

SURVEY TELESCOPE OPTICS

SURVEY TELESCOPE OPTICS

Valery Yu. Terebizh

SPIE PRESS
Bellingham, Washington USA

Library of Congress Cataloging-in-Publication Data

Names: Terebizh, V. Yu., author.

Title: Survey telescope optics / V. Yu. Terebizh.

Description: Bellingham, Washington : SPIE, The International Society for Optical Engineering, 2019. | "The purpose of this book is to give a concise and simple, as far as possible, description of the ideas underlying the basic wide-field astronomical systems"—Page viii | Includes bibliographical references and index. | Summary: "This book presents astronomical optical systems in the simplest form, with an emphasis on clear explanations of the ideas that underpin various systems. At the same time, it explains the deep connection between classical and contemporary telescopes, as well as the continuity of ideas for telescope construction. A number of new designs are described, including those recently proposed and those already operational, that provide a previously unattainable field of view"— Provided by publisher.

Identifiers: LCCN 2019033155 | ISBN 9781510631281 (paperback) | ISBN 9781510631298 (pdf) | ISBN 9781510631304 (ebook) | ISBN 9781510631311 (kindle edition)

Subjects: LCSH: Imaging systems in astronomy. | Astronomical instruments. | Optics, Adaptive. | Telescopes. | Astronomy.

Classification: LCC QB51.3.I45 T47 2019 | DDC 522/.2—dc23

LC record available at <https://lccn.loc.gov/2019033155>

Published by

SPIE

P.O. Box 10

Bellingham, Washington 98227-0010 USA

Phone: +1 360.676.3290

Fax: +1 360.647.1445

Email: books@spie.org

Web: <http://spie.org>

Copyright © 2019 Society of Photo-Optical Instrumentation Engineers (SPIE)

All rights reserved. No part of this publication may be reproduced or distributed in any form or by any means without written permission of the publisher.

The content of this book reflects the work and thought of the author. Every effort has been made to publish reliable and accurate information herein, but the publisher is not responsible for the validity of the information or for any outcomes resulting from reliance thereon.

Central image: "3/4 view rendering of Large Synoptic Survey Telescope," LSST Project Office, reprinted with permission of Creative Commons license. Bottom image: "Orbital planet system," reprinted with permission from gettyimages.

Printed in the United States of America.

Last updated 24 October 2019

For updates to this book, visit <http://spie.org> and type "PM311" in the search field.

SPIE.

To Sanya

Contents

<i>Preface</i>	<i>xi</i>
1 Introduction	1
1.1 Preliminary Definitions	2
1.1.1 Types of telescopes	2
1.1.2 Image quality	4
1.1.3 Efficiency of a survey	4
1.1.4 Limiting stellar magnitude and survey speed	6
1.2 Cursory Review of Modern Wide-Field Telescopes	7
1.2.1 Large wide-field telescopes	7
1.2.2 Survey telescopes of moderate size	11
1.3 Some Attendant Issues of Optics	12
1.3.1 Aperture stop and pupils	12
1.3.2 Curvature of the focal surface	13
1.3.3 ‘Ideal’ wide-field telescope and Schmidt camera	14
1.3.4 Remarks on color correction in catadioptric systems	16
1.3.5 Basic types of optical surfaces	18
1.4 Matching of Optics and Detector with Atmospheric Image Quality	20
1.4.1 Detectors of light	20
1.4.2 Sampling factor	22
2 Reflective Telescopes	25
2.1 Single Paraboloid	26
2.2 Two-Mirror Systems	27
2.2.1 Basic relations	28
2.2.2 Classical telescopes: Mersenne, Gregorian, and Cassegrain	31
2.2.3 Approximate aplanatic telescopes: Schwarzschild, Ritchey–Chrétien, and Gregory–Maksutov; Hubble Space Telescope	32
2.2.4 General Schwarzschild aplanats	37
2.2.5 Mirror Schmidt; LAMOST system	40
2.3 Selected Three-Mirror Telescopes	41
2.3.1 Paul system	41

2.3.2	Korsch anastigmats; the SNAP design	44
3	Catadioptric Systems with a Lens Corrector in Converging Beam	47
3.1	Lens Corrector at a Prime Telescope Focus	48
3.1.1	Wynne designs for Ritchey–Chrétien and classical primaries	49
3.1.2	All-spherical three-degree corrector of single glass	51
3.1.3	Dark Energy Camera; the DESI project	54
3.1.4	Subaru Hyper Suprime Camera	57
3.2	Lens Corrector in a Secondary Telescope Focus	58
3.2.1	Quasi-Ritchey–Chrétien system; VST telescope	59
3.2.2	Corrected Cassegrain system; Pan-STARRS telescope	61
3.2.3	Corrected Cassegrain design with a 2.5-m aperture and 3° field	63
3.2.4	Corrected Gregorian telescope	65
3.2.5	Folded Gregory–Maksutov telescope with a lens corrector	67
3.3	Three-Mirror Paul Telescope with a Lens Corrector	70
3.3.1	LSST project	70
4	Catadioptric Systems with a Full-Aperture Lens Corrector	75
4.1	Singlet Full-Aperture Corrector	75
4.1.1	Classical Schmidt camera	77
4.1.2	Modifications of Schmidt camera	83
4.1.3	Maksutov telescope	88
4.2	Doublet Full-Aperture Corrector	91
4.2.1	Richter–Slevogt system	91
4.2.2	Symmetrical corrector	93
4.2.3	Hamiltonian telescopes	95
4.2.4	The Ω_2 design	96
4.3	Triplet Full-Aperture Corrector	98
4.3.1	Schmidt–Houghton systems	98
4.3.2	Baker–Nunn and Super-Schmidt cameras	101
4.3.3	Meniscus Schmidt design of Hawkins and Linfoot; VAU telescope	103
4.3.4	Family of Sonnefeld cameras; the Ω_3 system	104
4.4	All-Spherical System with an Extremely Large Field	107
4.4.1	Statement of the problem	107
4.4.2	Examples of designs with an ultra-wide field of view	107
	Afterword	111
	Appendices	113
	A. Limiting Stellar Magnitude and Sky Survey Rate	115
	B. Schwarzschild Aplanats	117
	C. The Complexity of Optical Surfaces	121

D. Base Prime-Focus Lens Corrector with a 2.5° Field	125
E. List of Referenced VT Designs	127
F. New Algorithm for Calculating Anastigmatic Three-Mirror Telescopes	129
<i>Bibliography</i>	133
<i>Index</i>	145

Preface

Simplicity is the highest goal, achievable when you have overcome all difficulties.

Frederic Chopin (1810–1849)

Since the first telescopic surveys of the sky by Charles Messier and William Herschel in the late 18th century, investigations of this kind delivered astronomers an immense amount of information. In recent decades, the need for deep optical surveys has become especially urgent. In particular, cosmologists hope that new surveys will help them to discover so-called *dark matter*, to clarify the model of the universe, to explore the effects of gravitational lensing in clusters of galaxies, and to understand deeper the nature of sources of gravitational waves and powerful x-ray bursts. Wide-field telescopes are also needed to search for the planets around stars, to detect asteroids that pass dangerously close to the Earth, and to monitor the system of satellites around the Earth. Perhaps the most ambitious goal of modern observational astronomy is the acquisition of data concerning the current positions and magnitudes of all celestial objects brighter than approximately 24th magnitude in the visible waveband with the time scale of the order of one day.

A recent description of the purposes and results of sky surveys across the spectrum is provided by S. Djorgovski et al. (2012), who state that, “Surveys are now the largest data generators in astronomy, propelled by the advances in information and computation technology, and have transformed the ways in which astronomy is done. This trend is bound to continue, especially with the new generation of synoptic sky surveys that cover wide areas of the sky repeatedly, and open a new time domain of discovery.”

The subject of this book is the optical systems of telescopes that make it possible to implement a wide field of view in the visual waveband. As one can see, the key concept of ‘size of the field of view’ is vague without indicating the appropriate image quality of a point light source. Previously, with regard to wide-field telescopes, such requirements were rather mild—it was enough to provide images of stars with a diameter of about a dozen arc seconds in the integral waveband; since the beginning of this century, the requirements were toughened by an order of magnitude and approached the atmospheric resolution limit. This was abetted by the need to match optics

with detectors of light whose characteristics differ significantly from those of the photographic emulsion.

Over the past decades, the nature of design in optics has changed markedly due primarily to the increased power of computers and the sophistication of optical calculation programs. While analytical analysis relies mainly on a theory of third-order aberrations, a numerical approach takes full account of aberrations of complex systems. Charles Wynne, an outstanding creator of optical systems, wrote in 1968: “It was stated above that for Ritchey–Chrétien mirror systems the Seidel aberrations give for most purposes an adequate description of performance. For prime focus correctors consisting of systems of lenses, this is no longer the case.”

In this regard, it might seem that the analytical approach has already lost its significance, but it still lies at the root of the search for basic systems. Formally, the design of an optical system reduces to the search for a conditional minimum image quality function in the space of system parameters, the number of which is sometimes several dozen. The term ‘conditional’ is used because it is necessary to specify in detail the entire set of constraints and the desired performance. The case is radically complicated by the fact, discovered in the middle of the last century, that the quality function has a huge number of *local* minima in a multidimensional ‘optical’ space, but we are interested, as a rule, in a unique *global* minimum corresponding to the objectively best system. This mathematical problem does not yet have an exact solution, so the direct design of even a simple system can take an extremely long time with the most powerful computers. For this reason, the search for a best solution is largely based on the *understanding* of the desired optical system, which the approximate theory of aberrations gives.

Taken together, modern tools allowed the designs to reach a field of view measuring tens of degrees with image quality close to a diffraction-limited one.

The purpose of this book is to give a concise and simple, as far as possible, description of the ideas underlying basic wide-field astronomical systems. It is hoped that such an approach will be useful not only for professional optical designers but also for astronomers who are interested in creating survey systems. In the modern literature, it is not often possible to find a complete description of the new optical system, so many of the issues discussed are illustrated by our own designs.

It is a pleasure to thank my colleagues who have helped me for years, in particular, Mark Ackermann (University of New Mexico), Vadim Biryukov (Crimean Astrophysical Observatory), Yuri Petrunin (Telescope Engineering Company), Vladimir Skiruta (Crimean Astrophysical Observatory), and John Tonry (Institute for Astronomy, University of Hawaii).

Valery Terebizh
September 2019

Chapter 1

Introduction

The very topic discussed here suggests that we are interested in telescopes that combine a large field of view with a high survey speed of sufficiently faint objects. All of these interrelated concepts are largely determined by the goal of the observation.

To estimate the required speed of a sky survey S , as measured in square degrees per second (deg^2/sec), we assume that one needs to cover 10^4 deg^2 of sky in 3 hours. The specified area is a little smaller than the entire hemisphere visible above the horizon and free of absorption in the Milky Way and Earth's light pollution at large zenith angles, so our estimate matches the goals of real sky surveys. The resulting survey speed $S \simeq 1 \text{ deg}^2/\text{sec}$, which indicates that the problem is nontrivial.

Indeed, the field of view of a *classical Cassegrain* telescope (the parabolic primary and hyperbolic secondary mirrors; see Section 2.2.2) is only several arc minutes wide, so one would need to acquire about 10^6 images to cover the required area of sky, which is unrealistic even with multiple telescopes. The Ritchey–Chrétien telescope with both hyperbolic mirrors (Section 2.2.3), recently considered to be a wide-field instrument, also fails to solve the problem. The field of a Ritchey–Chrétien telescope does not exceed approximately $20'$, which might reduce the number of images mentioned above, but only by an order of magnitude. Thus, to perform a typical survey investigation, telescopes with an angular field diameter $2w$ of at least 1° are required. Most of the problems mentioned in the Preface need telescopes with a field from a few to tens of degrees in diameter (see Section 4.4.1).

There are two primary modes of surveying large areas of the sky: (i) we need to cover *sequentially* the area in reasonable time; and (ii) the sky area we are interested in should be under *continuous* observation. The problem of the first kind arises, for example, when we study the long-term variability of all objects on the celestial sphere brighter than a certain limit. The second mode is characteristic for cases where we look for fast transient objects, say, the counterpart of an x-ray burst.

The choice of mode is determined by the brightness and the characteristic time of evolution of the events under investigation. Of course, there are also intermediate situations.

In most of the current sky surveys, the faintest objects have about 19–22 magnitude in the visual range, which implies the use of telescopes at least 75 cm in diameter. However, a number of important problems, e.g., tracking asteroids dangerous to the Earth, can be solved with telescopes with a smaller aperture but a significantly wider field of view than conventional field of large instruments. It is rather difficult to set the lower boundary of the aperture dimension of a telescope that is useful as a survey instrument. In particular, interest in multi-lens systems of the type *Evrscope* (Law et al. 2015) with an aperture of about 10 cm is now noticeable. On the other hand, the achievement of a significant field of view with telescopes that have an aperture of more than 10 m is insufficiently studied, so the present discussion is confined to the above upper limit.

1.1 Preliminary Definitions

The variety of goals entails a wide diversity in size, type, and performance of survey telescopes. Before turning to a detailed discussion of the topic, it would be desirable to define the concepts of image quality, field of view, and classification of wide-field telescopes. We will specify these later, but for now it is enough to glance at the total set of wide-field telescopes in operation and those under construction.

1.1.1 Types of telescopes

Single-mirror telescopes are naturally subdivided according to the shape of the mirror surface. In the astronomical aspect, parabolic and spherical mirrors are of particular interest; the former because of the ability to form a diffraction image of an infinitely distant axial source of light (Section 2.1), and the latter due to the simplicity of the surface shape.

Following the common terminology (see, e.g., Schroeder 2000, Section 6.2), we call a Cassegrain system *classical* if its primary is a paraboloid. The *aplanatic Cassegrain* system,¹ or *Ritchey–Chrétien* (RC) telescope, consists of two hyperboloidal mirrors with specific values of eccentricities, which depend upon the layout's first-order parameters according to Eq. (2.16) of Section 2.2.3.

Further, a *Quasi-Ritchey–Chrétien* (QRC) system is a RC telescope with a lens field corrector between the secondary mirror and focal surface. The same term is often applied to similar systems, when both the mirrors and the

¹ *Aplanat* is an optical system in which both spherical aberration and coma are corrected.

corrector elements are slightly optimized as a whole, so the purely reflective two-mirror subsystem remains close to the strict RC. In other words, the two-mirror part of a QRC telescope should provide feasible images in the paraxial field.

The deep co-optimization of mirror optics and a lens corrector leads to a system whose parameters differ significantly from those for a QRC. For example, the Pan-STARRS telescope PS1 with a conic constant² of a secondary mirror equal to -21.4 cannot be regarded as an RC with a corrector or a QRC, as can be found in the literature. It is convenient to name such systems *Cassegrain telescopes with a corrector* or, for brevity, *corrected Cassegrain* systems.

Terms similar to those used for the Cassegrain system are appropriate for versions generated by a Gregorian system (Section 2.2.2). The *classical* Gregorian telescope has a paraboloidal primary mirror and an ellipsoidal secondary one. The corresponding aplanatic version of the Gregorian system was described for the first time by Maksutov (1932), so we call it the *Gregory–Maksutov* (GM) system (Section 2.2.3). Both mirrors of a GM telescope are ellipsoids, whose conic constants are given by the same Eq. (2.16). Finally, the *corrected Gregorian* telescope includes two mirrors and a lens corrector provided that the parameters of the entire optical system have undergone deep optimization. An example of such a system is given in Section 3.2.4.

We spoke above about single-mirror and two-mirror telescopes. The need to provide a large field of view for telescopes of considerable aperture leads to the development of purely reflective systems with a larger number of mirrors. Section 2.3 discusses only two such systems: the Paul and Korsch three-mirror telescopes. The first of them is a wide-field mirror analogue of the Schmidt camera with a practically plane-parallel beam of light going to the third mirror. The second system, a *three-mirror anastigmat* (TMA), is characterized by the complete elimination of third-order aberrations, which ensures excellent image quality within the field up to $2\text{--}3^\circ$. The problem of light vignetting, severe even in three-mirror telescopes, becomes critically acute for systems with a larger number of mirrors, which is addressed in the fairly extensive literature.

Adding lens optics to mirrors opens up a variety of catadioptric telescopes, which are discussed in Chapters 3 and 4. These systems are commonly referred to as “the discoverer.” The division of catadioptric telescopes according to the number of full-aperture lenses in the input corrector, which is used in Chapter 4, seems to be an adequate approach to the difficult task of classifying these systems.

² The conic constant is the square of the eccentricity, taken with the opposite sign.

1.1.2 Image quality

It is worth repeating that the angular diameter of the useful field of view $2w$ is determined by the quality of the images in it.³ The usual way to describe approximately the image quality provided by a telescope is to give the root-mean-square (RMS) angular diameter Δ''_{rms} of a star image in arc seconds (arcsec). It is more likely now to use another parameter, the angular diameter Δ''_{80} of a circle, which contains 80% of the energy in the image of a star. It is also popular in observational astronomy to specify $\Delta''_{1/2}$, i.e., the full width of a star image at the half maximum (FWHM). We omit further an upper symbol, measuring the image quality both in arcsec and microns. To distinguish Δ_{80} for a telescope alone from similar quantities, we designate it later as θ_{tel} .

For a Gaussian profile, we have approximately

$$\Delta_{80} \approx 1.269 \Delta_{rms} \approx 1.524 \Delta_{1/2}. \quad (1.1)$$

A word of caution is warranted against using $\Delta_{1/2}$ in cases where the profile of the image has a specific appearance. For example, sometimes it is a superposition of a relatively narrow central peak and a wide substrate, as it had a spot for the original Hubble Space Telescope. The same is particular to systems with rippled optical surfaces (O'Neill 1963, Chapter 6; Wetherell 1982; Suiter 1994, Chapter 13). In such cases, $\Delta_{1/2}$ and Δ_{80} may differ by several times, which is significant in the interpretation of photometric and spectroscopic observations.

Obviously, no strict definition for ‘wide-field telescopes’ exists; we merely propose a suitable working definition. For now, it is sufficient to consider a telescope as *wide-field* if its angular field of view, within which images of stars are not worse than a few arcsec, exceeds in size about 1° .

1.1.3 Efficiency of a survey

Along with a number of standard parameters of telescopes, it is useful to have a parameter that gives an idea of the efficiency of the telescope as a survey tool. To date, a widely used parameter is the *étendue*

$$E \equiv \pi w^2 \cdot \pi D_e^2 / 4, \quad (1.2)$$

a product of the observed sky area (deg^2) and the effective area of the telescope aperture (m^2). The *effective aperture* D_e takes into account the vignetting of useful light in the telescope, and with the significant role of this

³ The situation here resembles an old story about a woman who wanted to become a secretary. “Oh, can you really type at a rate of 200 words per minute?!” exclaimed the manager, looking at her resume. “Of course,” the woman replied, “but it ends up as nonsense. . .”

factor it can be noticeably inferior to the *entrance pupil diameter* D .⁴ For a conventional two-mirror telescope, we can use, as a good approximation, the relation

$$D_e \simeq D\sqrt{1 - \eta^2}, \quad (1.3)$$

where η is the *linear obscuration coefficient*, which approximately equals the ratio of the diameters of the secondary and primary mirrors.

The inadequacy of the étendue with respect to the problem of interest is clear from the fact that E does not take into account the quality of images provided by a telescope. Meanwhile, there is no doubt that with better angular resolution, higher survey efficiency can be achieved.

An adequate measure of the survey efficiency, the *sky survey rate* Γ , is defined, up to a constant factor, as the ratio of the observed sky area πw^2 to the exposure time T needed to achieve the required S/N value (Terebizh 2011). It is not difficult to show (Appendix A) that such a definition leads to the following expression:

$$\Gamma \equiv \frac{\pi w^2 \cdot \pi D_e^2 / 4}{\theta^2} = E / \theta^2, \quad (1.4)$$

where θ is the so-called *delivered image quality*:

$$\theta \equiv \sqrt{\theta_{atm}^2 + \theta_{tel}^2 + p^2}, \quad (1.5)$$

and θ_{atm} , θ_{tel} , and p are the angular image sizes due to, respectively, atmospheric turbulence, telescope aberrations, and the finite size of the detector pixels. The first two of these parameters correspond to an 80% level of energy.

As expected, the image quality naturally entered into Eq. (1.4), and its influence is even more significant than the area of the aperture and field of view, because it is in the denominator of this expression. In essence, Γ is the product of the number of resolution elements in the observed region of the sky and the effective area of the telescope aperture.⁵

A convenient practical unit of measurement for the sky survey rate is

$$\textit{herschel} \equiv 1 \text{ m}^2 \text{ deg}^2 / \text{arcsec}^2, \quad (1.6)$$

named after William Herschel (1738–1822). The rest of this book will use the abbreviation H for this unit.

⁴ The diameter of the paraxial image of the stop in object space. See Section 1.3.1.

⁵ Tonry (2011) proposed a more detailed approach to the evaluation of the survey efficiency, which includes consideration of the *point spread function* form and its alignment with the pixels of the detector.

1.1.4 Limiting stellar magnitude and survey speed

The notion of the *sky survey rate* Γ introduced above describes well the capabilities of the telescope itself, while the observer and the developer of a survey project also need the estimates of the stellar magnitude achievable with the instrument for a fixed exposure time and the corresponding survey speed. For our purposes, it is desirable to get sufficiently accurate values that are reasonably consistent with the observational data and, at the same time, do not enter into details that are superfluous in this context.

Such compromise calculations are given in Appendix A. We have for a limiting stellar magnitude:

$$m_{lim} = \mu/2 + 1.25 \log_{10}(N_0 \cdot q \cdot U \cdot \delta\lambda \cdot \epsilon \cdot T) + 2.5 \log_{10}[D/(\theta \cdot S/N)], \quad (1.7)$$

where

- μ (magnitude/square arcsec) is the sky surface brightness,
- N_0 (photons/sec cm² μm) is the photon flux from a star of zeroth magnitude,
- $q = q_{atm} \cdot q_{tel}$ is the total transparency, including the atmosphere and telescope,
- $U \simeq 1 - \eta^2$ is the fraction of unvignetted rays in a telescope,
- $\delta\lambda$ (μm) is the waveband width,
- ϵ (photo-events/photon) is the quantum efficiency of the detector,
- T (sec) is the exposure time,
- D (cm) is the telescope entrance pupil diameter,
- θ (arcsec) is the *delivered image quality* defined by Eq. (1.5), and
- S/N is the threshold signal-to-noise ratio adapted for observations.

It is sufficient for us to assume $N_0 = 1 \cdot 10^7$ photons/sec cm² μm in the visual region of the spectrum.

Values of m_{lim} according to Eq. (1.7) are in agreement with the estimates of the SIGNAL package created by the team of the *Isaac Newton Group of Telescopes* (<http://catserver.ing.iac.es/signal/>). However, we do not require the calculations to exactly match the real data, as our primary goal is to evaluate the comparative characteristics for the various types of optical systems.

As for the survey speed S , in the usual case, when the field of view has the form of a circle of diameter $2w$ (deg), and a square detector is inscribed into the field, we have

$$S = \frac{2w^2}{T + T_d} \text{deg}^2 / \text{sec}, \quad (1.8)$$

where T_d (sec) is the ‘dead time’ (or ‘slew time’), corresponding to telescope repositioning and data readout. Obviously, if the entire field of view is filled with a detector, then 2 should be replaced by π in Eq. (1.8).

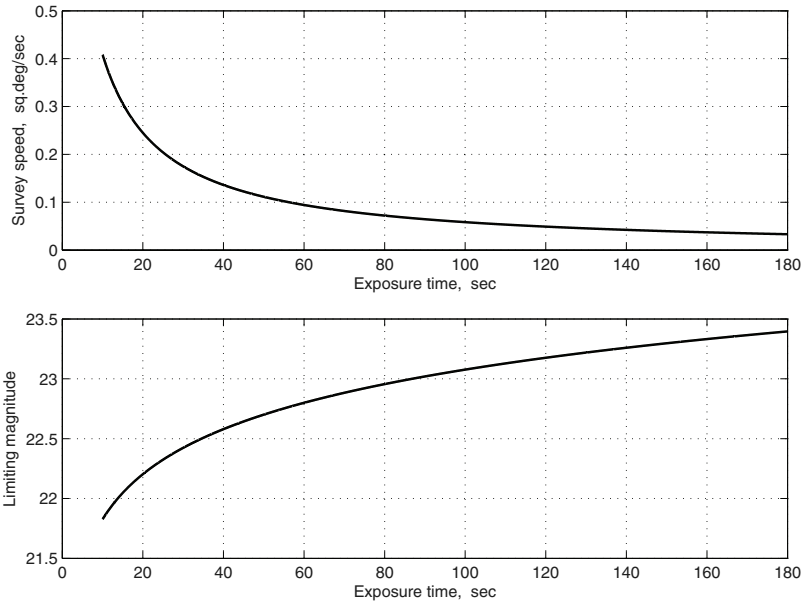


Figure 1.1 Limiting magnitude and survey speed as the functions of exposure time for the 1-m VT-056y design with a 3.5° field of view.

An example of functions $m_{lim}(T)$ and $S(T)$ is shown in Fig. 1.1. The design VT-056y represents a one-mirror telescope with a prime focus lens corrector (Terebizh 2016b). We assumed that $D = 1$ m, $F = 2.183$ m, $2w = 3.5^\circ$, $q = 0.75$, $U = 0.85$, $\theta_{tel} = 0.65''$, $\theta_{atm} = 1.5''$, $\mu = 21^m/\text{arcsec}^2$, and the object zenith angle is 30° . The spectral bandwidth is $0.50 \mu\text{m}$, and the dead time is 5 sec. As a detector, the STA1600 CCD with $10.56\text{-}K \times 10.56\text{-}K$ pixels of $9\text{-}\mu\text{m}$ size was selected; its quantum efficiency $\epsilon = 0.85$. The threshold value $S/N = 7$ corresponds to the accepted field and detector sizes.

Naturally, as the exposure time increases, weaker objects are achievable; however, the loss of time for each exposure reduces the survey speed. Knowing the survey speed allows us to estimate the total time T_{obs} , which is required for viewing the sky area A (deg^2), namely, T_{obs} (sec) = A/S . The latter relation, together with Eq. (1.7) and Eq. (1.8), defines an important relationship between m_{lim} , S , and T_{obs} , in which the exposure time T serves as a convenient parameter. Thus, using such simple calculations, one can create the initial basics of a project, which will then be refined as the project details.

1.2 Cursory Review of Modern Wide-Field Telescopes

1.2.1 Large wide-field telescopes

Table 1.1 gives a list of 23 telescopes with an aperture diameter D larger than 1 m and a sufficiently wide angular field of view $2w$ (see also reviews of

Table 1.1 Wide-field telescopes with an aperture diameter D larger than 1 m. F is the effective focal length, and $2w$ is the field of view.

No.	Name	D (m)	F (m)	$2w$ (deg)	Optical system type
1	LSST	8.4	10.3	3.5	Paul + 3-lens corrector
2	Subaru HSC	8.2	18.7	1.5	5-lens prime focus corrector
3	SPM-Twin	6.5	29.3	2.0	3-lens Cassegrain corrector
4	DCT	4.2	9.7	2.0	6-lens prime focus corrector
5	VISTA	4.1	12.1	1.65	3-lens Cassegrain corrector
6	LAMOST	4.0	20.0	5.0	Reflective Schmidt
7	DESI	4.0	11.5	3.2	6-lens prime focus corrector
8	Blanco DECam	3.93	11.5	2.2	5-lens prime focus corrector
9	AAT	3.9	12.7	2.0	4-lens prime focus corrector
10	DSST	3.5	3.5	3.5	Paul + 3-lens corrector
11	WIYN ODI	3.5	22.1	1.4	2-lens Cassegrain corrector
12	VST	2.61	14.5	1.47	4-lens Cassegrain corrector
13	T250 ACTUEL	2.5	9.1	3.0	3-lens Cassegrain corrector
14	Steward 90"	2.3	6.83	1.1	4-lens prime focus corrector
15	SNAP	2.0	21.4	1.5	3-mirror Korsch
16	Pan-STARRS	1.8	8.0	3.0	3-lens Cassegrain corrector
17	KMTNet	1.6	5.2	2.8	4-lens prime focus corrector
18	SkyMapper	1.3	6.23	3.4	3-lens Cassegrain corrector
19	UKST	1.24	3.1	9.3	Schmidt
20	Oschin Schmidt	1.22	4.6	5.7	Schmidt
21	ESO Schmidt	1.0	3.1	6.4	Schmidt
22	OMI	1.0	2.5	3.11	4-lens prime focus corrector
23	GEODSS	1.0	2.2	2.1	3-lens prime focus corrector

Notes to Table 1.1

1. LSST: Large Synoptic Survey Telescope. Allsman et al. (2006), Ivezić et al. (2008), Gressler (2009).
2. Subaru HSC: Subaru Hyper Suprime Camera. Komiyama et al. (2010).
3. SPM-Twin: Spectroscopic telescope, San Pedro Martir NAO Mexico. Gonzalez (2007), Gonzalez and Orlov (2007).
4. DCT: Discovery Channel Telescope. MacFarlane and Dunham (2006). The DCT will also feature a Ritchey–Chrétien focus with a two-lens corrector.
5. VISTA: Visible and Infrared Survey Telescope for Astronomy. Etedgui-Atad and Worswick (2003).
6. LAMOST: Large Sky Area Multi-object Fiber Spectroscopic Telescope. Cui et al. (2000).
7. DESI: Dark Energy Spectroscopic Instrument based on the Mayall 4-m telescope of KPNO. Martini et al. (2018), Miller et al. (2018).
8. Blanco DECam: Dark Energy Camera based on the Blanco 4 m telescope of CTIO. Kent et al. (2006), Flaughner et al. (2015).
9. AAT: Anglo-Australian Telescope. Jones (1994), Taylor and Gray (1990, 1994).
10. DSST: DARPA Space Surveillance Telescope. Curved focal surface. Grayson (2002).
11. WIYN ODI: WIYN Observatory One Degree Imager. Harmer et al. (2002).
12. VST: VLT Survey Telescope. Mancini D. et al. (2000).
13. T250 ACTUEL: Benitez et al. (2009), Cenarro et al. (2010).
14. Steward 90" (Bok Telescope). Williams et al. (2004).
15. SNAP: Super-Nova Accelerating Probe. Lampton et al. (2002).
16. Pan-STARRS: Panoramic Survey Telescope and Rapid Response System (PS1). Kaiser et al. (2002), Hodapp et al. (2004), Morgan and Burgett (2009), Chambers et al. (2016).
17. KMTNet: Korean Microlensing Telescope Network. Kim, et al. (2010, 2011).
18. SkyMapper: Rakich et al. (2006).
19. UKST: United Kingdom Schmidt Telescope. Wynne (1981).
20. Palomar 48-inch Schmidt – Samuel Oschin Telescope has been upgraded at first to a Palomar Transient Factory (Law et al. 2009), and then to the Zwicky Transient Facility (Smith et al. 2014).
21. ESO Schmidt: Wilson (1996).
22. OMI: Canadian One-Meter Initiative. Roy (2010).
23. GEODSS: Two identical Ground-based Electro-Optical Deep Space Surveillance telescopes. Jeas and Anctil (1981).

Ackermann et al. 2010, Djorgovski et al. 2012). Strictly speaking, the purely spectroscopic telescopes SPM-Twin, LAMOST, and N. U. Mayall telescope with the DESI corrector should be considered separately. Some of the telescopes are not yet operational, but the current state of the projects is not considered here, since we are interested in the optics of wide-field telescopes itself. For the same reason, we are referring not only to existing telescopes but also systems for which non-trivial optical solutions were found but have not yet been implemented. An example is a three-mirror Korsch anastigmat with an aperture of 2.0 m and a 1.5° field of view proposed in the Super-Nova Acceleration Probe (SNAP) project. Readers interested in the results of the survey studies should turn to the discussion by Djorgovski et al. (2012).

In the following chapters, we describe some of the telescopes listed in Table 1.1 in more detail, namely, LSST (Section 3.3.1), Subaru HSC (Section 3.1.4), LAMOST (Section 2.2.5), Blanco DECam and Mayall DESI (Section 3.1.3), VST (Section 3.2.1), SNAP (Section 2.3.2), and Pan-STARRS (Section 3.2.2).

The $[D_e - 2w]$ diagram corresponding to the data in Table 1.1 is shown in Fig. 1.2. The effective diameter D_e values were evaluated according to Eq. (1.3).

The first thing to note in Fig. 1.2 is the especially large field sizes of the three Schmidt telescopes. This is exactly Schmidt's breakthrough. In the second half of the 20th century, sky surveys with Schmidt telescopes contributed most of the progress in extragalactic astronomy. It is enough to

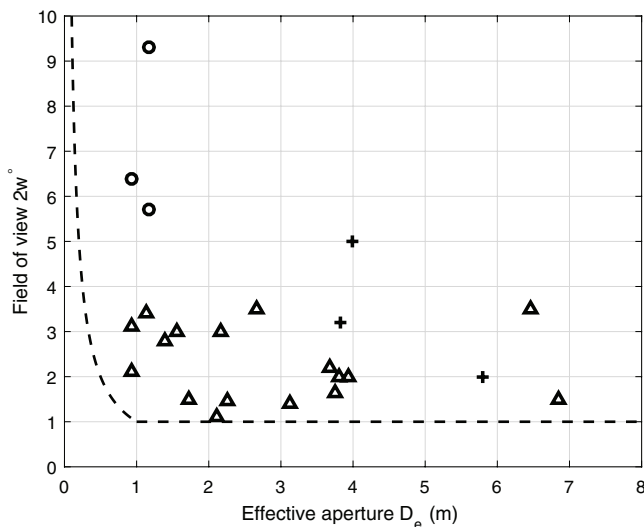


Figure 1.2 Effective aperture diameter (m) vs. angular field of view (deg) for the telescopes listed in Table 1.1. Spectroscopic telescopes are shown as crosses and Schmidt systems as circles. The dashed line separates the wide-field region according to Eq. (1.9).

recall the Palomar Sky Survey, made with the help of a 48-inch Schmidt camera, that served as the basis to identify extragalactic radio sources, which led, in particular, to the discovery of quasars.

Unfortunately, modern technology does not allow us to make lenses larger than about 1.5 m. Above this value, telescopes are distributed in the diagram more or less evenly in the $1.0\text{--}3.5^\circ$ band, with the exception of the gap in the region of $D_e \simeq 5$ m. An important fact is the limit of the field size from above for the telescopes that don't belong to the group of Schmidt cameras and spectroscopic systems. Indeed, the area $2w < 3.5^\circ$ is occupied by diverse mirror telescopes equipped with comparatively small lens correctors in a converging beam (Chapter 3), and it turns out that, regardless of the particular optical layout of a telescope, its angular field size is bounded above by the same value.

The simplest explanation of the latter fact holds that the angular field of view $2w \simeq L/F \simeq L/(\phi D)$ radians, where L is the linear size of the detector, and $\phi \equiv F/D$ is the *focal ratio*.⁶ It is possible now to implement a *flat* field of a relative size $L/D \sim 1/10$, while ϕ has to be reduced to about 1.5–2.0 in order to simplify the optical design and to decrease the size of the telescope. Hence, an obvious way to further expand the field in large telescopes uses big detectors on a curved focal surface.

As regards the aforementioned lack of systems with an effective aperture of about 5 m, it seems to be a correctable omission. The efficiency of such systems would be sufficient to advance the problems mentioned in the Preface, while difficulties in manufacturing and operating, as well as cost, would be substantially reduced compared to those for larger telescopes. As an example of the systems in question, consider the design of the corrected Gregorian telescope, which is presented in Section 3.2.4.

With the commissioning in 2012 of Blanco DECam and Subaru HSC, wide-field observations reached a new level, characterized by a conjunction of depth of investigation and a large field of view. An analysis of such a vast flow of information assumes the joint efforts of consortiums of astronomers.

It is desirable sometimes to have, for cataloging purposes, a formal definition of a wide-field optical system. Figure 1.2 suggests the simple definition of a boundary that separates wide-field telescopes from the others:

$$2w^\circ = \begin{cases} 1/D_e & \text{if } D_e \leq 1 \text{ m,} \\ 1 & \text{if } D_e > 1 \text{ m,} \end{cases} \quad (1.9)$$

where the field angle is measured in degrees and the effective diameter in meters.

⁶ In older sources, the focal ratio was denoted most often by *f*/#. We also use this designation sometimes, but only ϕ is used in the mathematical context.

Note that the Ritchey–Chrétien telescope with a field of nearly $20'$ does not fall into the class of wide-field systems. Equation (1.9) gives reasonable estimates even for smaller apertures. For example, the field of view of a survey system should be not less than 10° for a 10-cm objective (such as a commercial *Canon 200* lens), $2w \geq 4^\circ$ for a 25-cm camera, and $2w > 2^\circ$ for a 0.5-m telescope.

1.2.2 Survey telescopes of moderate size

Just as a navy cannot be restricted to aircraft carriers only, in a survey case it is reasonable to distribute tasks between instruments with various apertures and field sizes. A substantial part of the survey data is now obtained using telescopes with a diameter of less than 1 m, and there are reasons to expect that wide-field telescopes of moderate size will be manufactured even after the commissioning of the Large Synoptic Survey Telescope.

The telescopes discussed would be presented in Fig. 1.2 in the domain $D < 1$ m, $2w < 50^\circ$. Virtually all of these systems are successors of the classical Schmidt camera (Sections 1.3.3 and 4.1.1). From an optical point of view, the wide-field telescopes of moderate aperture have interesting variations in design, which is not possible in larger telescopes (see especially Köhler 1948, Buchroeder 1971). The basic information for these telescopes will be given in Chapter 4, along with descriptions of individual systems. This section discusses only some productive sky surveys aimed at finding near-Earth objects (NEOs), in particular, the potentially hazardous asteroids or comets with orbits that closely approach the Earth and are of a size large enough to cause significant regional damage in the event of impact.

The Catalina Real-Time Survey (Steward Observatory Station, Tucson, Arizona, USA) is a NASA-funded project supported by the NEOs Observation Program (Drake et al. 2009). The project utilized a 1.5-m $f/2$ telescope with a 1.1° field diameter and a 68-cm $f/1.7$ Schmidt telescope with a 3.4° field. In 2017, all operating observatories found a little more than 2,000 NEOs; almost half of them fell to Catalina Survey.

The Pan-STARRS survey (see Section 3.2.2), which uses the 1.8-m PS1 telescope with a field of 3.0° , provided about 43% of the total number of NEOs discovered in 2017.

One of the new projects is the Asteroid Terrestrial-impact Last Alert System (ATLAS), the first stage of which entered operation in 2015 (Tonry 2011, Tonry et al. 2018). This system, funded by NASA and developed by the University of Hawaii, comprises two observatories separated by about 100 km that simultaneously scan the complete northern sky every two days to a stellar magnitude fainter than 19. So far, each of the locations has one telescope with the Schmidt system, equipped with a three-lens focal corrector (Section 4.1.2); in the future, the number of observatories and telescopes is expected to increase. Table 1.2 shows the main characteristics of the base telescope.

Table 1.2 Specifications of the ATLAS Schmidt telescope.

Parameter	Value
Aperture	50 cm
Effective focal length	100 cm ($f/2.0$)
Field of view	7.5°
Detector	STA1600, $10.56K \times 10.56K$ CCD
Pixel size	$9 \mu\text{m}$ ($1.86''$)
Effective PSF FWHM at $1.5''$ seeing	$2.5''$
Nominal exposure time	30 sec
Readout time	6 sec

Since the ATLAS used previously made telescopes primarily to debug the software before moving on to new instruments, it was possible to optimize the entire observation channel, including the telescopes, their location, detectors, and data analysis. This ensures the opportunity to reach faint objects with telescopes of moderate aperture. Together with a high cadence, this makes the system an effective means of detecting new objects, as well as tracking variables and transient phenomena in the sky.

1.3 Some Attendant Issues of Optics

Although this book is devoted to the optical systems of telescopes, we will only briefly touch on the basic results of classical optics, since they are excellently described in fundamental monographs, starting with Born and Wolf (1999), Hecht (1998), G. Smith (1998), and Geary (2002) and ending with special handbooks on astronomical optics by Danjon and Couder (1935), Dimitroff and Baker (1945), Maksutov (1946), Wilson (1996, 1999), and Schroeder (2000). The purpose of this section is to focus on some issues of particular interest in the development of wide-field optical systems. In passing, this will allow us to avoid repetitions when discussing the seemingly different optical layouts.

1.3.1 Aperture stop and pupils

In optics, including its astronomical part, the concept of the system's *aperture stop* and the related concepts of *entrance* and *exit pupils* are of great importance (Born and Wolf 1999, Section 4.8.2).

The axial beam of light passing through the system is limited by the diaphragms, if they exist, and by the frames (or edges) of the optical elements, which can also be considered as diaphragms. The *aperture stop* is the diaphragm that limits the beam of light to the greatest extent. In other words, it determines the cross-section of the beam that forms the image. The *entrance pupil* is the image of the aperture stop created by the part of the optical system that precedes the stop; the *exit pupil* is the image of the aperture stop created by the

part of the system that follows the stop. Evidently, both pupils are mutual images of each other with the forward and backward rays. Like every image of a physical object (in our case, of the stop), pupils can be real or virtual.

These notions can be illustrated with an example of a two-mirror telescope in which the light beam coming from a star is bounded by the mounting of the primary mirror (Fig. 1.3). In this case, the mounting's edge coincides with both the aperture stop and the entrance pupil of a telescope. As seen in Fig. 1.3, the Cassegrainian convex secondary mirror forms a virtual exit pupil, which is placed before the secondary in the path of the incident light beam, whereas the concave secondary mirror of the Gregorian telescope forms a real exit pupil towards the primary mirror.

It is important to keep in mind, in connection with the subsequent discussion, that the focal surface of an optical system is illuminated in such a way that the light beams appear to originate from the system's exit pupil.

1.3.2 Curvature of the focal surface

For wide-field telescopes (and we are only interested in such systems), the curvature of the focal surface becomes particularly tangible. This aberration is usually called the *field curvature*; its effect on image quality is closely related to *astigmatism*. Both of these aberrations are proportional to the square of the field angle, that is, they increase rapidly with an increasing field.

In the presence of astigmatism, as is the case with the Ritchey–Chrétien two-mirror telescope, we have two focal surfaces—for tangential and sagittal sections of the light beams, respectively—and these surfaces are essentially curved (Born and Wolf 1999, Section 5.5.3). Two focal surfaces coincide if spherical aberration, coma, and astigmatism are eliminated, but, generally speaking, the common focal surface remains curved. This surface becomes a plane if, in addition, the *Petzval condition* is satisfied. The above is true only in the framework of the third-order theory of aberrations, which has limited value for wide-field systems.

In the context of astronomical observations, where the focal lengths are usually large, a significant angular field is combined with the large linear

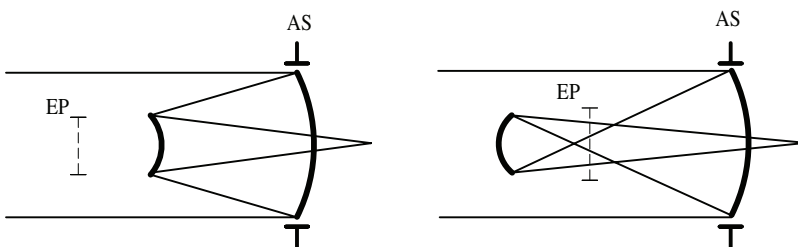


Figure 1.3 Positions of the aperture stop (AS) and exit pupil (EP) in the Cassegrain and Gregorian telescopes.

dimensions of the detector. This problem became imperative after Schmidt (1931) invented a camera with a field of view of about 10° . Until then, when calculating optical systems, the main goal was to achieve a flat focal surface to use common detectors. This approach is adopted in most of the systems considered in this book. Meanwhile, the field of view is sometimes so great that it should be left curved. It is time for us to understand that the curved focal surface is just as natural for telescopes as for the eyes of living beings.

The following ways seem to be preferred now in this regard: (i) the use of large detectors with a curved surface; (ii) applying the long-known technology based on a plurality of delicate waveguides with a curved-in-aggregate input surface (figured fiber-optic plates); and (iii) the faceting of the curved focal surface, i.e., the use of relatively small, flat detectors equipped with local field-flattening optics.

In the old days, either a photographic plate or a film were bent along a curved focal surface at wide-field observations, but these detectors are no longer used because of their low quantum efficiency. The principal issues and examples of modern curved detectors were discussed by Iwert and Delabre (2010) and Iwert et al. (2012); the first of these articles includes a photograph of a curved detector with a size of $60\text{ mm} \times 60\text{ mm}$ and a curvature radius of 500 mm . There are also working examples of curved detectors of this type. In particular, a mosaic of curved detectors has been implemented in the DARPA-developed 3.5-m Space Surveillance Telescope (Blake et al. 2013).

The second option (figured fiber-optic plates) considered in a modern context involves a number of technological problems. The basic difficulties may be overcome within the framework of the program announced by the European Space Agency, which provides a solution for mapping a curved image field onto a flat imaging detector array.⁷

In connection with the third option, it is appropriate to mention the 95-cm Kepler space telescope with the equivalent field diameter of 11.6° . Its detector consists of 21 pairs of ordinary $59\text{-mm} \times 28\text{-mm}$ CCDs covered by sapphire field-flattening lenses. An analogous procedure is applicable in other systems discussed here.

The future development of wide-field systems will be based on the first way, which involves the creation of large detectors with a curved surface.

1.3.3 'Ideal' wide-field telescope and Schmidt camera

The term 'ideal' was employed by Karl Strehl (1905) to describe the system in Fig. 1.4(a). The system is simple: it includes only a spherical mirror and a diaphragm located in the center of the sphere. A huge field of view is available

⁷ The details can be found in a note from 19 March 2013 at [http://www.esa.int/Our Activities/Space Engineering & Technology/](http://www.esa.int/Our_Activities/Space_Engineering_&Technology/).

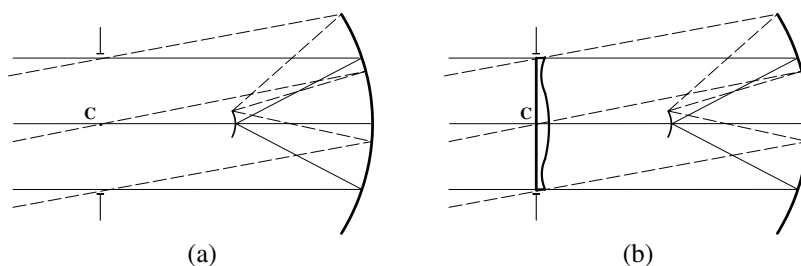


Figure 1.4 The two steps in the design of the Schmidt camera: (a) ‘Ideal’ telescope of Strehl. (b) Lens corrector at the center of curvature C .

to the system, since there is no accentuated optical axis in it: all of the beams passing through the center are equal. Therefore, the images of stars within the field are the same; they are located on a spherical surface approximately in the middle between the diaphragm and the mirror.

However, images in the ‘ideal’ telescope are far from perfect, because they are spoiled by *spherical aberration*. The latter consists in the fact that the rays from the edge zone of the wide light beam form the image closer to the mirror than the rays reflected from the central zone⁸ (Fig. 1.5). The great invention of Schmidt (1931) was the design and creation of a single-lens corrector placed at the center of curvature of a spherical mirror [Fig. 1.4(b)]. The ordinary corrector is a glass plate with one surface that has a substantially aspheric shape to compensate for the spherical aberration of the mirror. Namely, the central part of the corrector acts as a positive lens, which shortens the focal length, while its outer part acts as a negative lens [see Figs. 1.4(b) and 1.5].

In such a way, a field of view of about 10° can be attained (Section 4.1.1). To properly assess this achievement, recall that the field of a classical telescope is only a few arc minutes. The essence of the new optical system was clearly expressed by G. H. Smith (1998, p. 380): “There is now point

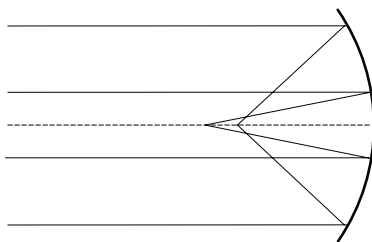


Figure 1.5 Spherical aberration of a spherical mirror.

⁸ Since spherical aberration can be characteristic of both spherical and aspheric optical elements, Maksutov (1946) considered it more appropriate to call it *zonal aberration on the axis*.

symmetry about the center of the stop (and the center of curvature of the mirror), rather than rotational symmetry about an axis. This point symmetry is the basis of the Schmidt telescope.” Thus, the core of the centenary path from the ‘ideal’ telescope to the modern versions of the Schmidt camera can be summarized as follows:

The really wide field of view can be provided by placing an aperture stop at the center of curvature of the spherical mirror and subsequent correction of spherical aberration by elements of low optical power.

Shortly after Schmidt’s discovery, Maurice Paul (1935) used this approach to propose a three-mirror wide-field telescope, which is the basis of the most ambitious modern project, the Large Synoptic Survey Telescope (Sections 2.3.1 and 3.3.1). The core two-mirror subsystem in the Paul telescope, imitating the Schmidt corrector, is a Cassegrain telescope; a similar three-mirror generalization with a Gregorian core telescope was suggested by James Baker (see Dimitroff and Baker 1945).

The life of Bernhard Schmidt (1879–1935) and the history of his discovery are covered in a book by Mursepp and Weismann (1984) and articles of Wachmann (1955), Osterbrock (1994), and Busch, Ceragioli, and Stephani (2013). (Schmidt’s mastery is all the more striking because he lost his right hand in his youth.) It is worth mentioning that Karl Strehl was not the first: the same system was discussed in the 19th century by Joseph Petzval and Hermann Vogel (Walter Stephani 2015, private communication). Strehl and Schmidt knew each other even before 1910. An important role in the spread of the new system was played by a young friend of Schmidt, Walter Baade, who prompted him to write a short article and later drew the attention of American astronomers to the extraordinary capabilities of a wide-field telescope. In the 1940s, Baade’s studies at Mount Wilson Observatory led to a two-fold change in the estimation of the size of the known universe.

1.3.4 Remarks on color correction in catadioptric systems

Compensation of chromaticity in lens optics has been repeatedly described in the literature (see, e.g., Hecht 1998, Smith 1998, and, for historical perspective, King 1955). The paucity of a set of optical glass led Isaac Newton to doubt the possibility of compensating for this aberration in a lens-based system. Only a relatively recent study of Newton’s diaries (Turnbull 1959, Whiteside 1969) revealed that his search for achromatic systems was more extensive than is commonly believed.⁹ In 1673, Newton found another way to compensate for the longitudinal color of a single lens: by combining it with a meniscus lens-mirror, which was later named a *Mangin mirror*. The rays of different wavelengths are focused by a single lens

⁹ I am grateful to M. R. Ackermann, who has drawn my attention to this fact.

from blue to red in order of increasing distance from the lens, and in reverse order—by a Mangin mirror.

The corresponding telescope was patented much later by W. F. Hamilton (1814), so the systems like that shown in Fig. 1.6 with a separated lens/mirror-lens pair are known as *Hamiltonian telescopes*. The achromatic doublet of Chester Hall had already been well studied early in the 19th century, but flint glass was expensive, so Hamilton proposed the combination of a large crown lens with a smaller flint color-correcting element (Wilson 1996, p. 212). In fact, it is sufficient, and often preferable, to use the same type of glass for both elements.

Let us add that the known *medial* design by Schupmann (1899) introduces to the layout in Fig. 1.6 a small field element (a lens or a simple mirror) that projects an image of the front lens onto a correcting element in the form of a meniscus mirror-lens (Baker 1954, Daley 1984).

The above concerns only a change in the axial position of the focus depending on the wavelength, i.e., the *longitudinal chromatic aberration* (longitudinal color). In catadioptric systems, there is also the *lateral chromatic aberration* (lateral color, or more strictly, *chromatic difference of magnification*), and all of the “colored” varieties of monochromatic aberrations, among which we will distinguish *spherochromatism*. The lateral color is caused by the dependence of the effective focal length on the wavelength. As a result, images in different wavelengths have a different transverse scale. In particular, images of stars stretch radially into colored stripes whose length grows to the edge of the field of view. Spherochromatism means the dependence of spherical aberration on the wavelength. All types of chromatic aberrations, more or less distinct in simple optical systems, are intertwined with each other in wide-field telescopes in a fanciful way.

Nowadays, the Hamiltonian approach has led to elegant wide-field telescopes with closely sized optical elements; a detailed discussion will be given in Sections 4.2.3, 4.2.4, and 4.3.4. From a practical point of view, the production and use of Hamilton systems is somewhat more complicated than systems that contain conventional mirrors. Simple consideration shows that the free surface of the Mangin element should be made twice as accurately as

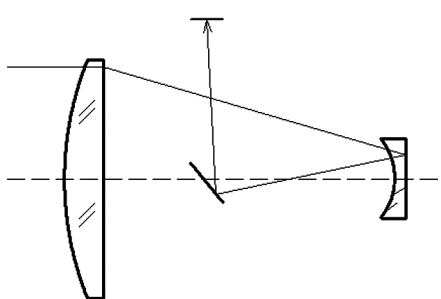


Figure 1.6 The W. F. Hamilton (1814) catadioptric system.

the surface of an ordinary lens, whereas the accuracy of the mirror's surface should be 6 times higher than the surface of the lens. This circumstance complicates the fabrication, but it also determines the tougher requirements for the temperature regime during both manufacturing and further operation.

In general, since most catadioptric telescopes have a high speed (low $f/\#$), the correction of longitudinal chromaticity, and especially spherochromatism, constitutes a challenging problem. This task is often placed upon either a purely lens-based portion of the system or shared between the two components by the Hamiltonian method. Both ways have their difficulties, so it is useful to bear in mind an old recipe, which was summarized by Maxwell (1972, Section 2.1) as follows:

By locating the focal power in reflecting surfaces and the aberration correction in refracting components, the effects of chromatic aberration may be minimized.

For example, both the Schmidt camera (Fig. 4.1) and the Richter–Slevogt system (Fig. 4.8) follow this rule. In the latter, a two-lens input corrector is essentially afocal, whereas a single lens in the Maksutov telescope (Fig. 4.7) has some optical power and as such needs to correct the spherical aberration of the primary mirror and compensate for its own chromatism simultaneously. For that reason, the two-lens corrector is better suited as a starting point for developing a wide field of view.

A good example of the potency of the described approach is an all-spherical system with a field of near-diffraction-quality images with an angular diameter of more than 45° (Terebizh 2016a). In particular, the four-lens corrector of one glass in the VT-119g model with a 30° field (Fig. 4.23) is nearly afocal ($f/44$), so chromatic aberrations are negligible.

1.3.5 Basic types of optical surfaces

Since the very first steps of optics, most optical surfaces have become conic sections. The reason for this is understandable, because it is the paraboloid that forms the perfect axial image of a distant star. Then the ellipsoid (in the Gregorian system) or the hyperboloid (in the Cassegrain system) transfers this image into a more convenient place while increasing the focal length.

The corresponding type of surfaces became *standard* in optical calculation programs. The equation of a conic section that has rotational symmetry about the z axis is

$$r^2 = 2R_0z - (1 + b)z^2, \quad (1.10)$$

where $r = (x^2 + y^2)^{1/2}$ is the radial coordinate, R_0 is the paraxial radius of curvature, and the conic constant $b = -\epsilon^2$ is the negative squared eccentricity. It is suitable in optical ray tracing to solve Eq. (1.10) with respect to the surface sag z , so a standard surface is defined by

$$z = \frac{r^2/R_0}{1 + \sqrt{1 - (1 + b)(r/R_0)^2}}. \quad (1.11)$$

The scarcity of the set of conic sections became increasingly clear as the field of view expanded, so a polynomial in the radial coordinate was added to the sag representation by Eq. (1.11). For example, an *even asphere* surface is defined as follows:

$$z = \frac{r^2/R_0}{1 + \sqrt{1 - (1 + b)(r/R_0)^2}} + \alpha_1 r^2 + \alpha_2 r^4 + \dots + \alpha_N r^{2N}. \quad (1.12)$$

In addition to the basic version, there are dozens of surface types in the developed programs of optical calculations. These surfaces are quite useful in practice, but limitations are apparent when we enlarge the system's aperture, speed, or the field of view. A power series slowly converges to a desired function (see, e.g., Lanczos 1988, Chapter 7; Press et. al. 1992, Section 5.1). In optics, we seek the most accurate approximation of a (maybe unknown) theoretically optimal surface profile, so we are greatly interested in a quickly converging series. Meanwhile, the convergence of the power series representation (Eq. (1.12)) is especially slow for the fast optical systems with a large aperture because it deals with powers of the ratio r/R_0 , which is not particularly small near the edge of an aperture.

For these reasons, we can use another polynomial approximation to attain the higher speed of convergence, namely,

$$r^2 = 2R_0 z - (1 + b)z^2 + a_3 z^3 + a_4 z^4 + \dots + a_N z^N. \quad (1.13)$$

The coefficients (a_3, a_4, \dots, a_N), along with R_0 and b , define a polynomial representation of a surface in the sag z but not in the radial coordinate r . Even for fast surfaces, we usually have $z \ll r$, so the **polynomial** expansion in the **sagitta** (*polysag*) is expected to converge more quickly than the series in Eq. (1.12). Besides, the direct extension of Eq. (1.10) in powers of the sag appears to be a more logical approach than adding a series in r powers to its solution with respect to the sag.

The generalization of the basic class of conic sections in the form of Eq. (1.13) has been known for a long time (see, e.g., Rusinov 1973), but as far as we know, it had never been applied systematically in optical design. For these reasons, the polysag surface type was added to the user-defined surfaces in ZEMAX (Terebizh 2008), so it becomes possible to use new surfaces with reflective and refractive optics.

The aspheric surface is usually tested with the help of an auxiliary optical device, a *null-corrector* (also called a *compensator*), which transforms the

reflected wavefront of the complicated form into the spherical wavefront (Wilson 1999, Section 1.3.4; Terebizh 2014). Since the null-corrector for a polysag surface would be designed in the same way as for a habitual asphere, the manufacturing of the polysag surfaces should not hold any surprises.

An example of the use of polysag surfaces will be given in Section 2.3.1. Of course, the properties of these surfaces deserve further study.

1.4 Matching of Optics and Detector with Atmospheric Image Quality

The practice of designing various telescopes shows that the desired optical layout essentially depends on the initial and final factors, i.e., the problems being solved and the given detector of light. The latter may seem less important, but keep in mind the importance of matching the resolving power of optics with that of the detector. Besides, the limited size of the detector often dictates the focal length of the telescope, and thus its speed and the optical layout itself. Finally, the optical layout of the wide-field telescope cannot be chosen independent of the supposed shape of the surface of the detector.

1.4.1 Detectors of light

Many publications are devoted to charge-coupled devices (CCDs) in optical astronomy, in particular, the *Handbook of CCD Astronomy* by Howell (2000); a later ESO Workshop *Detectors for Astronomy* (Oct. 2009) is also informative. Thus, it is inappropriate to discuss the topic extensively in this text. However, for proper matching of resolutions, the following typical characteristics of detectors should be taken into account:

- The spectral range. In wide-field observations, the designs are limited usually by the bandpass of the filters *g* (0.40–0.55 μm), *r* (0.56–0.69 μm), and *i* (0.69–0.82 μm). Regarding the optical calculations, the expansion of the waveband to the blue region is fraught with difficulties both in the selection of glass and the increase in the dispersion of light. Both difficulties are significantly mitigated when moving to the infrared region.
- The pixel size p . In detectors for wide-field observations, the most popular values are $p \simeq 9\text{--}15 \mu\text{m}$. Smaller values reduce the pixel's *full well capacity* (see below), whereas larger values impair resolution.
- The detector format, i.e., the number of pixels and the detector linear dimensions on both coordinates. In single-chip flat CCD detectors, the range for a format extends from 4096×4096 to 10560×10560 (STA1600) pixels. For a 9-micron pixel, this corresponds to linear dimensions of $36.9 \times 36.9 \text{ mm}$ and $95.2 \times 95.1 \text{ mm}$, respectively; the

corresponding diagonal lengths are 52.1 mm and 134.5 mm. In calculations, detectors are usually assumed to be inscribed into the circular field of view of the telescope. Obviously, the dimensions of composite detectors can be very large. For example, in a DECam system with a 4.0-m aperture and a 2.2° field, a detector consisting of $15\text{-}\mu\text{m}$ pixels has a 45-cm diameter (Section 3.1.3). The linear diameter of the field of view of the Subaru Hyper Suprime Camera is 50 cm; it is even larger (64 cm) on the LSST.

- The *quantum efficiency* (QE) of the detector as a function of the wavelength, i.e., the average number of photo-events that one photon of a given wavelength causes. QE is noticeably different for the *front-illuminated* and *back-illuminated* CCDs. For the former, the peak QE is usually in the range of 55–60%, while for the latter it can reach 90% and even higher. For example, the QE of the E2V CCD 230-42 is 92% at $0.60\ \mu\text{m}$; the QE of the large-format STA1600 CCD is 87% at $0.60\text{--}0.65\ \mu\text{m}$.
- The full well capacity (FWC), i.e., the maximum number of events that a pixel can accumulate. Typically, the FWC of CCDs is in the range $(0.80\text{--}5.0) \times 10^5$ events. The larger the FWC is, the greater the dynamic range and the better the linearity of the detector.
- The dark current (DC), i.e., the average output signal in one pixel per hour at zero illumination. The dark current consists mainly of electrons thermally generated within the semiconductor material. For good back-illuminated CCDs, DC is less than 1 event/pixel/hour.
- The read-out noise, i.e., the random noise from the detector output stage in the absence of signal. A good value is considered to be several events (RMS) per reading.

So far we have only dealt with detectors of the CCD type. There are nearly the same CMOS-type (complementary metal-oxide semiconductor) light detectors, but they only recently began to compete with CCDs. Previously, CMOS detectors were too small, and they had insufficiently high quantum efficiency and unstable noise compared to scientific CCDs, but they read charge faster and had lower average readout noise. All mentioned shortcomings have been overcome now to a large extent, while preserving the merits (Zimmer, McGraw, and Ackermann 2016). In general, modern CCD and CMOS detectors have similar characteristics, so the choice of the detector depends on the specific problem being solved.

The present-day wide-field systems for telescopes of moderate and large size would be impossible without the rapid development of mosaic CCD technology. The latter provides a fairly quick reading of information from a set of CCDs with a total size of up to 1 m, whereas the gaps between the individual chips are negligible.

It is also worth adding that modern image detectors require a significant *back focal length* (BFL) for the telescope's optics, i.e., the distance from the

last optical surface to the light detector, especially accounting for the filter wheel, the focusing device, and the shutter. For wide-field telescopes with a moderate aperture, this can become a serious problem, the standard solution for which involves Newtonian or Cassegrainian image transfer outside the telescope tube.

1.4.2 Sampling factor

According to the Fourier theorem, almost every function can be represented as a superposition of harmonic oscillations of different frequencies, taken with due weight. If we are talking about a function of time, then the corresponding time frequency ν (cycles/sec) is inversely proportional to the time period of the harmonic oscillations. Similarly, the spatial frequency is defined as $f = 1/P$, where P is the period of the spatial harmonic of the function being studied, say, the image brightness distribution. Accordingly, the dimension of f is the number of cycles per unit length, usually cycles/mm.

The distributions encountered in practice often either do not change at a space scale smaller than some limit value a or high-frequency variations are not of interest. In other words, the spatial frequencies of real distributions are usually bounded from above by the value of the *cutoff frequency* $f_c \equiv 1/a$; such distributions are classified as the *functions of a bounded spectrum*.

Figure 1.7(a) shows a monochromatic distribution of brightness in the image of a star, i.e., the *point spread function* (PSF), which was obtained using the perfect paraboloid at zero vignetting of light. For ideal conditions, such as shown here, the PSF is called the *Airy pattern*. The radius of the central peak, known as an *Airy disk*, is $r_A \simeq 1.44\lambda\phi$, where λ is the wavelength, and $\phi \equiv F/D$ is the focal ratio; $r_A \simeq 2.9 \mu\text{m}$ in this case. The Airy disk includes about 84% of all energy in the image of a point light source; thus, an Airy diameter of $2r_A$ is close to D_{80} . The spatial spectrum of the PSF, which is called the *modulation transfer function* (MTF), is identically equal to zero at frequencies above 500 c/mm in this example [Fig. 1.7(b)].

The last property is not an exception (Born and Wolf 1999, Section 9.5.2). The spatial spectrum of any, even perfect, optical system is bounded from above by the cutoff frequency

$$f_c = 1/(\lambda\phi), \quad (1.14)$$

i.e., of about the inverse Airy radius.¹⁰ The reason for the strict cutoff of frequencies in optical systems is the diffraction of light, that is, due to its wave nature. Thus, when considering optical images, the minimum scale is $a = \lambda\phi$, and the cutoff frequency is $f_c = 1/a$. In the above example, we had $\lambda = 0.5 \mu\text{m}$ and $\phi = 4.0$, so $f_c = 500 \text{ c/mm}$.

¹⁰ If the wavelength is measured in microns, then f_c (cycles per mm) is $1000/(\lambda\phi)$.

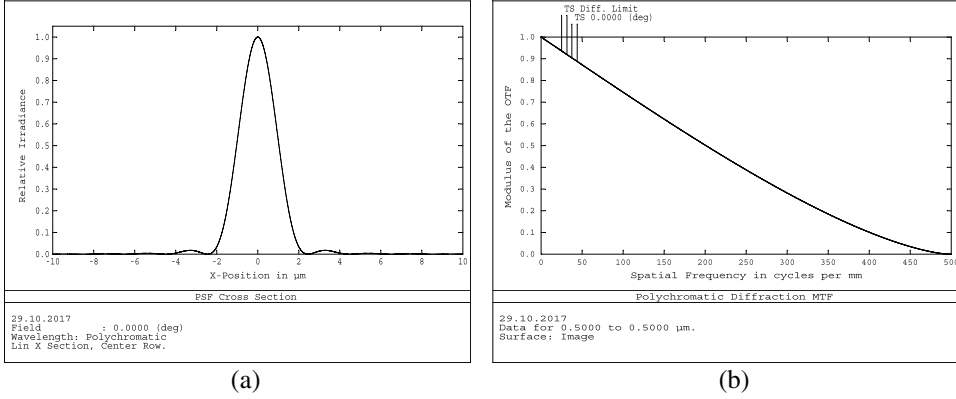


Figure 1.7 (a) Cross-section of a PSF formed by perfect paraboloid (diameter = 1 m, focal length = 4 m) in monochromatic light with a wavelength of 0.5 μm . (b) Spatial spectrum of the PSF.

The continuous distributions are an idealization. In practice, we are dealing with discrete samples, most often made with some constant step δx . This leads to the appearance of a second characteristic frequency, called the *Nyquist frequency*:

$$f_{Ny} \equiv 1/(2 \cdot \delta x). \quad (1.15)$$

Comparative values of the two characteristic frequencies f_c and f_{Ny} determine the quality of the picture obtained as a result of the sampling of a continuous distribution.

According to the *sampling theorem* by E. Whittaker, V. Kotel'nikov, and C. Shannon (see, e.g., Press et al. 1992, p. 500), to completely restore a function of a bounded at some cutoff frequency f_c spectrum, the following condition must be met:

$$f_{Ny} \geq f_c, \quad (1.16)$$

or, equivalently, the sampling step

$$\delta x \leq 1/(2f_c) = a/2. \quad (1.17)$$

It is said sometimes that for a complete reconstruction of a function, the *sampling frequency* $f_s \equiv 1/\delta x = 2f_{Ny}$ must at least double the cutoff frequency. In optics, Eq. (1.17) takes the form

$$\delta x < \lambda\phi/2. \quad (1.18)$$

In the context of astronomical observations, sampling is specified by the pixel size p , so that the Nyquist frequency $f_{Ny} = 1/(2p)$, and Eq. (1.18) requires

that $p \leq \lambda\phi/2 \simeq r_A/2$: the pixel should be less than about half the Airy radius. It is more convenient to write this inequality as

$$r_A/p \geq 2. \quad (1.19)$$

Images in telescopes, especially in wide-field ones, are by no means always diffractive. As said previously, the value of θ_{tel} characterizes the image quality provided by a telescope alone. Usually, it varies from about $0.5''$ up to a few arcsec, i.e., has the same order of magnitude as the typical atmospheric blurring θ_{atm} . For our purposes, it is enough to accept that the angular diameter of a star image due to these two factors is

$$\theta = \sqrt{\theta_{atm}^2 + \theta_{tel}^2}. \quad (1.20)$$

After setting the image quality, it is reasonable to generalize the above Eq. (1.19) as follows:

$$\chi \equiv \theta/p \geq 4, \quad (1.21)$$

where the ratio χ of the diameter of the star image to the pixel size is called the *sampling factor*. Thus, one usually should have at least 4 pixels covering the diameter of a star image. Taking into account random fluctuations of the light flux, this value is usually increased to 8 for precise photometric measurements (e.g., $\chi \simeq 7$ for the Kepler space telescope). On the other hand, for surveys where detecting faint objects is of primary importance, the sampling factor is reduced to 1–2.

For the design VT-056y that used as an example in Section 1.1.4 (Fig. 1.1), $\theta_{atm} = 1.5''$, $\theta_{tel} = 0.65''$, $p = 0.85''$, so $\theta = 1.63''$, and $\chi = 1.9$. Hence, the design is well suited to searching or exploratory observations.

Naturally, if the condition in Eq. (1.21) is violated, i.e., pixels are too rough, the object's image is irreversibly smoothed. In the frequency domain, this means that the spatial spectrum located above the Nyquist frequency is superimposed on the low-frequency region; this phenomenon is called *aliasing*.

In addition to sampling, further smoothing is caused by averaging over the pixel's area. The last factor is formally reduced to multiplying the original spectrum by $\text{sinc}(pf)$, where the known function

$$\text{sinc}(z) \equiv \sin(\pi z)/(\pi z), \quad -\infty < z < \infty. \quad (1.22)$$

The first positive zero of function $\text{sinc}(pf)$ is at the frequency $f_{01} = 1/p$, so that smoothing due to the finite pixel size becomes significant at a frequency twice the Nyquist frequency.

Chapter 2

Reflective Telescopes

The area of research named in this chapter is well investigated and covered by a number of monographs, in particular, the classic books of Danjon and Couder (1935), Dimitroff and Baker (1945), and modern studies by Schroeder (2000), Wilson (1996), and Korsch (1991). Therefore, we confine our discussion to brief general remarks and give basic calculation formulas for two-mirror systems.

Undoubtedly, it would be easiest to observe at the focus of a single concave mirror, and this was the first operating model of a reflecting telescope, made by Isaac Newton (1643–1727) around 1668 (presented to the Royal Society in 1671). Observations by William Herschel (1738–1822) and William Parsons (Earl of Rosse, 1800–1867) at the prime focus of a large parabolic mirror laid the foundations of modern astronomy. Unfortunately, the field of view of a single mirror is strongly limited by off-axis aberrations, primarily coma (Section 2.1). Thus, for two centuries two-mirror telescopes were the main observation tools.

By themselves, two-mirror telescopes without additional optical elements (Section 2.2) do not provide a wide field of view in the sense discussed in Section 1.1.2. There are simply too few degrees of freedom in a two-mirror system, that is, parameters that determine the shape of mirrors and their spacing. However, the two-mirror systems serve as the basis for numerous advanced telescopes, so understanding their properties is important.

A purely reflective Schmidt camera, using a mirror corrector instead of a transparent corrector plate, would be very attractive to observers, but it faces all of the difficulties common to off-axis systems. Nevertheless, the recently implemented LAMOST system (Wang et al. 1996, Zhao 2012) allows us to hope for a wider distribution of mirror Schmidt cameras as the technology develops.

Only three-mirror, purely reflective systems have sufficient degrees of freedom to provide a field of view larger than about 1° (Section 2.3). Of the many existing axisymmetric systems, we distinguish the designs by Maurice Paul (1935) and Dietrich Korsch (1972, 1977, 1980), as their development has become firmly embedded in modern practice. In addition, Appendix F

presents a new simple algorithm for calculating anastigmatic three-mirror telescopes.

In recent decades, a number of axisymmetric anastigmatic four-mirror solutions were found (see Wilson 1996 for references). It seems that the size of the field of view attained in these designs does not justify the complexity of the mirror surfaces and the whole system. The problem of light vignetting, generally a challenge in axisymmetric, purely reflective optics, becomes practically unsolvable for wide-field systems as the number of mirrors increases.

This last reason prompted opticians to look for off-axis mirror systems, which were subsequently designed (Owen 1990; Wilson 1996, Section 3.7). However, until now the manufacture of off-axis wide-field telescopes was hampered by technological problems and tight tolerances for positional and optical parameters.

2.1 Single Paraboloid

As mentioned earlier, the field of view of a single mirror is limited primarily by the coma. The emergence of coma is due to two factors: the difference in the magnifications of the axial and external zones of the optical system, as is the case with spherical aberration (Fig. 1.5), and the axial symmetry breaking of a wide oblique light beam. According to the theory of coma (Plummer 1902; Wilson 1996, Eq. (3.199)), the length of the comatic star's image in arc seconds is

$$\theta'' = \frac{45}{4\phi^2} w', \quad (2.1)$$

where $\phi \equiv |F|/D$ is the focal ratio of a mirror, and w' is the field angle in arc minutes. Equation (2.1) is valid for mirrors of both parabolic and spherical shape. In the latter case, there is also a spherical aberration, so we will leave it aside. Assuming $\theta \leq 1''$, we get the following estimate for the paraboloid's field diameter, within which the image of a star does not exceed 1 arcsec:

$$2w'(\theta \leq 1'') = \frac{8}{45} \phi^2 \simeq 0.178\phi^2. \quad (2.2)$$

Thus, the size of the field of view due to coma increases in proportion to the square of the focal ratio, but the proportionality factor in Eq. (2.2) is too small to achieve an acceptable field size for a compact telescope.

The following will use the simplified notation $2w(1'')$ instead of $2w(\theta \leq 1'')$. Figure 2.1 illustrates Eq. (2.1) in the case of an $f/4$ paraboloidal mirror. As can be seen, the size of the comatic image increases linearly with the increasing field angle, and the proportionality coefficient is close to $45/64 \simeq 0.70$, which occurs under the given conditions. The prediction $2w(1'') \approx 3'$ of Eq. (2.2) is also in agreement with analytical calculations.

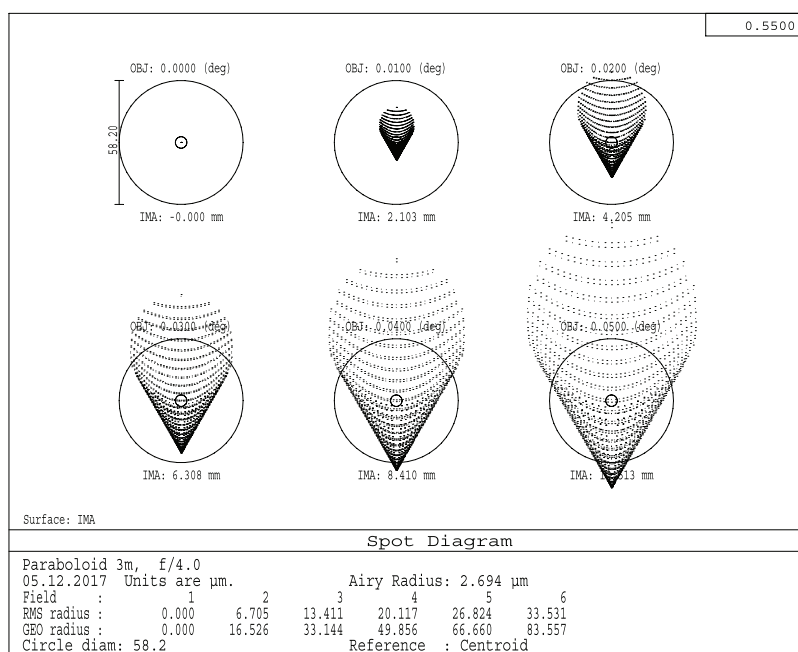


Figure 2.1 Spot diagrams at a wavelength of 0.55 μm for a 3-m, $f/4$ paraboloid. A large circle of diameter 58.2 μm corresponds to 1", and the small circle to the diffraction Airy disk. Diagrams are shown for the optical axis and field angles of 0.6', 1.2', 1.8', 2.4', and 3.0'.

Although other aberrations begin to appear as the field size increases, coma remains the dominant factor, which substantially limits the use of the prime focus of telescopes. Thus, we are forced to explore systems with two or more mirrors to achieve at least a moderate field.

2.2 Two-Mirror Systems

In the middle of the 17th century, lens telescopes with acceptable chromaticity became too long, so Marin Mersenne (1588–1648) proposed in 1636 a compact, purely specular telescope. Namely, he suggested to look through a small hole in a concave parabolic mirror to a similar smaller mirror. The foci of mirrors were assumed to be coincident, and thus the Mersenne telescope was afocal.

The idea of James Gregory (1638–1675), described in his book *Optica Promota* (1663), was to combine the focus of the paraboloid with one of the ellipsoid foci in order to transfer the image of a star to another ellipsoid focus located more conveniently (Fig. 2.2). Similarly, Laurent Cassegrain (1629–1693) suggested in 1672 using a convex hyperbolic secondary mirror instead of a concave ellipsoidal secondary, which further compacted the telescope (Fig. 2.3).

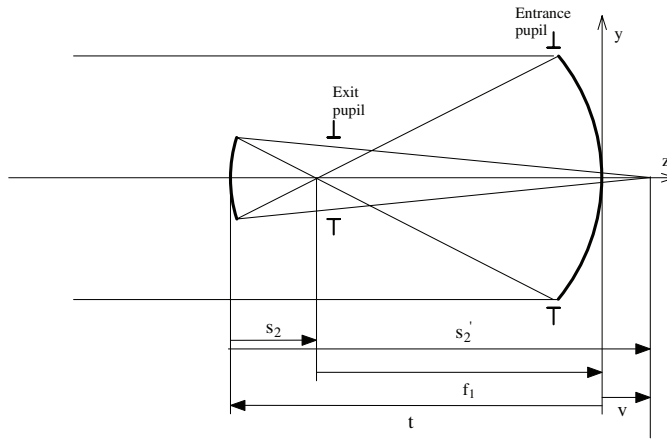


Figure 2.2 Optical layout of the Gregorian telescope. Positive variables are indicated by arrows pointing to the right, and negative by arrows pointing to the left. The Mersenne system responds to a parallel outgoing beam of light.

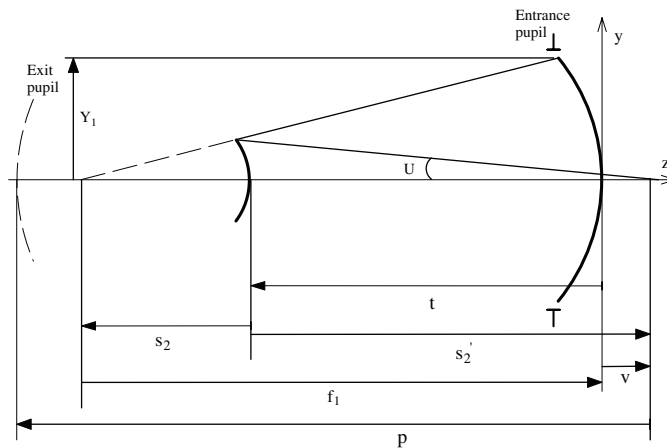


Figure 2.3 Optical layout of the Cassegrain telescope. Positive variables are indicated by arrows pointing to the right, and negative by arrows pointing to the left. The Mersenne system responds to a parallel outgoing beam of light.

The development of the theory of two-mirror systems consistently reflects the prolonged efforts of astronomers and opticians to expand the field of view of telescopes. The result of these efforts is quite impressive: the size of the field with good images has increased from a few angular minutes per order of magnitude (King 1955, Schroeder 1993, Wilson 1996).

2.2.1 Basic relations

To set the geometric configuration of a two-mirror telescope, irrespective of its system, several initial parameters have to be selected. Following Maksutov

(1932, 1946), we choose as such the telescope aperture size D , the equivalent focal length F , and two dimensionless ratios:

$$q \equiv -s_2/f_1, \quad \beta \equiv -s_2/s'_2, \tag{2.3}$$

where f_1 is the focal length of the primary mirror (as usual, we assume $f_1 = -R_1/2 > 0$ for a concave mirror with a paraxial radius of curvature $R_1 < 0$), s_2 is the spacing between the secondary mirror and the primary focus, and s'_2 is the spacing between the secondary mirror and the system focus ($s'_2 > 0$). Figures 2.2 and 2.3 illustrate the ordinary sign convention for the Cassegrain and Gregorian telescopes, whereas Fig. 2.4 gives an idea of the configurations of all possible two-mirror systems.

To explain the meaning of the entered parameters, note that $|q| = D_2^{(0)}/D \equiv \eta$ is the linear obstruction ratio for the incident axial beam, and β is the inverse magnification $m = F/f_1$ of the secondary. Thus, the basic parameters can also be determined by the following formulas:

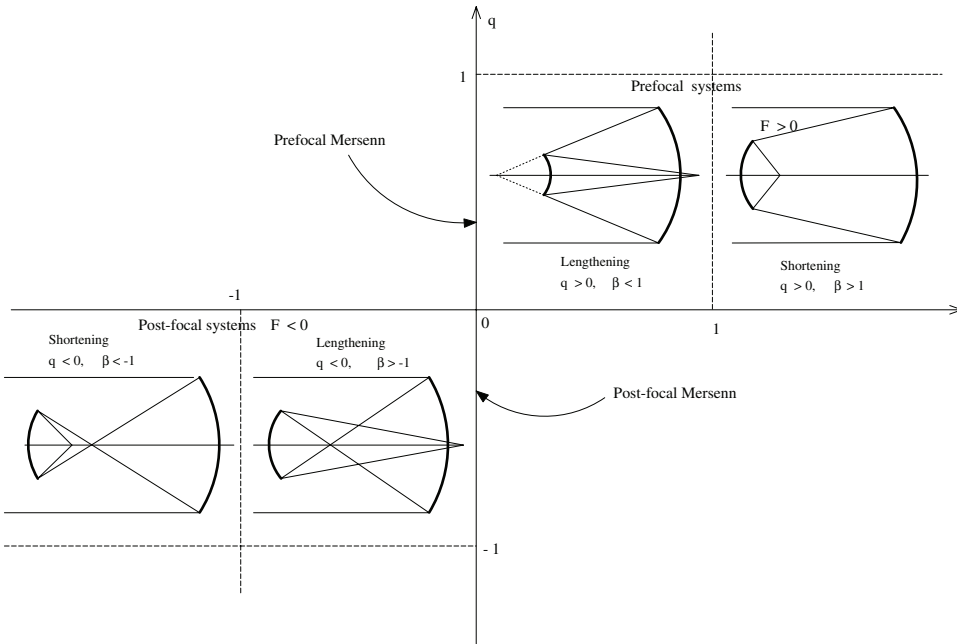


Figure 2.4 Schematic representation of two-mirror telescopes on the Maksutov diagram. First and third quadrants correspond to systems in which the secondary mirror is located, respectively, before the primary focus and behind it; two other quadrants correspond to systems with virtual images. Further subdivision of systems is determined by whether the focal length of the primary mirror is lengthened or shortened by the secondary mirror. Mersenne systems correspond to the $\beta = 0$ axis.

$$q = s'_2/F, \quad \beta = f_1/F. \quad (2.4)$$

We have $F > 0$, $0 < q \leq 1$, $0 < \beta \leq 1$ for a Cassegrain system, and $F < 0$, $-1 < q \leq 0$, $-1 < \beta \leq 0$ for a Gregorian (Fig. 2.4). As one can see, q and β always have the same signs for telescopes with real images. The corresponding conditions for a Mersenne system are $-1 < q < 1$ and $\beta = 0$, so $F = \infty$ while $\beta F = f_1$.

Given the set $\{D, F, q, \beta\}$, all other parameters of the two-mirror telescope can be written as follows:

The equivalent focal ratio

$$\phi = |F|/D; \quad (2.5)$$

the distance from the secondary mirror to the prime focus

$$s_2 = -q\beta F; \quad (2.6)$$

the distance from the secondary mirror to the system focus

$$s'_2 = qF; \quad (2.7)$$

the paraxial radius of curvature of the primary mirror

$$R_1 = -2\beta F; \quad (2.8)$$

the paraxial radius of curvature of the secondary mirror

$$R_2 = -\frac{2q\beta}{1-\beta}F; \quad (2.9)$$

the spacing between mirrors

$$t = -(1-q)\beta F; \quad (2.10)$$

and the distance between the primary vertex and the system focus

$$v = [q - (1-q)\beta]F. \quad (2.11)$$

Most often, the aperture stop of the system coincides with the frame of the primary mirror; however, it is of interest the case when the distance ζ between these elements is positive. Then the distance from the system focus to the exit pupil is

$$p = -\frac{qF}{1 - (1-q)\beta - q\zeta/F}, \quad (2.12)$$

and the exit pupil diameter

$$D_p = |p|/\phi = \left| \frac{q}{1 - (1 - q)\beta - q\zeta/F} \right| D. \quad (2.13)$$

Sometimes a different arrangement of the aperture stop is used, in particular, on the frame of the secondary mirror.

Using the above equations, it is not difficult to find various relations between the parameters of the telescope, e.g., $1/F = -2/R_1 + 2/R_2 - 4t/(R_1 R_2)$, $R_2 = qR_1/(1 - \beta)$, etc. Among them, we give only the frequently used relation

$$\left. \frac{\partial v}{\partial t} \right|_{R_1, R_2} = 1 + m^2, \quad (2.14)$$

which allows us to find the change in the image offset v as the mirror spacing t changes (note that v and t have opposite signs, and $m = 1/\beta$).

Curiously, a two-mirror analogue of the ‘ideal’ Strehl telescope exists (see Section 1.3.3). Namely, a two-mirror telescope will acquire complete point symmetry if we require that the mirrors be concentric and place an aperture stop at the common center of curvature. As Eq. (2.12) shows, the exit pupil of the resulting system is also located at the center of symmetry when $\zeta = -R_1$. Herewith, the images are the same in a wide field of view, but as in the ‘ideal’ telescope, they are spoiled by spherical aberration. Subsequent optimization improves the image quality significantly, but the system remains too long.

The convenience of Maksutov’s choice of initial parameters is largely due to the fact that a simple representation exists in the plane (q, β) not only for the so-called *lengthening* Gregorian and Cassegrain telescopes described above but also for the *shortening* systems (see Fig. 2.4). These terms have arisen because systems with $|\beta| = 1/|m| = |f_1/F| < 1$ increase the absolute value of the equivalent focus in comparison with the focus of the primary mirror, while the systems with $|\beta| > 1$ shorten it. Figure 2.4 shows a general diagram of two-mirror configurations in the (q, β) -plane, with mirrors not only in the form of a conic section but also with an arbitrary shape.

2.2.2 Classical telescopes: Mersenne, Gregorian, and Cassegrain

The above formulas describe only the geometric configuration of any two-mirror system, whereas the shape of the mirrors remains arbitrary. In general, it is determined by the requirement of proper image quality in a sufficiently wide field of view.

By definition, *classical two-mirror telescopes* are those for which the primary mirror has the form of a paraboloid, while the secondary one is an ellipsoid, for a Gregorian system, or hyperboloid, for a Cassegrain system (see, e.g., Schroeder 2000, p. 62; Wilson 1996, p. 86). Within the framework of the theory of third-order aberrations, a classical telescope is specified by two

conditions relating to the axial images of a star: (i) spherical aberration is corrected at the prime focus, and (ii) spherical aberration is corrected at the secondary focus, that is, of the entire system.

Obviously, these requirements are of a limited nature: only the third order of the theory of aberrations is taken into account, the images are considered only on the optical axis, and only spherical aberration is considered. It was the consistent rejection of these limitations that led to progress in the performance of two-mirror systems.

The two above requirements lead to the following relations for the conic constants¹ of the primary and secondary mirrors of the classical telescope:

$$b_1 = -1, \quad b_2 = -\left(\frac{1 + \beta}{1 - \beta}\right)^2. \quad (2.15)$$

Thus, for the prefocal systems (when $\beta > 0$), the secondary mirror is a hyperboloid, whereas for the postfocal systems it has the shape of an ellipsoid. The latter becomes a sphere when $\beta = -1$.

The image quality provided by a classical telescope has been deeply studied analytically within the framework of aberration theory, and this book does not repeat the known results. The most important conclusion is that the size of the comatic image is exactly the same as for a single paraboloid, i.e., it is given by Eq. (2.1). Accordingly, the field of view, within which the size of a star image is less than 1 arcsec, $2w(1'')$, does not usually exceed $10'$. This problem became particularly challenging after the creation of large classical telescopes up to the 5-m Palomar reflector in the middle of the 20th century. It prompted the search for two-mirror systems free of both spherical aberration and coma, i.e., *aplanats*.

2.2.3 Approximate aplanatic telescopes: Schwarzschild, Ritchey–Chrétien, and Gregory–Maksutov; Hubble Space Telescope

As stated above, the shape of mirrors in a classical telescope is specified by requirements to correct spherical aberration in both the prime and secondary focal points of the telescope. In this case, the remaining aberrations (and above all, the most harmful for the expansion of the field, coma) remain uncompensated. The idea of Karl Schwarzschild (1873–1916), expressed by him at the beginning of the 20th century, was to allow spherical aberration at the prime focus but eliminate both spherical aberration and coma at the secondary focus, i.e., implement an *aplanatic* two-mirror telescope. For this, an additional degree of freedom appears: the eccentricity of the primary mirror. If observations at the primary focus also have significance, then a suitable lens corrector can be installed.

¹ That is, the squares of eccentricities, taken with the opposite sign: $b_1 = -\epsilon_1^2$, $b_2 = -\epsilon_2^2$.

According to modern concepts, it is appropriate to call *approximate aplanats* optical systems in which spherical aberration and coma are eliminated only within the framework of the theory of third-order aberrations. The general analytic theory by Schwarzschild (1905) not only provides for the correction of the third-order coma but also proposes a deeper consideration based on the known *sine condition* (Hecht 1998, Section 6.3). As long as observations with low-sensitivity photographic plates required fast telescopes, Schwarzschild focused on the so-called *shortening prefocal aplanat* in the region $q > 0, \beta > 1$ (see Fig. 2.4). We will discuss Schwarzschild’s approach in the next section, but for the present note that this theory can be extended to the whole (q, β) -plane.

After the untimely death of Schwarzschild, one of the most outstanding researchers in the history of astronomy, his studies remained incomplete. A special case of his general theory for not-too-fast (when $\phi \gg 1$) lengthening prefocal systems in a region $q > 0, \beta < 1$, was clarified by Henry Chrétien (1879–1956), who initiated George Ritchey (1864–1945) to make the first such telescope (Chrétien 1922, Ritchey and Chrétien 1927). All other aplanatic systems of the third order, namely, postfocal systems with $\beta < 0$ and $\phi \gg 1$ (Fig. 2.4), were first found by Dmitry Maksutov (1896–1964).²

To avoid misunderstandings, the classification of two-mirror approximate aplanats is summarized in Table 2.1. In all of these systems—Ritchey–Chrétien, Schwarzschild and Maksutov—the mirrors are conic sections, which are characterized by the following conic constants:

$$b_1 = -1 - \frac{2q\beta^2}{1-q}, \quad b_2 = -\left(\frac{1+\beta}{1-\beta}\right)^2 - \frac{2\beta^2}{(1-q)(1-\beta)^3}. \quad (2.16)$$

Recall that the parameters q and β are defined by Eq. (2.3). A comparison of the last expressions with those in Eq. (2.15) shows that the aplanatism of the system is due to the appearance of the second terms in Eq. (2.16).

Table 2.1 Types of two-mirror aplanats.

System	Lengthening	Shortening
Prefocal $F, q, \beta > 0$	RC $0 < \beta < 1$	Schwarzschild $\beta > 1$
Postfocal $F, q, \beta < 0$	Maksutov $0 < \beta < 1$	$ \beta > 1$

² In his reports of 1924, Maksutov described aplanatic systems in the entire (q, β) -plane unaware of the Schwarzschild and Chrétien investigations, but he succeeded in publishing his studies only eight years later (Maksutov 1932).

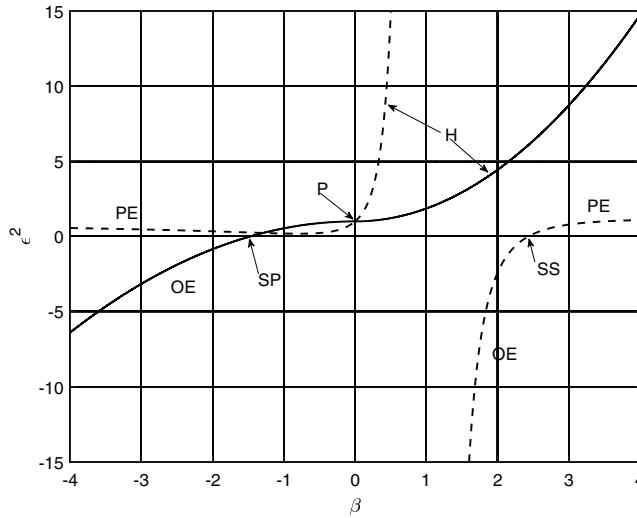


Figure 2.5 Squares of eccentricities of the primary (solid line) and secondary (dashed lines) mirrors versus β for aplanatic telescopes at $|q| = 0.30$. Notation is as follows: P – paraboloid, H – hyperboloid, PE – prolate ellipsoid, OE – oblate ellipsoid, SP – spherical primary mirror, and SS – spherical secondary mirror.

Figure 2.5 gives an idea concerning the types of optical surfaces of aplanatic two-mirror telescopes according to Eqs. (2.16). A detailed discussion of the related issues, including the manufacturing, was given by Maksutov (1932; 1946, Section 21), Wetherell and Rimmer (1972), Wilson (1996, 1999), and Schroeder (2000).

The first large RC telescope was an 84-inch (213.4-cm) reflector at the Kitt Peak National Observatory, which entered operation in 1964.

Table 2.2 provides a summary of the parameters for another known RC system, the Hubble Space Telescope (Burrows 1990, p. 25). This list can be also considered as a control example for the whole set of equations outlined above for two-mirror telescopes. Note the large equivalent focal distance, which provides sufficient scale at the focal surface for the set of auxiliary devices, and the corresponding choice of small q and β parameters in order to compensate for a large F and thereby achieve an acceptable telescope length and negligible obstruction of incident light.

In the context of this book, the most interesting question is how much aplanatism allows for the expansion of the field of view of the two-mirror telescope. Since third-order spherical aberration and coma are eliminated in aplanatic telescopes, the size of the field is determined by astigmatism and curvature of the focal surface. As is known (see, e.g., Hecht 1998, p. 266), the best astigmatic images are formed on the *surface of medium curvature*, where they take the form of so-called *circles of least confusion*. Simple calculations

Table 2.2 Parameters of the Hubble Space Telescope.

Initial Parameter	Value	Calculated Parameter	Value
D	2400.0 mm	ϕ	24.000
F	57599.859 mm	s_2	-613.929 mm
q	0.111219023	s_2'	6406.200 mm
β	0.095833569	t	-4906.071 mm
		R_1	-11040.000 mm
		R_2	-1358.000 mm
		v	1500.129 mm
		p	-7002.651 mm
		D_p	291.778 mm
		b_1	-1.002299
		b_2	-1.496860

that we omit give the following expression for the radius of this surface in approximate two-mirror aplanats:³

$$R_m = -\frac{q\beta F}{\beta + (1 - q)(1 - \beta^2)}, \tag{2.17}$$

while the angular size of astigmatic spots in the medium surface is

$$\theta = \frac{w^2}{4\phi} \left| \frac{2 - (1 - q)\beta}{q} \right|, \tag{2.18}$$

where θ and the field angle w are measured in radians. Note the simplicity of these relations written in Maksutov's variables. The limiting diameter of the field, within which the astigmatic image of a star is less than 1", follows from Eq. (2.18) when $\theta = 1/206265$:

$$2w(\theta \leq 1'') \simeq a(q, \beta)\sqrt{\phi}, \tag{2.19}$$

where the field angle is measured in arc minutes, and the function

$$a(q, \beta) \equiv 30'.28 \left| \frac{q}{2 - \beta(1 - q)} \right|^{1/2}. \tag{2.20}$$

The contour map of the function $a(q, \beta)$ for prefocal systems is shown in Fig. 2.6.

First of all, after the quadratic dependence on ϕ due to coma has been eliminated, the size of the field increases slowly with increasing focal ratio, in proportion to $\phi^{1/2}$ [compare Eq. (2.19) with Eq. (2.2)].

³ The corresponding equation for a classical telescope differs from Eq. (2.17) only by a factor of 2 before β^2 .

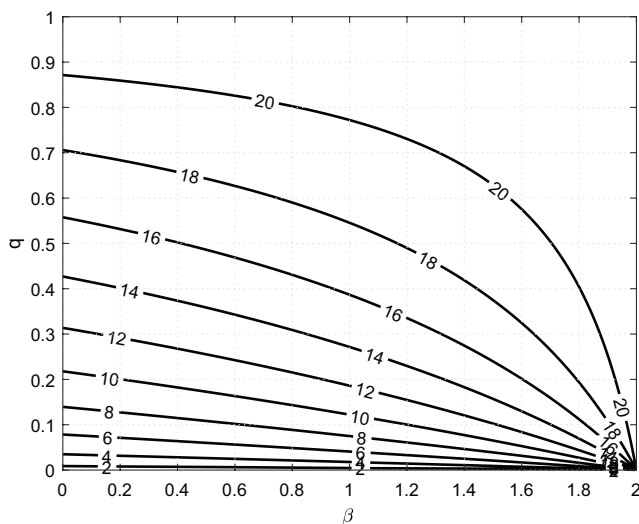


Figure 2.6 Contour map of the function $a(q, \beta)$ (arcmin) according to Eq. (2.20) in the region of prefocal Cassegrain and Schwarzschild systems.

As for the dependence on the parameters (q, β) , the Cassegrain type is more preferable compared to the Schwarzschild version. Generally, the small β (large magnification on the secondary mirror) and large axial obstruction ratio q are more advantageous for the extension of the field, but the second option is evidently limited by q values of about 0.3–0.5. Thus, a simple estimate is often sufficient for the subsecond field diameter of a typical RC telescope (Terebizh 2005b, p. 21):

$$2w(\theta \leq 1'') \simeq 12' \sqrt{\phi} \quad (2.21)$$

Again, at typical values of the focal ratio for aplanatic telescopes $\phi \simeq 8 - 12$, we should get $2w \simeq 34' - 42'$ for the field diameter.

To verify these estimates, we designed, with the help of the ZEMAX program, the four RC-type systems, all with an aperture diameter of 2 m and an axial obstruction ratio $q = 0.25$, but the following other parameters: (a) $\beta = 0.1$, $\phi = 8.0$; (b) $\beta = 0.3$, $\phi = 8.0$; (c) $\beta = 0.1$, $\phi = 12.0$; and (d) $\beta = 0.3$, $\phi = 12.0$. The expected subsecond field diameters for these cases, according to Eq. (2.19), are $31'$, $32'$, $38'$, and $39'$, respectively. In exact designs, the field of view, restricted by condition $2R_{rms} = 1''$ in spot diagrams, was $36'$, $36'$, $44'$, and $45'$, respectively. Thus, the analytical prediction according to Eq. (2.19) slightly (by about 14%) underestimates the field sizes.

A special case is the Hubble Space Telescope, in which both q and β are chosen to be unusually small, of the order of 0.1, but $\phi = 24$ is deliberately large (see Table 2.2). According to Eq. (2.19), one could expect the field

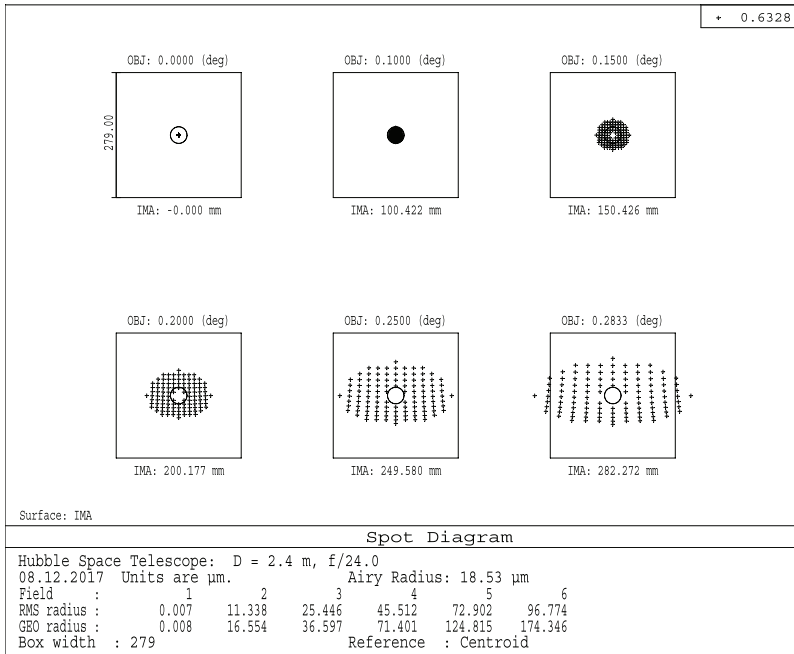


Figure 2.7 Spot diagrams of the Hubble Space Telescope for the field angles 0, 6', 9', 12', 15', and 17' on a curved image surface with a radius of -635 mm. The box width is $279 \mu\text{m}$ ($1''$), and the wavelength is $0.6328 \mu\text{m}$.

diameter $7\sqrt{24} \approx 34'$; the corresponding spot diagrams shown in Fig. 2.7 are in good agreement with this estimate.

The results above correspond to a curved focal surface, but the back focal length (BFL) remained optimal only for the axial image. Optimization of both the BFL and the radius of curvature of the image surface slightly expands the field (in the case of the HST, from $34'$ to $42'$). On the other hand, the requirement that the focal surface be flat substantially reduces its size (for the HST, down to $18'$). We do not enter here into further details; our goal is to show the range of the angular field characteristic of a given system. We also add that the consideration of postfocal telescopes leads to similar inferences.

When developing two-mirror systems, one needs to keep in mind that the design of the optimal baffle system to prevent direct sky background light in two-mirror telescopes is a non-trivial problem, for which extensive literature is devoted (see Wilson 1999, Section 7.2). An exact algorithm was proposed by Terebizh (2001a) that assumes mirrors of arbitrary shape and a non-zero size of the field.

2.2.4 General Schwarzschild aplanats

In a series of papers written a century ago, Schwarzschild laid the foundations of the modern aberration theory of optical systems, including telescopes (Born

and Wolf 1999, Chapter 5; Wilson 1996, Section 3.2). By that time, a few types of two-mirror telescopes with mirrors in the form of conic sections already existed. Appealing specifically to conic sections was a natural step when providing only the paraxial image of a distant source. Schwarzschild was interested in a more general question: *What form should the mirrors have in a two-mirror system, which has the widest field of view?*

The last section in Part II of this series (Schwarzschild 1905) is devoted to seeking an aplanatic two-mirror telescope, more precisely, a system in which both spherical aberration and coma are rigorously corrected near the optical axis. Schwarzschild managed to derive closed analytical formulas that described the shape of the mirror surfaces in such a telescope. Subsequently, Born and Wolf (1999, Section 4.10.2) gave a general formulation of the problem of the simultaneous correction of spherical aberration and coma in an arbitrary optical system, while Lynden-Bell (2002), and Willstrop and Lynden-Bell (2003) have repeated, in a different form, some of the conclusions of Schwarzschild's study.

Because the analytical description of mirror surfaces in exact Schwarzschild aplanats is complicated (see Appendix B), the image quality provided by these telescopes has remained unclear for a long time. Only approximations of the surfaces by conic sections admissible for systems with large focal ratios were considered. The expansions that emerge in this case were found by Schwarzschild (1905) himself. Then, Chrétien (1922) and Maksutov (1932) concretized these expansions for the Cassegrain and Gregorian systems, respectively, which gave rise to telescopes aplanatic in the third order of the aberration theory. The merits of these systems and the discovery of a fast wide-field camera by Schmidt (1931) were responsible for the prolonged lack of interest in Schwarzschild's exact theory.

This situation was explicable so long as the diameter of Schmidt telescopes corresponded to the needs and technology capabilities of the time. At present, there are several problems in observational astronomy that compel a return to Schwarzschild's theory to ascertain the image quality achievable with exact aplanats. In addition to the known problems of background astronomy, we mention, as an example, far-ultraviolet observations from spaceborne platforms, suggesting the use of telescopes with a minimum number of reflective surfaces.

The context in which Schwarzschild discussed the problem and the example mentioned above influenced the widely held view that Schwarzschild's theory is applicable only to prefocal reducing systems. Meanwhile, this theory, with proper modifications, covers not only all prefocal systems, including Cassegrain telescopes, but also postfocal Gregorian systems. Schwarzschild formulas that define the mirror surfaces in an aplanatic telescope can be brought to a form that is valid for an arbitrary two-mirror system (Terebizh 2005a). These equations are given in Appendix B; this section concerns only the initial formulation of the problem and some

numerical results. For the latter, it was necessary to extend the set of surfaces embedded into ZEMAX.

It is known (see, e.g., Hecht 1998, Section 6.3) that the necessary condition for the absence of coma is the satisfaction of the *sine condition* discovered by Ernst Abbe and Hermann Helmholtz in 1873. In the case of interest for us, when an object of observation is at an infinitely large distance, this condition reduces to a simple relation:

$$Y_1 / \sin U = F = \text{const} \tag{2.22}$$

for all of the incident ray heights Y_1 and aperture angles U (see Fig. B1). In fact, this relation means that the wavefront in the exit pupil of the telescope must have a spherical shape.

Schwarzschild combined the sine condition with the ordinary equations of ray optics and thereby found the optimal shape of the primary and secondary mirrors. As mentioned previously, he was looking for a system as fast as possible, for which prefocal shortening configurations were needed. A numerical example of such a system, given by Schwarzschild, corresponds to $q = 0.50$, $\beta = 2.50$ in Maksutov's variables. Schwarzschild compared the exact expressions for surfaces in his theory with conical sections and came to the conclusion that the exact surfaces of the primary and secondary mirrors can be approximated, respectively, by a hyperboloid and an ellipsoid up to the system focal ratio $\phi \approx 3$.

Figure 2.8 illustrates the possibilities of the exact Schwarzschild system for $q = 0.50$, $\beta = 2.50$, and $\phi = 3$. As can be seen, the field of view with image quality better than $1''$ reaches 0.7° , but there is a strong astigmatism in the system. Couder (1926) noted that astigmatism of the Schwarzschild system

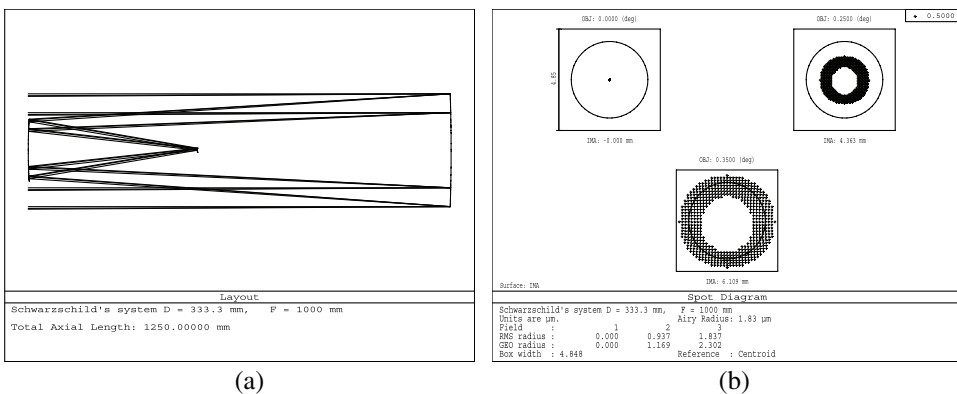


Figure 2.8 (a) Optical layout and (b) spot diagram of the Schwarzschild aplanat with an aperture of 0.333 m and a focal length of 1.0 m. The field angles are 0, 15', and 21'; the box width is 4.85 μm ($1''$).

can be eliminated at $\beta = 2/(1 - q)$, but as shown by Eq. (2.10), the length of the system becomes exactly twice as large as the equivalent focal length.

For these reasons, the Schwarzschild system and its special case, the Couder anastigmat, are rarely addressed now. However, the Cassegrainian versions of Schwarzschild general theory remain attractive in terms of image quality and light loss. Figure 2.9 gives an idea of the capabilities of such systems with the example of a fairly large telescope with a very high speed, at $\phi = 1.2$; the initial design parameters are $q = 0.30$, $\beta = 0.65$ (Terebizh 2005a, 2011). A diameter of the field of view, $2w(\theta \leq 1'') \simeq 16'$ is completely unattainable by the Ritchey–Chrétien aplanat at this speed.

Undoubtedly, the strict Schwarzschild aplanats deserve further study.

2.2.5 Mirror Schmidt; LAMOST system

The disadvantages of the original Schmidt system are, in particular, the chromatic effects and impossibility to manufacture a corrector plate with a diameter of more than about 1.5 m. Soon after the creation of the Schmidt camera, researchers realized that an appropriate corrector mirror can replace the glass plate in the original layout, thereby eliminating both of the above drawbacks. To avoid severe vignetting, the axes of the corrector and the spherical mirror should not coincide (Fig. 2.10), so the profile of the corrector mirror not only is aspheric but also has no axial symmetry.

Owing to these complexities, the first such small telescopes were made only three decades later (Epstein 1967, 1973). The relevant basic theory was laid by Korsch (1974), Lemaitre (1976, 2009), and Schroeder (1978).

At the turn of the century, the reflective Schmidt system was revived in the LAMOST project (Large sky Area Multi-Object fiber Spectroscopic Telescope; Wang et al. 1996, Zhao et al. 2012). Both the spherical primary

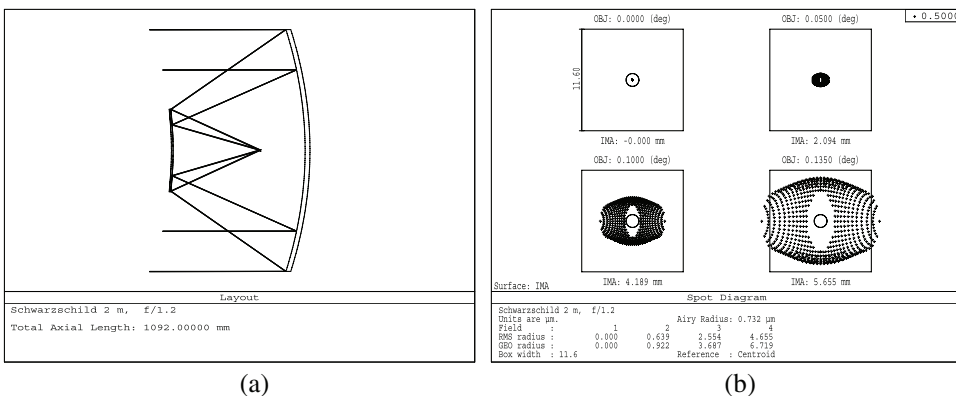


Figure 2.9 (a) Optical layout and (b) spot diagram of the Schwarzschild aplanat with an aperture of 2.0 m and a focal length of 2.4 m. The field angles are 0, 3', 6', and 8.1'; the box width is 11.6 μm (1'').

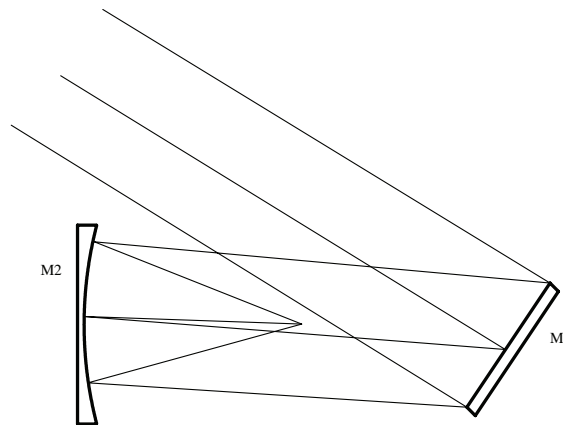


Figure 2.10 Sketch of the all-reflective Schmidt camera. M1 is the corrector mirror with a surface of complex shape, and M2 is the spherical mirror.

and the corrector mirror are complicated multi-element systems that continuously change their shape under computer control. The telescope is intended for spectrographic observations; it has a wide field of view of 5° in diameter and, at the same time, a large effective aperture that varies from 3.6 to 4.9 meters in diameter, depending on the direction of pointing. The capabilities of LAMOST are evidenced by the fact that the telescope enables one to get 4000 spectra in a single exposure to a limiting magnitude as faint as $r = 19$ at resolving power $R \approx 1800$.

2.3 Selected Three-Mirror Telescopes

As mentioned at the beginning of this chapter, we limit ourselves here to a general description of only Paul and Korsch three-mirror systems. For a detailed description of numerous versions of three-mirror telescopes, refer to the monographs by Korsch (1991), Wilson (1996), Schroeder (2000), and the journal literature cited there.

2.3.1 Paul system

Shortly after the creation of the Schmidt camera, Maurice Paul (1935) generalized the basic Schmidt idea to a three-mirror system. The starting point for the Paul investigation was the Mersenne afocal system, consisting of two confocal paraboloids (Fig. 2.11), which he considered as a compressor of the collimated beam ('feeder'). An important property of this system is the absence of third-order spherical aberration, coma, and astigmatism (see Schroeder 2000, Section 6.2f for the proof).

Recall that all of the light beams leaving an optical system appear to originate from its exit pupil (Section 1.3.1). In this respect, the exit pupil

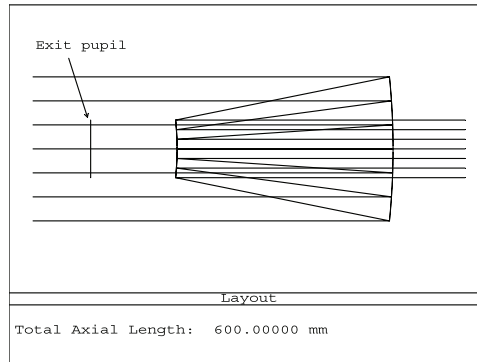
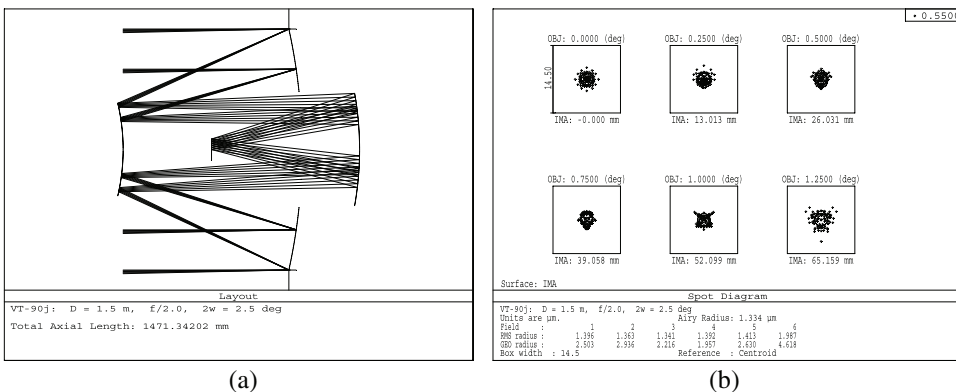


Figure 2.11 Exit pupil in a Mersenne system.

operates as an aperture stop in the 'ideal' telescope [Fig. 1.4(a)]. The second step made by Paul was the placement of a concave spherical mirror in such a way that its center of curvature coincides with the center of the exit pupil of a Mersenne two-mirror system (Fig. 2.12). Evidently, the spherical tertiary mirror plays the same role in a Paul telescope as a primary mirror in the Schmidt camera, whereas the two-mirror Mersenne system is intended both for the compression of the incident beam and the formation of an appropriate entrance pupil for the sphere.

Continuing the analogy with the classical Schmidt camera, we can expect that there is spherical aberration in the Paul system as the collimated beams fall on the *spherical* tertiary mirror. The natural solution is to cause the two-mirror beam compressor to introduce a spherical aberration of the opposite sign; for this purpose, Paul replaced the parabolic secondary mirror with a sphere, thereby achieving a three-mirror telescope with a negligible third-order spherical aberration, coma, and astigmatism. The only serious



(a)

(b)

Figure 2.12 (a) Optical layout and (b) spot diagrams of VT-090j design of a Paul type with an aperture of 1.5 m, focal length of 3.0 m, and the flat field of 2.5°. Field angles are 0, 0.25°, 0.50°, 0.75°, 1.0°, and 1.25°; the box width is 14.5 μm (1").

shortcoming was the curved field. The modifications necessary to eliminate this fault were found by Baker (1969). He also noted the possibility of a similar three-mirror system in the case where the base system is a Gregorian telescope (see Dimitroff and Baker 1945).

Unfortunately, the original Paul-Baker design had an insufficiently wide field. Subsequent investigations by Angel, Woolf, and Epps (1982) and Willstrop (1984) show that it is possible to widen the field by adjusting the conic constants and adding the polynomial aspheric terms to equations of the mirror surfaces, as in Eq. (1.12). This three-mirror design lies at the heart of the Large Synoptic Survey Telescope. However, even with aspheric terms up to eighth order, the image quality was not good enough, so a three-lens corrector has been introduced just prior to the focal plane (Section 3.3.1).

Figure 2.12 shows an example model VT-090j of a reflective Paul telescope with an aperture diameter of 1.5 m. This design has a flat field 2.5° in diameter (130.3 mm). The conic constants of the primary, secondary, and tertiary mirrors are, respectively, -1.0 , 0.0 , and 0.0 , just as Paul suggested in 1935, but the surfaces of mirrors slightly differ from the paraboloid and two spheres due to the presence of even aspheric terms of fourth and sixth orders. These terms were added to get good image quality in a rather wide and flat field and to avoid the too-large vignetting. Nevertheless, the latter is quite significant, so linear obstruction is 0.48 across the field.

Another important characteristic is the *asphericity gradient* G_{\max} , which represents the highest rate of surface deviation from the nearest sphere. For example, $2 \mu\text{m}/\text{mm}$ means that the considered surface deviates from the nearest sphere by $2 \mu\text{m}$, when one moves by 1 mm along the radius (see the more detailed discussion in Appendix C). The corresponding value for the primary mirror, $2.65 \mu\text{m}/\text{mm}$, should be considered acceptable.

Figure 2.13 depicts an example of a purely reflective flat-field telescope with polysag-type surfaces, which were described in Section 1.3.5 (Terebizh 2008). The VT-061b design is of interest in comparison with the DARPA Space Surveillance Telescope (Table 1.1), which in addition to three mirrors includes a three-lens corrector but does not attain a flat image surface (Ackermann et al. 2006). Terebizh (2008) also describes an example of a purely reflective 8.4-m telescope based on the polysag surfaces.

The above designs demonstrate the typical difficulties encountered when designing a Paul system, namely, the complexity of the shape of the surfaces of mirrors, their considerable steepness, and the significant vignetting. These problems seem unjustified with a relatively small size of the aperture and field, because the catadioptric telescopes with a lens corrector in the converging beam offer much simpler solutions (Chapter 3). However, when we examine systems with an aperture of the order of several meters, the Paul system is almost the only reasonable solution, so researchers face difficulties that grow rapidly as the aperture and field of view increase.

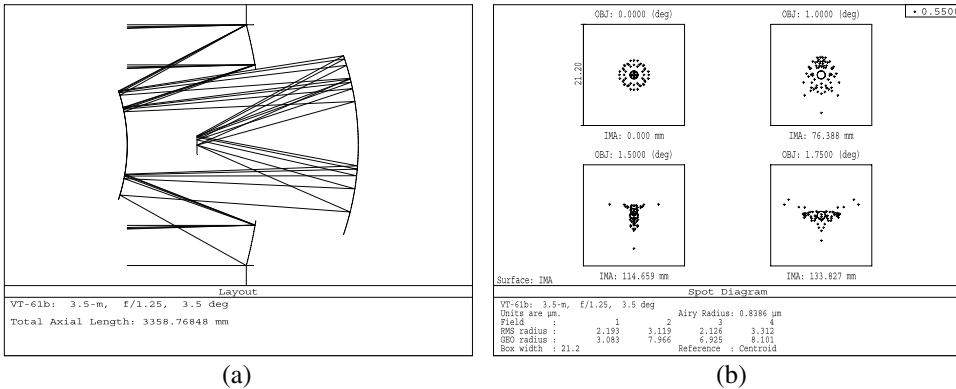


Figure 2.13 (a) Optical layout and (b) spot diagrams of a Paul-type $f/1.25$ design VT-061b with an aperture of 3.5 m and flat field of 3.5° in diameter. Field angles are 0° , 1.0° , 1.5° , and 1.75° ; the box width is $21.2 \mu\text{m}$ ($1''$).

The Paul telescope serves as a good example of how old ideas in optics, going back to the 17th century and the beginning of the 20th century, form the basis of the newest developments in astronomical optics.

2.3.2 Korsch anastigmats; the SNAP design

By introducing the proper spherical aberration, the two-mirror Cassegrain subsystem of the Paul telescope imitates an aspheric lens corrector of the Schmidt camera. Hence, according to the idea of the latter, light beams incident on the spherical tertiary mirror are nearly collimated. Generally speaking, we can abandon this requirement and move away from the Schmidt configuration, but then we have to deal with a not-so-large field of view, which is achieved by using all of the resources of the multi-mirror system. A characteristic feature of systems of this kind is the presence of an intermediate image of the object.

There are five monochromatic aberrations of the third order: spherical aberration, coma, astigmatism, field curvature, and distortion. On the other hand, the insertion of each new reflecting surface in the form of a conic section adds three new degrees of freedom: the paraxial radius of curvature, the conic constant, and the distance to the next surface. In a three-mirror telescope, the number of degrees of freedom becomes enough to correct all of the third-order aberrations of the system mentioned above. Dietrich Korsch (1972, 1977, 1980, 1991) managed to solve this problem analytically, and as a result he wrote explicit expressions for all parameters of a perfect system with three mirrors, which thus belongs to the class of third-order *anastigmats* (see also Wyman and Korsch 1974a,b). It is remarkable that mirrors are simple conic sections with moderate eccentricities, i.e., the steepness of the mirror surfaces is feasible for all but very fast telescopes.

It was an apparent success, both in the theory and practice of telescope manufacturing. Since then, many versions of the Korsch three-mirror anastigmats have been made, in particular, the telescope for the IKONOS satellite with an aperture of 0.7 m destined to study the Earth’s surface with resolution of 1–4 m (Kramer 2002). The 6.5-m James Webb Space Telescope (JWST), which is also a three-mirror anastigmat of Korsch, is planned to launch in 2021. Observations in space, and even more so in the wavelength range of 0.6–29.0 μm , determine the specific features of the JWST optical layout (Gardner et al. 2006). Figuratively speaking, the main task of the JWST is not so extensive in coverage but rather the deep physical study of space objects; therefore, a field with an effective diameter of 14.5 angular minutes was considered sufficient.

The axially symmetric Korsch system includes usually one or two auxiliary flat mirrors to reduce vignetting. For example, IKONOS has two flats, whereas a telescope planned for the space project Super-Nova Acceleration Probe (SNAP) manages only one flat [Fig. 2.14(a)]. The field of view of IKONOS is nearly 1° , so it is located at the boundary of the region of wide-field telescopes (Fig. 1.2), whereas the 2-m SNAP system with a field 1.5° in diameter, even with the obscured 0.75° central part, lies in the wide-field region. The spot diagrams in Fig. 2.14(b) illustrate the excellent image quality provided by this design.⁴

Despite the attractive properties of the Korsch folded telescopes, the general trouble of vignetting in all-reflective systems remains a serious problem, especially for wide-field systems. For example, the folding mirror in the SNAP is ~ 0.75 m in diameter: a large value for top-quality flats. Although some other layouts of two-axis telescopes have been proposed (see, e.g., Barbe

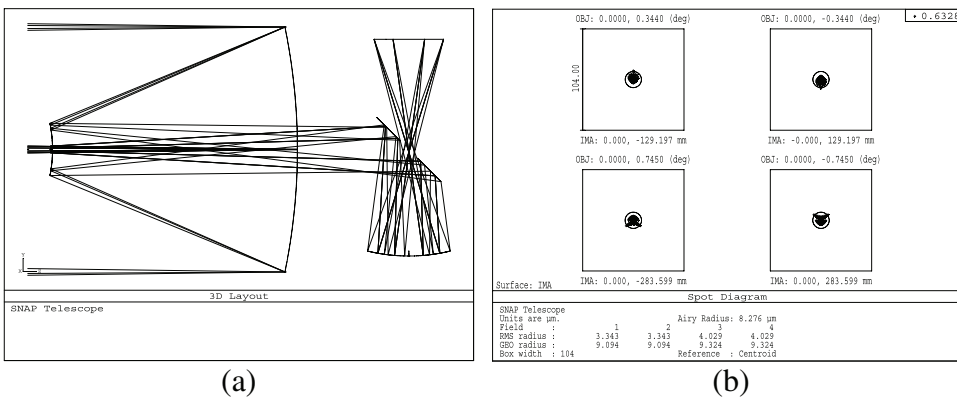


Figure 2.14 (a) Optical layout and (b) spot diagrams of SNAP design. The field angles are $\pm 0.344^\circ$ and $\pm 0.745^\circ$; the box width is 104 μm ($1''$).

⁴ The implementation of the SNAP is postponed, but this does not reduce the attractiveness of the developed optical layout.

et al. 1997), the necessity to eliminate the large auxiliary optics remains. This can be attained in a single-axis Korsch system, but then there are serious difficulties with eliminating the direct background light and baffling.

We also add that Robb (1978) explicitly wrote all of the relations for the third-order aberrations in the three-mirror system; unlike Korsch, he did not seek an inverse solution in analytical form but left it for numerical optimization. Robb argued in favor of this approach in that the equations of Korsch “are lengthy, and little or no insight is to be gained.”

Mention should also be made of an analytical study by Lee and Yu (2009). The approach allows one to preselect the appropriate configuration for a specific application, but the calculation procedure is unstable with respect to input data variations.

As this book was being prepared, an algorithm was developed to calculate three-mirror systems free of spherical aberration, coma, astigmatism, and field curvature (see Appendix F). The algorithm is stable and requires the natural input data. Thus, it becomes possible to get a wide-angle system with a flat field close to the theoretical best; if necessary, the latter is achieved through slight optimization.

Turning to the monographs by Korsch (1991), Wilson (1996), and Schroeder (2000), one can find numerous examples of attractive solutions for three-mirror telescopes. However, the abundance of approaches shows the lack of a general description of three-mirror systems. An important step in this direction was made by Mikhel’son (1980), who expanded Maksutov’s classification described above to three-mirror systems.

Chapter 3

Catadioptric Systems with a Lens Corrector in the Converging Beam

Reflecting telescopes, which we have considered so far, have their unique advantages, in particular, the ability to reach large dimensions and operate in a very wide spectral range. On the other hand, their capabilities are limited to either a small number of degrees of freedom (in two-mirror systems) or by vignetting (in multi-mirror telescopes). Thus, it is natural to combine the possibilities of purely reflective optics with those of lenses, i.e., turn to catadioptric systems.

There are two main directions in this regard.

The first takes into account the limited size of the lenses and therefore places them in a beam converging at the focus. In this case, the dimensions of the mirrors may significantly exceed those for the lenses. Such systems are discussed in this chapter. The characteristic of interest to us—the size of the field of view—reaches several degrees in systems with a corrector in a converging beam.

The next chapter is devoted to the second direction, to systems in which lenses and mirrors have comparable dimensions. Obviously, the aperture of such systems is inferior to that of the telescopes of the first group, while the proper use of lens properties allows one to achieve nearly-diffraction-limited images over a field of the order of a few tens of degrees at apertures reaching 1 m.

Lens correctors in a converging beam look diverse, but it became clear over time that in each configuration, both at the prime and secondary foci, there are some fundamental features of the corrector, so specific conditions require only a moderate variation of the parameters of a basic optical layout.

Recall the general rule given in Section 1.3.4, which researchers have long relied upon to develop catadioptric systems: *The best way to get rid of chromaticity is to assign the optical power mainly to the mirrors, leaving the*

lens component to fix geometric aberrations without introducing its own chromaticity.

3.1 Lens Corrector at a Prime Telescope Focus

Presumably, the earliest lens correctors were proposed by Ralph A. Sampson (1913a, b), first for the secondary focus of a two-mirror telescope and then for the primary focus of a large parabolic mirror. Already in these investigations, the principle mentioned above was fully used: the corrector was afocal, while its lenses were supposed to be made of a single glass.

All of these designs, as well as several other early proposals, were not implemented. Practical success was achieved by Frank E. Ross, whose corrector was installed on several large telescopes (Ross 1935). According to Wynne (1965), the subsecond field of view of Ross's corrector for the 200-inch (508-cm) Palomar telescope was about $10'$. This is noticeably superior to the field of an $f/3.3$ primary mirror without a corrector, which, as it follows from Eq. (2.2), is only about $2'$.

In subsequent years, various types of correctors were proposed, mainly using aspheric surfaces and special types of glass (Wilson 1996, Section 4.3). Since the late 1960s, an all-spherical three-lens system of one glass devised by Charles G. Wynne (1911–1999) has become the standard lens corrector for the RC hyperboloidal and classical paraboloidal primaries.¹ They will be the focus of Section 3.1.1.

Wynne correctors provide a flat field of view of a subsecond quality up to 1° in diameter. The four-lens system of that field size for a parabolic mirror was further developed by Rakich and Rumsey (2013). In the early 2000s, with the advent of a new generation of telescopes with a diameter of about 4 meters and partly in connection with the redesign of existing Ritchey–Chrétien telescopes with a close diameter, it became necessary to develop correctors with a flat field of the same image quality up to 3° in size. The corresponding optical layouts are described in Sections 3.1.2–3.

Somewhat different are the corrector for the 8.2-m Subaru telescope and the DESI corrector for the 4-m N. U. Mayall telescope of the Kitt Peak National Observatory (KPNO); the first is due to the large size of the primary

¹ “Charles Wynne was the most distinguished lens designer of the postwar era. His work influenced the design of practically every lens and optical system manufactured today, including the modern camera lens, the esoteric optics used in the manufacture of silicon chips, and the giant telescopes used by astronomers. . . Wynne recognized in the 1950s that the then-new electronic computers could be used for ray tracing; however, what was needed was some means of getting the computer itself to find the best lens design, a process known as optimization. Wynne showed this could be done using a technique known as *damped least squares*, or DLS. His discovery revolutionized the process of lens design.” [“Lens-design legend Charles Wynne dies,” *OE Reports* **193**, <http://www.spie.org/web/oer/january/jan00/wynne.html> (January 2000)]

mirror and its high speed, whereas the second is due to the specifics of spectroscopic observations using optical fibers.

3.1.1 Wynne designs for Ritchey–Chrétien and classical primaries

Since the hyperbolic primary mirror of a Ritchey–Chrétien telescope does not allow the prime focus to be used directly, it is the correctors for RC telescopes that have been given more attention. In addition, the rapid development of computers and related software coincided in time with the implementation of large RC telescopes.

Perhaps the best way to illustrate the topic is to give concrete examples of the optical systems under discussion. Figure 3.1 illustrates the three-lens prime focus corrector devised by Wynne for the 150-inch (3810-mm) RC reflector of the KPNO. A general description of the primary focus mode is given in Table 3.1.

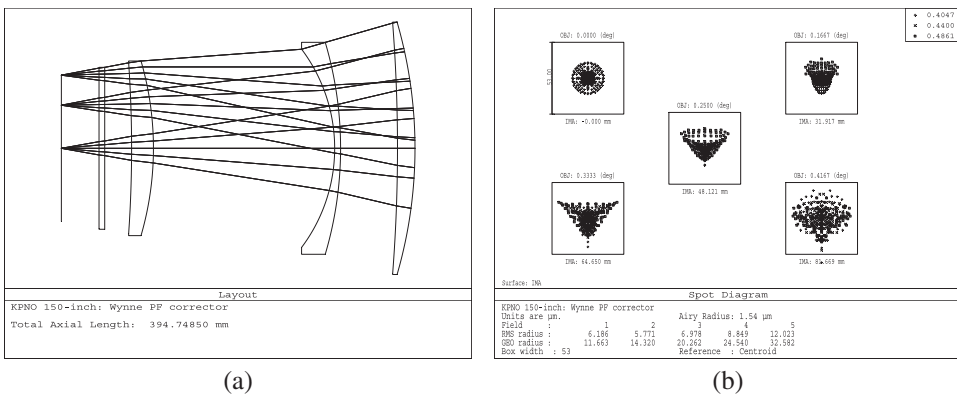


Figure 3.1 (a) Optical layout and (b) spot diagrams of a Wynne (1968) corrector for the $f/2.80$ hyperbolic primary mirror of the KPNO 150-inch telescope in the waveband 0.4047–0.4861 μm . The field angles are 0, 10', 15', and 25'; the box width is 53 μm (1").

Table 3.1 Performance of the KPNO 150-inch telescope with the Wynne (1968) three-lens corrector.

Parameter	Value
Primary diameter	3810.0 mm
Primary focal ratio	2.800
Primary conic	-1.095412
Final focal ratio	2.868
Spectral range	0.4047–0.4861 μm
Angular field	50'
Linear field	163 mm
Maximum distortion	+2.76% at 0.44 μm
Form of surfaces	All spheres
Glass grades	All Schott UBK 7
Maximum lens diameter	282 mm

For all its simplicity, the Wynne RC corrector provides subsecond images within the field, which is much wider than the values previously achieved. It should be said, however, that the spectral range is too narrow by modern concepts; nevertheless, there is noticeable chromatic aberration, both longitudinal and transverse. In this regard, Wynne wrote: “Correctors of this type, redesigned for different spectral ranges, show closely similar image spreads for wavelength intervals for which the change of refractive index of the glass is similar. A considerably wider spectral range of good resolution would be possible with correctors of this form if a smaller field angle were accepted.” The modern means of optimization allows one to significantly expand the spectral range while maintaining the size of the field of view. As for monochromatic aberrations, all third-order aberrations are corrected acceptably; nevertheless, the fifth-order triangular coma is 0.83λ (RMS) at the edge of the field, and further attempts to eliminate it in a three-lens system are unsuccessful.

Wynne designed prime-focus correctors for a number of other RC-type telescopes, in particular for the McDonald Observatory 105-inch (267-cm) telescope and the European Southern Observatory (ESO) 3.5-m telescope. The appearance of the Wynne corrector is unique to each telescope; in spite of this, the invariance of the basic features, namely, the sufficiency of only three spaced spherical lenses made of one glass, allows us to consider them as systems of the same type. Moreover, even the slight aspherisation of some surfaces, which is easy to accomplish with modern optical programs, preserves Wynne’s design as a basic prime-focus corrector system.

Shortly after designing the RC corrector described above, Wynne (1973) devised the four-lens correctors with one glass for a classical paraboloid. Meanwhile, the aberrations of the parabolic and hyperbolic mirrors differ only in that the former lacks spherical aberration, and therefore the difference is not so great at moderate speed as to exclude the possibility of a three-lens all-spherical corrector for a parabolic mirror. Indeed, Wynn (1974) soon found such a solution.

Figure 3.2 shows an example of the Wynne corrector for a classical paraboloid. Note the much wider spectral range in comparison with the KPNO corrector and the more pronounced increase of the focal length.

It is important to understand why the Wynne corrector has become the basic system for many telescopes. To this end, we have carried out a deep optimization of the above corrector for the KPNO 150-inch telescope with the help of modern tools. During optimization, a few parameters were retained, i.e., those for the primary mirror, the first lens maximum diameter, and the spectral range; only the central and edge thicknesses of the two lenses were slightly enlarged to facilitate their manufacture. The result was indicative: Wynne’s original design changed very little with virtually the same image quality.

Thus, Wynne managed to achieve a solution close to the *global* minimum of the merit function in the multidimensional (in this case, 14-dimensional)

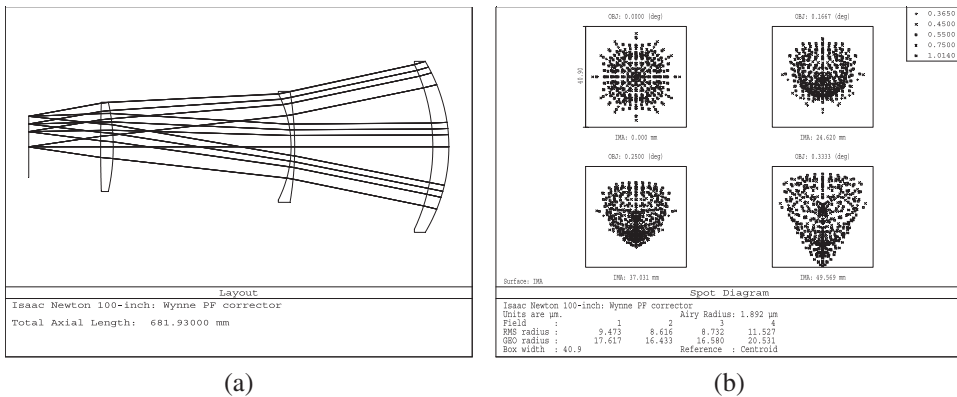


Figure 3.2 (a) Optical layout and (b) spot diagrams of a Wynne (1974) corrector for the $f/3.05$ parabolic primary of a Newtonian 100-inch telescope in the $0.365\text{--}1.014\ \mu\text{m}$ waveband. The field angles are $0, 10', 15',$ and $20'$; the box width is $40.9\ \mu\text{m}$ ($1''$). The final focal ratio is 3.45.

space of optical parameters. In the middle of the 20th century, it became clear that the ‘optical space’ is filled with many local minima scattered across the extensive valleys with a slight slope. The detection of the globally deepest minimum means the design of the best possible system under the given conditions (see also the relevant explanations in the Preface).

Wynne’s three-lens spherical correctors made of glass of the same type reach the practical limit with respect to the size of the field of view and the width of the spectral range. A useful development of such a system for an $f/2.5$ parabolic primary mirror was suggested by Rakich and Rumsey (2013). Their four-lens corrector also contains only spherical surfaces and is made of the same type of glass. The task was to improve the quality of images in a 1° field and to provide a nearly telecentric (plane-parallel) path of the rays in the image space. The latter is desirable for matching the corrector with the fiber cable for multi-object spectral observations. These goals have been achieved. Along the way, the details were clarified regarding the mutually complementary relationship between the size of the field of view and the width of the spectral interval.

3.1.2 All-spherical three-degree corrector of single glass

The optical layout of the corrector discussed in this section was devised by Terebizh (2003, 2004) in connection with the AURA Request for Bid *Concept Optical Design for a Very-Wide Field Corrector for the Blanco 4-meter Telescope* (2003). This telescope, located near La Serena, Chile, belongs to the Cerro Tololo Inter-American Observatory. According to the *Statement of work*, the product of the corresponding study should be “. . . Two new designs, which may allow production of a new type of wide field corrector, rather than production via rescaling of traditional prime focus corrector designs.”

An important feature of the project was the possibility to create a powerful survey telescope quickly and inexpensively. Besides, at a diameter of 4 m and a focal ratio $\phi \sim 3$, a primary mirror with a roughly afocal field corrector can be reasonably matched in modulation transfer function with ordinary detectors that have pixels about $15 \mu\text{m}$ in size. Thus, the problem of matching optics with a detector, which is not easy to implement at the Cassegrain focus, is solved here in a natural way.

In fact, three versions of the basic optical layout were presented with a field 2.12° , 2.40° , and 3.00° in diameter; they were called, respectively, Blanco-R (VT-014d), Blanco-S (VT-014e), and Blanco-T (VT-014f). The last two systems are considered to be principals, while the system Blanco-R has been specially designed with a reduced size of the front lens.

All three versions of the corrector are similar to each other, so we show in Fig. 3.3 only the corrector for Blanco-S. Special measures have been taken to equalize the size of stellar images across the field of view. This was done both to simplify frame processing and because of the larger area of the outer part of the field. Table 3.2 summarizes the performance of the three corrector versions.

The basic optical layout of the corrector can provide a flat field up to 3° in diameter at the subsecond image quality in a wide integrated spectral range. Since observations are generally carried out in relatively narrow spectral ranges rather than in integral light, the corresponding image quality is better than shown in Table 3.2. The refocusing range when passing from one spectral band to another is only a few hundredths of a millimeter; such a small value is attributable to the optimization of the system in integrated light.

The main features of the corrector basic optical layout are as follows:

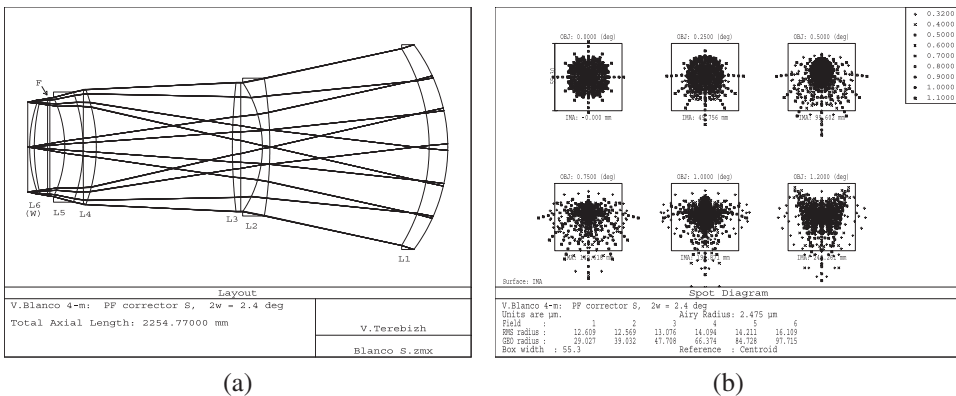


Figure 3.3 (a) Optical layout and (b) spot diagrams of the Terebizh (2003, 2004) Blanco-S corrector for the $f/2.7$ hyperbolic primary of the V. M. Blanco 4-m telescope. The spectral range is $0.32\text{--}1.10 \mu\text{m}$. The field angles are $0, 0.25^\circ, 0.5^\circ, 0.75^\circ, 1.0^\circ$, and 1.2° ; the box width is $55.3 \mu\text{m}$ ($1''$). 'F' denotes a filter; the last lens L6 is also a detector window.

Table 3.2 General characteristics of the correctors for the Blanco telescope. The axial curvature radius of the primary mirror is -21311.6 mm, and its conic constant is -1.09763 .

Parameter	Corrector		
	“R”	“S”	“T”
Angular field of view	2.12°	2.4°	3.0°
Effective focal length with the telescope, mm	11 506.7	11 400.4	11 505.9
Effective focal ratio	2.92	2.90	2.92
Scale, $\mu\text{m}/\text{arcsec}$	55.79	55.27	55.78
Linear field of view, mm	427	481	606
Spectral range	0.32–1.10 μm	0.32–1.10 μm	0.32–1.10 μm
Image RMS-diameter over field (center-edge)	26.4–31.2 μm 0.48″–0.56″	24.8–31.2 μm 0.44″–0.56″	28.6–39.6 μm 0.52″–0.70″
Image D_{80} diameter over field (center-edge)	33.2–38.5 μm 0.60″–0.70″	31.8–38.0 μm 0.58″–0.68″	36.0–45.0 μm 0.64″–0.80″
Maximum distortion	0.42%	0.60%	0.61%
Maximum clear aperture, mm	900	1100	1300
Number of lenses		Everywhere 6	
Shape of lens surfaces		All spheres	
Lens material		All fused silica	

A. The key role in expanding the field is played by doublets L2/L3 and L4/L5, each of which is, by itself, an effective compensator of coma.² The lens L6 serves simultaneously as the field flattener and the detector window. Doubling the number of lenses in comparison with the Wynne corrector provides an increase in the area of survey by an order of magnitude. With modern broadband coatings (see Section 3.1.3 for the relevant discussion), the overall transparency of the system remains high; it is worth recalling in this regard the common objectives with the number of lenses reaching two dozen.

B. The fact that all optical surfaces are spheres is important for several reasons. The obvious ones are ease of manufacturing and comparative cheapness of the design. More significant is the *mildness of the tolerances for all parameters*, because the slopes and transverse shifts of a spherical surface mutually compensate each other, which is impossible for aspheres. Equally important is the *smoothness of surfaces*, which is easily achieved for spheres. On the contrary, a steep asphere is difficult to make without ripples, which spreads a significant part of light into the wings of the image (O’Neill 1963; Wetherell 1980, 1982; Schroeder 2000, Sections 11.1.c, 18.1.c, and Appendix C). In such a case, the image D_{80} diameter is much larger than the frequently used full width at half maximum (FWHM). Finally, Saunders et al. (2014) have shown that there is still room in large optics for the

2 Similar coma compensators were described by M. Rusinov (1979, p. 371) irrespective of telescope optics. Lens L3 has been applied by B. Delabre in a corrector with a 0.95° field of view (2002, not published). Delabre’s system consists of three lenses and a detector window that has an optical power.

compensation of atmosphere dispersion by means of tiny transverse displacements of a pair of spherical elements in opposite directions, but this cannot be done with aspheric surfaces. In the latter case, two complex optical elements have to be additionally introduced (see Fig. 3.5).

C. It is not necessary to explain the benefits of using of a single glass, especially fused silica, which is stable and transparent in a very wide range of spectrum.

D. Although the corrector was developed for a particular primary mirror of a hyperbolic shape (and thus the corresponding degrees of freedom were fixed initially), its overall structure remains unchanged with reasonable variations in the size of the field, as well as the shape and speed of the primary. This stability indicates that the global minimum in the optical space was reached during optimization, as in the case of the Wynne triplet.

The corrector is close to an afocal system, so the focal length of the telescope exceeds that of the primary mirror only slightly (Table 3.2). The *sampling factor* χ , which was defined by Eq. (1.21) as the ratio of the D_{80} diameter of a star image to the pixel size, is approximately 1.5–2.5 for a pixel size of 15 μm (0.27"), given by the *Statement of work*. Thus, matching the optical system with the detector is satisfactory.

The positive ('pincushion') distortion in the system Blanco-S reaches its maximum at the edge of the field of view in the ultraviolet; the exact value is 0.61% for a field angle of $w = 1.2^\circ$ and a wavelength of 0.32 μm . This value may be considered negligible if we do not pose a special astrometric problem or use an observation mode, which involves sliding the image along the detector. Otherwise, being constant with time, the distortion can be taken into account when processing the data.

For linear fields of view about half a meter in size, it is not so much the image distortion but rather its variation with wavelength that is hazardous. In our case, the maximum (in absolute value) distortion gradient $-2.25 \times 10^{-4} \mu\text{m}^{-1}$ may be considered acceptable.

The stability of the structure of the lens corrector described here with respect to variations in the shape of the primary mirror allows the use of some base model when creating any particular design with a prime focus corrector. Such a model, VT-014j, is presented in Appendix D. The design includes a 4-m parabolic primary mirror and an all-spherical lens corrector made of fused silica. This simple system provides about 0.4" images within a flat field with a diameter of 2.5° (integral waveband 0.40–1.00 μm).

3.1.3 Dark Energy Camera; the DESI project

The lens corrector known as the Dark Energy Camera, or DECam, was mounted in 2012 at the prime focus of the V. M. Blanco 4-m telescope, which was discussed in the previous section. The DECam consists of 5 lenses made of fused silica and provides a field 2.2° in diameter (Kent et al. 2006,

Doel et al. 2008). A detailed description of the DECam, including a prescription of the optical layout, is presented in the definitive paper of Flaughner et al. (2015).³

A comparison of Tables 3.2 and 3.3 shows that the DECam occupies, relative to the sizes of a field and the front lens, an intermediate position between the Blanco-R and Blanco-S correctors. At the same time, along with the external similarity of the Blanco-RST and the DECam correctors seen in Figs. 3.3 and 3.4, there is an essential difference between them in the optical sense. As noted in the previous paragraph, lenses L2–L4 of the Blanco-RS are not mutually independent but make up two pairs, each of which is a powerful coma suppressor. In the DECam, the second pair of lenses is replaced by a single lens, one of whose surfaces is a highly steep asphere.⁴

For many years, the steepest aspheric surfaces were mirrors of the 1.8-m Vatican Advanced Technology Telescope (West et al. 1997), whose asphericity gradients (see Appendix C) are $3.9 \mu\text{m}/\text{mm}$ and $3.6 \mu\text{m}/\text{mm}$ for the primary and secondary mirrors, respectively. These mirrors were successfully manufactured by the University of Arizona’s Steward Observatory Mirror Laboratory and the Space Optics Research Laboratory (Chelmsford, MA). In the DECam, the asphericity gradient is $6.0 \mu\text{m}/\text{mm}$ on the concave surface of the second lens along the path of light rays (Fig. 3.4) and reaches $21.2 \mu\text{m}/\text{mm}$ on the convex surface of the fourth lens. This means

Table 3.3 General characteristics of the DECam at the Blanco telescope.

Parameter	Value
Angular field of view	2.2°
Telescope effective focal length	11732 mm
Effective focal ratio	3.08
Scale in the focal plane	$56.9 \mu\text{m}/\text{arcsec}$
Linear field of view	452 mm
Spectral range	$0.40\text{--}1.0 \mu\text{m}$
Image RMS diameter, center-edge of field	$15.0\text{--}55.4 \mu\text{m}$ ($0.26''\text{--}0.97''$)
Image D_{80} diameter, center-edge of field	$19.2\text{--}71.5 \mu\text{m}$ ($0.34''\text{--}1.26''$)
Maximum distortion	0.30%
Number of lenses	5
Maximum clear aperture of corrector	932 mm
Lens material	All are of fused silica
Shape of lens surfaces	Two are aspheres of eighth order

³ The two surfaces of the DECam are aspheric. The data in Table 2 of that paper concerning these surfaces are erroneously assigned to the opposite sides of the lenses C2 and C4.

⁴ A decade after the start of the project, Saunders, Gillingham, Smith, Kent, and Doel (2014) noted that “The Terebizh design has been adapted and implemented for the Dark Energy Camera (DECam) on the Blanco telescope, including a reduction in lens count to 5.” It is difficult to agree with this opinion, because just the destruction of the second doublet in the Blanco-RST systems necessitated the introduction of steep aspheres with all of the consequences specified in point B of Section 3.1.2.

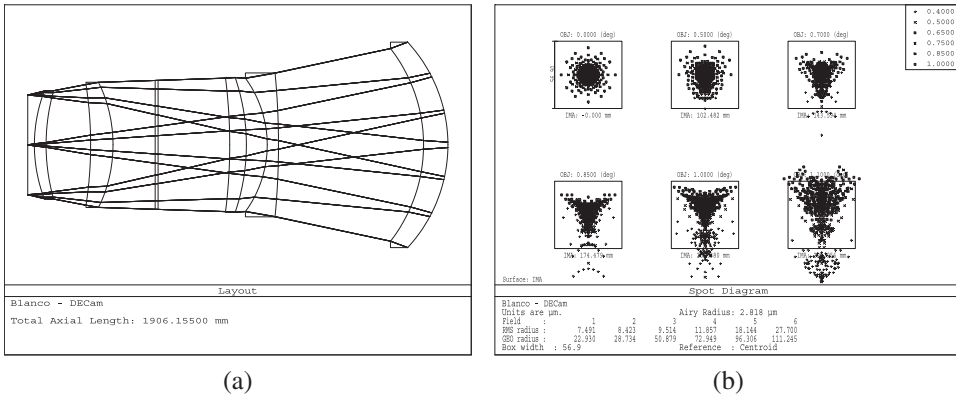


Figure 3.4 (a) Optical layout and (b) spot diagrams of DECam at the prime focus of the V.M. Blanco 4-m, $f/2.7$ hyperbolic mirror. The spectral range is 0.40–1.00 μm . Field angles are 0, 0.5°, 0.7°, 0.85°, 1.0°, and 1.1°; the box width is 56.9 μm (1"). The last lens is also a detector window.

that the surface leaves the nearest sphere by about 34 wavelengths of the common He-Ne laser, when one moves along the radius by 1 mm.

The DECam was optimized for a spectral range of 0.40–1.00 μm , within which the nominal g , r , i , and z bands are located; then the filters for Y (0.95–1.065 μm) and u (0.30–0.40 μm) bands were added. According to the first public data release of the Dark Energy Survey (Abbott et al. 2018), the median FWHM is about 1" in the above bands; the D_{80} values are not given.

An important problem for multi-lens systems is the loss of light when reflected from surfaces. For a lens made of fused silica, the fraction of energy reflected from one uncoated surface is about 3.5%, so that nearly 30% of light will be lost in the five-lens system. To reduce the loss of light in the DECam, modern capabilities have been applied to lens coatings. Namely, surface reflectance less than 1.5% in the wavelength range 0.34–1.08 μm and less than 1.2% in the wavelength range 0.48–0.69 μm has been required with a nonuniformity less than 0.7%. Thus, the loss of light in one lens is only 2.5–3.0%.

With a linear diameter of the focal surface of about half a meter, the implementation of a proper detector is not an easy task. Since a similar problem is typical for all large wide-field telescopes, we give an appropriate brief description from the aforementioned paper by Flaugher et al. (2015): "The 570-megapixel focal plane comprises 62 2K \times 4K CCDs for imaging and 12 2K \times 2K CCDs for guiding and focus. The CCDs have 15 μm \times 15 μm pixels with a plate scale of 0.263"/pixel. A hexapod system provides state-of-the-art focus and alignment capability. The camera is read out in 20 s with 6–9 electron readout noise." The fully depleted red-sensitive back-illuminated CCDs were developed by the Lawrence Berkeley National Laboratory.

Flaugher et al. (2015) also provide a valuable experience concerning the mechanical design and alignment of a lens system of such a large size.

The DESI corrector

Currently, a close twin of the Blanco telescope, the 4-m N. U. Mayall telescope of the Kitt Peak National Observatory, is being renewed (Martini et al. 2018, Miller et al. 2018). The telescope will be equipped with a prime-focus lens corrector—the *Dark Energy Spectroscopic Instrument* (DESI)—but unlike the DECam, it is intended to record spectra of the objects in the field with a resolution of 2000–5000 in the range of 0.36–0.98 μm . For this, 5000 fibers are used, which transmit light to the slits of spectrographs. Obviously, the focal surface need not be flat to place in it numerous fibers, so its shape is not spherical but rather aspheric with moderate curvature.

From the optical point of view, the use of fibers also determines another important difference between the DESI and conventional correctors, namely, the matching of the corrector with fibers requires that the chief rays were oriented near local normals to the focal surface. This condition reduces the number of degrees of freedom and complicates the design of the optical system (Sholl et al. 2012).

For a number of reasons outside the scope of this discussion, the primary focal ratio of $f/2.81$ has been magnified to $f/4.5$, which caused the appearance of chromatic aberration. Thus, it was necessary to find a trade-off between the possibility of curving the focal surface, the condition of the normality of the chief rays, and the level of chromatic aberration. The resultant six-lens optical layout of the corrector provides a field 3.2° (80 cm) in diameter. Two spherical lenses made of Schott N-BK7 are destined to correct for atmosphere dispersion; of the remaining four lenses made of fused silica, two are spherical, and two have one aspheric surface each. The asphericity gradient is limited to 30 $\mu\text{m}/\text{mm}$.

3.1.4 Subaru Hyper Suprime Camera

The Subaru telescope of National Astronomical Observatory of Japan (Mauna Kea, Hawaii), with an aperture of 8.2 m, was designed according to the $f/12.2$ Ritchey–Chrétien scheme. To expand the field of view, the 1.5° prime-focus lens corrector, known as the *Subaru Hyper Suprime Camera* (HSC), was installed in 2013 in lieu of the secondary mirror. A recent special issue of the *Publ. Astron. Soc. Japan* (2018), V. 70, No. SP1, is devoted to the Subaru HSC; we will also rely on a patent by Matsuda (2015).

It is understandable that the manufacture of a field corrector at the prime focus of a very large telescope faces significant difficulties due to the limited size of lenses. The Subaru telescope is twice as large as the Blanco reflector, so the angular size of the field had to be reduced, but it remained significant at such an aperture (Komiyama et al. 2010, Miyazaki et al. 2018). The light

diameters of the largest lenses in both systems are of the same order: 932 mm in the DECam, and 820 mm in the Subaru HSC.

The flat field of the subarcsec quality in the integral waveband 0.40–1.1 μm is provided by a five-lens system made by Canon of the Ohara catalog glasses and fused silica; a two-lens atmosphere dispersion corrector (ADC) is also inserted into the optical system (Fig. 3.5). The authors of the optical system proceeded from the classical Wynne (1965, 1968) triplet, which is represented in Fig. 3.5 by lenses L1, L2, and L5 (see also Fig. 3.1). The L3/L4 doublet is considered as a chromatic aberration compensator, whereas the built-in ADC is almost afocal.

The above data regarding the dimensions of the image and the input lens of the DECam and the Subaru HSC do not fully describe the difficulty of implementing the latter design. The matter is that the f -numbers of the primary mirrors of these two telescopes are very different: $f/2.8$ for the DECam, and $f/1.8$ for the Subaru HSC. In both systems, the correctors slightly extend the focal length; the final speed values are $f/3.1$ and $f/2.2$, respectively. Bearing in mind the high speed of the Subaru primary and a limited choice of types of glass, the field diameter of 1.5° seems too wide for the corrector to be made with sufficiently simple surfaces. Indeed, one of two surfaces of each of five lenses is a deep asphere of the 16th order of the expansion Eq. (1.12) in even aspheres. The corresponding asphericity gradients range from 7 $\mu\text{m}/\text{mm}$ to 125 $\mu\text{m}/\text{mm}$ (!), that is, about 200 wavelengths of a red He-Ne laser at a radial displacement of 1 mm.

3.2 Lens Corrector in a Secondary Telescope Focus

The previous section showed that placing a few spherical lenses near the focus of an ordinary hyperbolic or parabolic mirror makes it possible to provide a flat field with an angular diameter of up to 3° and a linear size of about half a

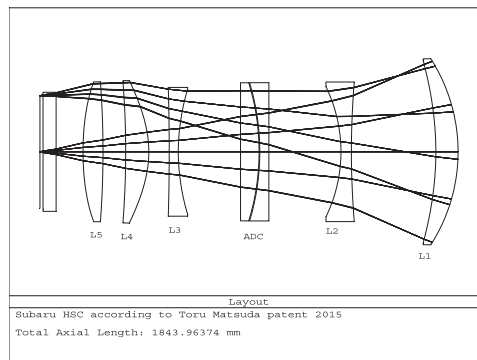


Figure 3.5 Optical layout of the Subaru Hyper Suprime Camera with a flat field of 1.5° (Matsuda 2015). The atmosphere dispersion corrector is designated as ADC.

meter. This way should be considered quite simple and reliable, but the telescope becomes too long with a fairly large feeding mirror, so a large and expensive dome is required. In this regard, it is natural to try compact two-mirror systems with a lens corrector, especially since the entering of a secondary mirror adds a few degrees of freedom. At first glance, it seems strange that the goal of expanding the field with additional degrees of freedom is weakly realized. Before entering the related details, let us make a few general comments on the subject.

First of all, an opportunity to use a lens corrector near the secondary focus of the Ritchey–Chrétien telescope deserves attention, because the RC system itself has a field of view of about 0.5° . The resulting system is called a *Quasi-Ritchey–Chrétien* (QRC) telescope; it can achieve a field 1.5° – 2.0° in diameter.

Meanwhile, with a few corrector lenses, it is no longer necessary to correct aberrations of a base two-mirror system separately: all optical elements, mirrors and lenses, may be optimized together. In this case, we get a system called the *corrected Cassegrain* telescope in Section 1.1.1. Of course, a similar *corrected* Gregorian telescope exists. As shown in the following paragraphs, these systems provide a field of about 3° with a primary mirror size of the order of 2–3 m.

Let us now return to the question of why the image quality in corrected Cassegrain systems depends weakly on the shape of the secondary mirror, so that even the values of the conic constant of order -20 which sometimes occur (e.g., in the Pan-STARRS-1 telescope) help slightly. The reason is that the secondary mirror of a survey telescope should be equally suited for the light beams falling on it at very different angles, but this is possible only when the surface of the mirror is close to a sphere (Lynden-Bell and Willstrop 2004). The fact that a simple spherical secondary mirror can be used in wide-field corrected Cassegrain telescopes was discovered by Harmer and Wynne (1976). With an infinitely large radius of curvature, the sphere turns into a plane, and indeed, sometimes a flat secondary mirror is applied, agreeing with a significant vignetting of light (e.g., in the ROTSE-III telescope; see Akerlof et al. 2003).

In view of the above, we are forced to complicate the shape of the surfaces of both mirrors and lenses in order to expand the field of view. Nonetheless, the field size in the corrected Cassegrain system is approximately the same as in a single-mirror telescope with the prime focus lens corrector.

Thus, when choosing the optical layout of a wide-field telescope, it is necessary to find a compromise between the total length of the system and the complexity of the optical surfaces.

3.2.1 Quasi-Ritchey–Chrétien system; VST telescope

Recall that the QRC system is an RC telescope (maybe slightly refined), equipped with a lens corrector. Most existing telescopes belong just to the

Ritchey–Chrétien type, so the need for lens correctors at the secondary focus is understandable. Of the many studies in this direction, those by Wynne (1968) and by Epps and Fabricant (1997) should be noted. These publications are divided by three decades, during which photographic emulsion ceased to be the main detector of light, and this function was accepted by CCDs. As a rule, CCDs have better resolution and require a larger back focal length; therefore, the last mentioned designs are more suitable for the current state of observation techniques.

Harland Epps and Daniel Fabricant (1997) presented their findings in a way that gives a clear idea of priorities in this area: “We describe a new family of two element field correctors that can provide excellent images ($\leq 0.2''$) over a field diameter exceeding 0.5° . These new correctors have five appealing features: (1) they are compact, (2) they use only spherical surfaces, (3) they are constructed from fused silica, with high transmission over the entire optical band, (4) ghost images are well controlled, and (5) one of the corrector elements can serve as the dewar vacuum window to minimize the number of glass-air surfaces.” (It is useful to compare this opinion with what was said in Sections 3.1.2 and 3.1.3.) The authors presented several specific corrector designs for existing RC telescopes.

Regarding the possibility of a slight change in the shape of mirror surfaces in the Ritchey–Chrétien system, the *VLT Survey Telescope* (VST) with an aperture of 2.61 m and a field of view of 1.47° is a good example (Sedmak et al. 1999, 2007).

The optical system of this telescope (Fig. 3.6) consists of two hyperbolic mirrors and three spherical corrector lenses made of silica. If we remove the corrector, the remaining two-mirror subsystem, described in the second column of Table 3.4, provides good images but only in a $20'$ field. By itself, this subsystem is not an RC telescope, but it is close to some ‘underlying’ RC

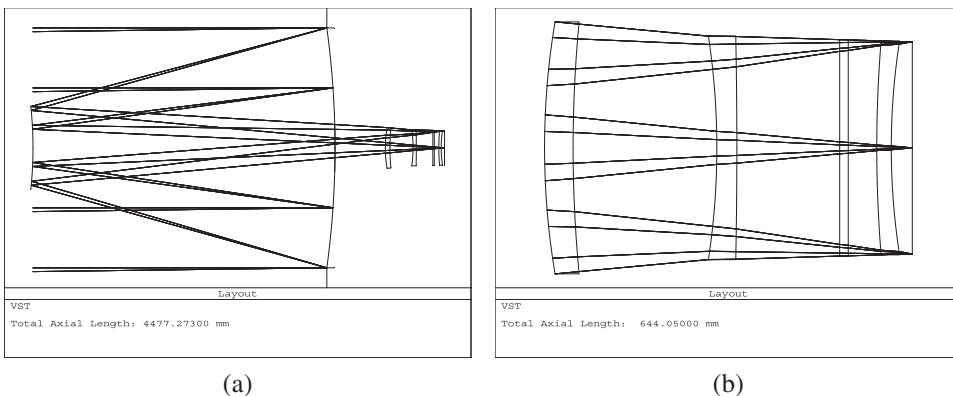


Figure 3.6 (a) Optical layout of the VST and (b) enlarged VST lens corrector. The flat filter is placed between the second and third lenses.

Table 3.4 Parameters of the VST two-mirror subsystem and of the underlying RC telescope.

Parameter	VST mirrors	RC
Field size $2\omega(1')$	20'	30'
Focal ratio	5.546	5.546
Primary curvature radius	−9509.0 mm	−9509.7 mm
Primary conic constant	−1.139899	−1.0965
Secondary curvature radius	−4374.0 mm	−4374.6 mm
Secondary conic constant	−5.421864	−4.9455
Mirrors spacing	−3285.873 mm	−3286.1 mm
Back focal length	1184.97 mm	1184.92 mm
Image curvature radius	−1525.6 mm	−1554.2 mm

telescope. The parameters of the latter can be found as follows. According to Section 2.2.1, any two-mirror telescope can be defined by four initial variables: the aperture diameter D , the equivalent focal length F , and the pair of dimensionless ratios (q , β). All of these variables are assumed to be the same as in the two-mirror VST subsystem, in particular, $q \approx 0.3089$, $\beta \approx 0.3285$, but conic constants should be obtained from Eqs. (2.16) for the aplanatic system. In this way, the values given in the third column of the Table 3.4 were obtained.

The data in Table 3.4 confirm the proximity of the real subsystem of the VST mirrors to some Ritchey–Chrétien system. Thus, a noticeable increase in the field of view, in this case, almost up to 1.5° , can be achieved by adding a few lenses to the appropriate RC system and then by moderately optimizing *the whole telescope design*. As a result, a balanced optical system was realized that met the stated goal.

Although QRC telescopes can provide a slightly larger field of view, this is not enough to study fast transient events.

3.2.2 Corrected Cassegrain system; Pan-STARRS telescope

The direct way to expand the field of view is to complicate the shape of the surfaces of both mirrors and lenses by deep optimization of the two-mirror system together with the lens corrector. The *Panoramic Survey Telescope and Rapid Response System* (Pan-STARRS) gives a specific example of a corrected Cassegrain system (Fig. 3.7).

The project is carried out by the University of Hawaii, Institute for Astronomy (Hodapp et al. 2004, Morgan and Burgett 2009). The prototype telescope, PS1, is located on the summit of Haleakala on the island of Maui, Hawaii. It started regular observations in March 2010 and soon showed a rather high efficiency of observations and, at the same time, problems with operation due to unreasonably tight tolerances.

Before considering the PS1, it is worthwhile to compare the approach of the Pan-STARRS project with that accepted by another advanced project, the

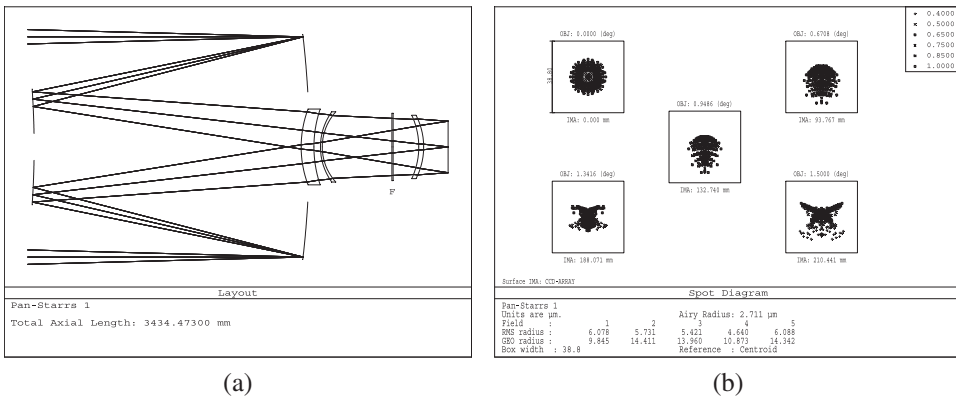


Figure 3.7 (a) Two-dimensional projection of a single optical subassembly $f/4.4$ Pan-STARRS (PS1) telescope (NOADC-M-4.0.ZMX). The aperture is 1.8 m, and the field is 3° in diameter. The filter is designated by 'F'. (b) Spot diagrams correspond to the waveband of $0.40\text{--}1.0\ \mu\text{m}$, the box width is $38.8\ \mu\text{m}$ ($1''$).

Large Synoptic Survey Telescope (LSST), which will be discussed in Section 3.3.1. Both projects impose extremely high demands on the level of optical manufacture, detector characteristics, and general technology. The LSST project assumes the fabrication of a sole wide-field telescope of 8.4 m in diameter and the effective aperture of about 6.7 m (Starr et al. 2002, Tyson and Wolff 2002). The Pan-STARRS project relies upon an array of 1.8-m wide-field telescopes, which will provide, in aggregate, at least the same survey efficiency (Kaiser et al. 2002). The main advantages of the latter approach are as follows:

- A large telescope necessarily should have very high speed, which strongly complicates its manufacture;
- A few telescopes of moderate size are cheaper and can be made in a shorter term than one giant instrument;
- The set of independent telescopes can register some area of sky at the same time, which improves the reliability of detecting the faint or variable objects;
- The dynamic range of the registration system is wider; and
- Special investigations with telescopes of about 2 m in diameter reveal an ability to compensate the atmospheric wavefront inclinations by controlling the charge accumulation in the detector.

The telescopes characteristics in both projects, in many respects, depend on the image detectors used. The relevant information, along with the survey programs and current status, are easy to find on the project websites and in the cited articles; we will concentrate here on the optical schemes of the telescopes.

Figure 3.7 shows the optical layout of the PS1 telescope. Its entrance pupil diameter and effective focal length are 1.8 m and 8.0 m, respectively.

The fraction of unvignetted rays is about 0.73, so the effective aperture diameter is 1.54 m. The primary and secondary mirrors are sixth-order even aspheres, as well as the two concave surfaces of the first and last lenses. The conic constant of the secondary mirror with a diameter of 917 mm is unusually high in its absolute value, -20.41 ; the corresponding gradient of asphericity $G_{\max} \approx 1.49 \mu\text{m}/\text{mm}$ (see Appendix C for definition). An analogous value for the concave surface of the last lens is larger, $G_{\max} \approx 5.50 \mu\text{m}/\text{mm}$, but still considered an acceptable value. To fully use the abilities of the large CCD array covering the image circle that is 421 mm in diameter, the grid distortion of the image has been reduced to a relatively low level, $\sim 0.5\%$. Finally, the total length of the system—the feature that has led to the corrected Cassegrain system instead of a prime focus corrector—is 3.54 m.

At first glance, the front corrector's lens is too thick, whereas the second lens is too thin: the ratios of the diameter to the thickness of the lenses are 5.6 and 37, respectively. The reason may be connected to the intention to replace the first lens with an atmospheric dispersion corrector, while the second lens is intended mainly for the focus correction in spectral wavebands.

As regards the use of four even aspheres, including both mirrors, it all depends on how far this solution was necessary to achieve a proper field. Our trial study showed the existence of designs with the same aperture, field of view, and distortion, in which both mirrors are simple conic sections, the fraction of unvignetted rays is 0.76 across the whole field, whereas the corrector lenses are all spherical and are made of fused silica. In one of the test models, the RMS diameter of stellar images in the integral wavelengths range $0.40\text{--}1.00 \mu\text{m}$ varies from $0.35''$ to $0.49''$ along the field radius; the asphericity gradients for the primary and secondary mirrors are $0.29 \mu\text{m}/\text{mm}$ and $0.054 \mu\text{m}$, respectively. Another example of a corrected Cassegrain system with simple optics is described in the next paragraph.

An excessive complexity of the optical design has led to the fact that⁵ “The PS1 images remain slightly less sharp than initially planned, which significantly affects some scientific uses of the data.” Nevertheless, due to the large field of view, PS1 remains an effective survey tool. Its sky-scan speed reaches 6,000 square degrees in one night, so that the entire sky available in Hawaii can be imaged in four nights. Since 2011, the contribution of Pan-STARRS to the near-Earth asteroid discoveries has steadily increased and reached 44% of the total world number in 2017.

3.2.3 Corrected Cassegrain design with a 2.5-m aperture and 3° field

Among the wide-field telescopes listed in Table 1.1, there is a 2.5-m system T250 with parameters not too different from those for PAN-STARRS1. According to Cenarro et al. (2010), T250 is an $f/3.6$ two-mirror Cassegrainian

⁵ <https://en.wikipedia.org/wiki/Pan-STARRS>

telescope equipped with a lens field corrector. The effective focal length of T250 is 9.1 m, the field of diameter 3.0° (476 mm) is flat. The telescope provides image quality $D_{80} \leq 20 \mu\text{m}$ ($0.45''$) in the waveband $0.33\text{--}1.10 \mu\text{m}$.

As far as we know, only a cursory description of the optical layout of the T250 was published. The aforementioned paper says: “The primary and secondary mirrors have an hyperbolic aspheric surface,” whereas the field corrector “. . . consists of 3 lenses of fused silica with aspheric surfaces and diameters in the range 500–600 mm.” Because of the insufficient information concerning the capabilities of an efficient corrected Cassegrain system, a close-to-T250 example, VT-137d, has been designed. However, the goal of maximizing the similarity of the designs was not posed; we only sought to find a reasonable solution. First, the focal length of 9.5 m was fixed, which provides the suitable scale in the focal plane and thus matches the pixels of about $15 \mu\text{m}$. Then, the $f/3.8$ focal ratio was adopted to keep the system compact.

The VT-137d design is shown in Fig. 3.8, and its general characteristics are collected in the Table 3.5. The main features of the design consist in the comparative simplicity of optical surfaces and the unusually low light vignetting for wide-field systems, so the effective aperture diameter reaches 2.3 m. Indeed, both mirrors have a hyperbolic shape of a moderate asphericity gradient, and all lens surfaces are spheres. The second of the above features is due to the placement of the aperture stop on the secondary mirror. With this, the primary mirror increases somewhat, but the high light efficiency of the telescope is more important. In addition, the stop on the secondary mirror facilitates the simplification of the lens corrector. As usual, we give the dimensions of the spot images in the integral light of the range indicated in Table 3.5.

Depending on the mode of observations, a low distortion of the images may or may not be required. We did not take efforts to reduce distortion, so it

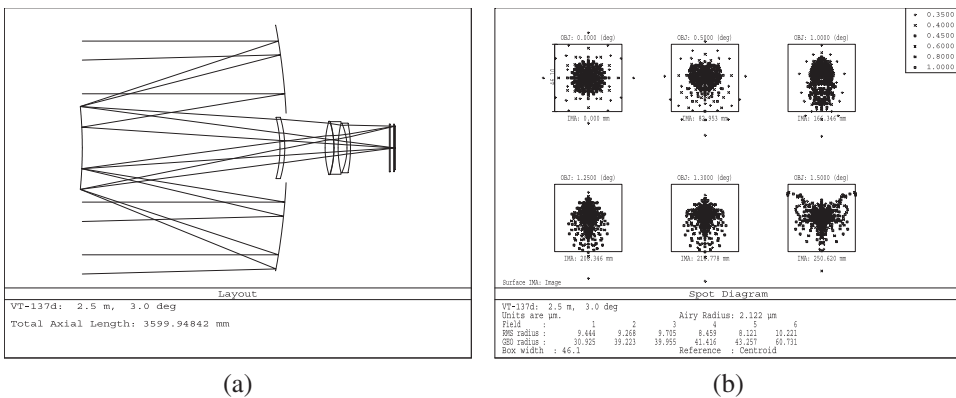


Figure 3.8 (a) Optical layout and (b) spot diagrams of the VT-137d design in polychromatic light $0.35\text{--}1.00 \mu\text{m}$. The box width is $46.1 \mu\text{m}$ ($1''$).

Table 3.5 General characteristics of the VT-137d design.

Parameter	Value
Entrance pupil diameter	2.5 m
Effective focal length	9.5 m ($f/3.8$)
Field of view	3.0° (501 mm), flat
Spectral range	0.35–1.0 μm
Fraction of unvignetted rays, center-edge	0.851–0.852
Effective diameter	2.3 m
Scale in the focal plane	46.1 $\mu\text{m}/\text{arcsec}$
Image RMS-diameter across the field	18.9–20.4 μm (0.41"–0.44")
Image D_{80} diameter across the field	22.3–26.4 μm (0.48"–0.57")
Conic constants of mirrors	–1.3124, –9.500
Asphericity gradients of mirrors	2.1 $\mu\text{m}/\text{mm}$, 2.2 $\mu\text{m}/\text{mm}$
Number of lenses	4
Shape of lens surfaces	All spheres
Diameters of lenses	570–700 mm
Lens material	All of fused silica
Total mass of lenses	167 kg
Total length of the system	3.6 m

is 0.76% at 0.45 μm . It is possible to reduce it to 0.3%, as in T250, while maintaining the key features of the design.

Obviously, in order to compete with 4-m telescopes equipped with the prime-focus correctors described in Sections 3.1.2 and 3.1.3, it would be desirable to create a reliable corrected Cassegrain system with an aperture diameter of no less than 3.5 m and a field of 2.5°–3.0°. A prototype of such design, VT-137q, is presented by Terebizh (2019). The system has an aperture of 3.6 m, a field of view with a diameter of 2.5° (474 mm), and at the same time is quite compact: its total length is 4.36 m. The primary and secondary mirrors are standard hyperboloids; all five corrector lenses are made of fused silica and have spherical surfaces. The D_{80} star diameter in the integral waveband 0.40–0.82 μm is about 0.4" across the flat focal surface. The comparative simplicity and compactness of the optical layout allow us to consider this system promising for conducting deep sky surveys.

3.2.4 Corrected Gregorian telescope

We mentioned in Section 1.3.1 that the Gregorian system has an attractive feature: its exit pupil is real, not virtual, as in the case of the Cassegrain system (see Fig. 1.3). This is true regardless of the shape of the mirrors surfaces, in particular, both for the classical system with a parabolic primary, and for the Gregory–Maksutov aplanat with elliptical mirrors. Usually, the Gregorian exit pupil is located close to the primary focus. Such a position allows us to place a correcting optical element directly into the exit pupil, which efficiently corrects the aberrations of a two-mirror system.

It seems that the superposition of wide light beams near the primary focus prevents the imposition of a lens corrector in the Gregorian system. However, it is possible to avoid additional vignetting, if we make a hole at the center of a front lens of the corrector and shift the rear its part closer to the primary mirror. As a result, we get a compact wide-field catadioptric system that consists only of the standard optical surfaces (Terebizh 2007a). Worth adding that the focal surface is well protected from direct and stray light.

An example of such a system, the design VT-050k with a 6-m entrance pupil diameter (5.1-m effective aperture), is shown in Fig. 3.9; its main characteristics are listed in Table 3.6. With an all-spherical corrector of one glass, the design provides image quality better than $0.5''$ in the integral light across a flat field 2.0° in diameter; the slight subsequent aspherization of some lens surfaces allows for the achievement of a field about 3° in diameter.

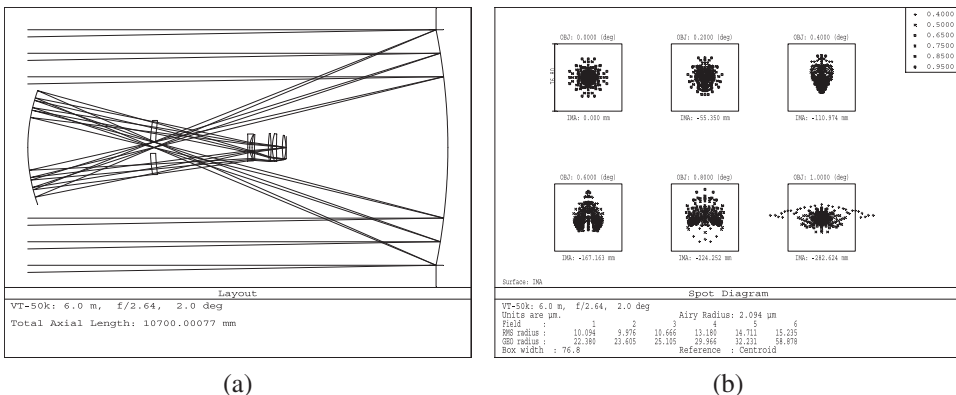


Figure 3.9 (a) Optical layout of design VT-050k with an aperture of 6 m and a 2° flat field. (b) Spot diagrams correspond to the integral waveband $0.40\text{--}0.95\ \mu\text{m}$; the box width is $76.8\ \mu\text{m}$ ($1''$).

Table 3.6 Performance of the VT-050k design.

Parameter	Value
Entrance pupil diameter	6.0 m
Effective focal length	15845 mm
Focal ratio	2.64
Scale in the image plane	$76.8\ \mu\text{m}/\text{mm}$
Angular field diameter	2.0°
Linear field diameter	565 mm
Fraction of unvignetted rays	0.715 across the field
Effective aperture	5073 mm
Waveband	$0.40\text{--}0.95\ \mu\text{m}$
RMS spot size	$20.2\text{--}30.5\ \mu\text{m}$ ($0.26''\text{--}0.40''$)
D_{80} image diameter	$27.4\text{--}36.6\ \mu\text{m}$ ($0.36''\text{--}0.48''$)
Total length of system	10.7 m

Both the primary and secondary mirrors are ellipsoids; the primary is close to a paraboloid, while the secondary mirror is close to a sphere.⁶ The asphericity gradients are $1.79 \mu\text{m}/\text{mm}$ and $1.82 \mu\text{m}/\text{mm}$ for the primary and secondary mirrors, respectively; they are far below the acceptable modern level (Appendix C). The lens corrector consists of six spherical lenses (including the curved detector window) made of fused silica. Apparently, the moderate steepness of the mirrors is the inevitable cost for a compact optical layout, large aperture, and the simple lenses of the corrected Gregorian telescope.

Generally speaking, one can apply the corrector's front lens without a hole, but it has a small influence on the image quality. On the other hand, the rejection of the front lens turns the system into a common corrected Gregorian telescope with a moderate field of view. Note that it is possible to expand the field in the system under discussion if we allow a curved focal surface, but even a telescope with a 5-m effective aperture and a 2° flat field of view would be a powerful observation tool. If it is nevertheless necessary to expand the field of view, then the aforementioned asphericization of the lens surfaces is preferable.

With a pixel size of about $15 \mu\text{m}$, the scale in the focal plane of the telescope VT-050k is suitable for performing photometric observations, but a smaller focal length is desirable for exploratory studies. To this end, a trial $f/2.05$ system VT-050m featuring the same aperture with a focal length of 12.3 m (scale is $59.6 \mu\text{m}/\text{mm}$) was designed. All six corrector lenses still have a spherical shape and are made of fused silica. The spot size in integral light is $0.34''$ – $0.72''$ across the 2° field. Evidently, faster designs can be found, if necessary.

Perhaps the corrected Gregorian telescope with a lens in the exit pupil could compensate for the lack of wide-field systems with a diameter of about 5 m, which was mentioned in Section 1.2.1.

3.2.5 Folded Gregory–Maksutov telescope with a lens corrector

To solve some astronomical problems, one needs a telescope whose characteristics seem, at first glance, to be mutually incompatible: a significant field of view with image quality close to the diffraction limit; the small vignetting of useful light; the wide spectral range extending from the ultraviolet to the infrared region of the spectrum; the absence of background illumination; the simplicity of optical surfaces; and the resulting comparative softness of tolerances on the parameters of the system.

As an example of such problems, we point out the space project MESSIER (Valls-Gabaud 2016, Hugot et al. 2014), aimed at searching for a cosmological structure of extremely low surface brightness. This project

⁶ Note that a concave ellipsoid is favorable to control the mirror's surface in the course of manufacturing.

further extends the requirements for the telescope by limiting the distortion of the image and refusing to use lenses because of the Cherenkov glow that appears in them when relativistic particles pass through.

Obviously, in these conditions it is not easy to find a suitable solution both in the class of axisymmetrical wide-field systems (Chapter 4; Terebizh 2011, 2016b) and among off-axial systems with aspheric and freeform optical surfaces (Hugot et al. 2014, Buffington 1998, Singaravelu and Cabanac 2014, Challita et al. 2014). We consider here a 400-mm model, which is a modified version of the folded aplanatic Gregorian telescope⁷ provided by a two-lens corrector protected from cosmic particles (Terebizh 2017). Although the model was designed to meet, as far as possible, the entire set of requirements listed above, we did not mean any specific project but wanted to give a general idea of the optical scheme of the desired instrument.

The model VT-133c is shown in Fig. 3.10 and is described in Table 3.7. Optical surfaces of power mirrors are ellipsoids; the primary mirror is close to the paraboloid, and the secondary mirror is close to the sphere. Two spherical lenses of the corrector are made of fused silica.

The insignificant obscuration of the incoming light flux (1.6%) and the absence of direct background illumination are provided by folding of the optical layout with the aid of a small flat mirror. This same feature maintains the axial symmetry of the system, which significantly simplifies the optical surfaces and makes the tolerances on the parameters far less tight

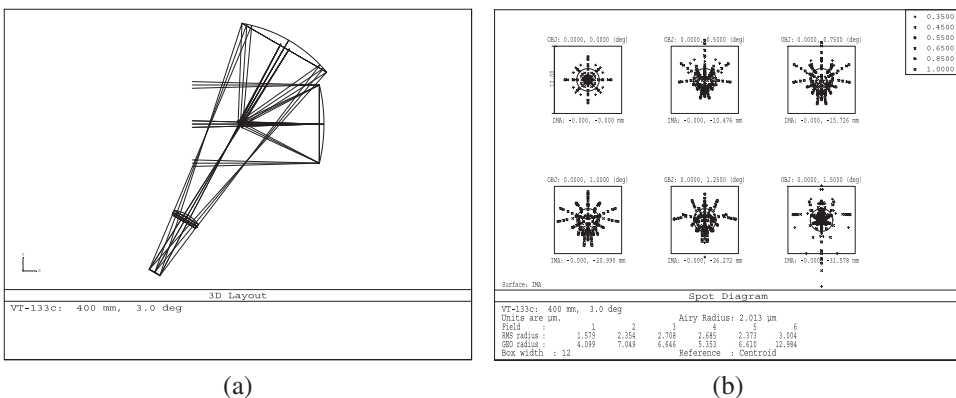


Figure 3.10 (a) Optical layout and (b) spot diagrams of the VT-133c design in polychromatic light 0.35–1.00 μm . The box width is 12 μm ($2''$). The Airy diffraction disk is shown by a circle.

⁷ Recall that the aplanatic version of the Gregorian system was proposed by Maksutov (1932). He also used the folding of the optical axis of the Gregorian system in a telescope mounted in the 1940s at the Yerevan Observatory, Armenia (Maksutov 1946).

Table 3.7 Basic characteristics of the VT-133c design.

Parameter	Value
Entrance pupil diameter	400 mm
Effective focal length	1200.2 mm (5.8 $\mu\text{m}/\text{arcsec}$)
Effective focal ratio	3.0
Field of view diameter	3.0°
Primary spectral waveband	0.35–1.0 μm
Linear obscuration	0.120
Fraction of unvignetted light, center - edge	0.984–0.984
Effective aperture diameter	397 mm
Maximum distortion	0.48%
Spot diameter in integral light, center - edge	2.8–5.1 μm (0.48"–0.88")
Diameter of a circle containing 80% of energy in a star image (D_{80}). Integral light, center - edge	5.9–8.2 μm (1.0"–1.4")
Maximum lens diameter	145 mm
Curvature radius of the image surface	195 mm

in comparison with off-axis systems. In addition, the folded layout makes it possible to reliably shield the lenses and the detector of light from cosmic particles. To fasten a fold mirror (in this example, with a diameter less than 43 mm), thin stretches can be used that introduce negligible light diffraction.

As seen in Fig. 3.10(b), the spot diameter of a star image in the polychromatic light 0.35–1.00 μm does not exceed 5.1 μm at the image scale of 5.8 $\mu\text{m}/\text{arcsec}$ and the diameter of the Airy disk of 4.9 μm for the central wavelength. The D_{80} diameter of images is less than 8.2 μm along the field of view. Thus, the system under consideration provides nearly diffraction-limited images in a sufficiently wide field of view and an extended spectral range.

The folded mirror obscures both the incoming light beam and the beam reflected by the secondary mirror; the latter factor is more significant. The angle of fracture of the initial optical axis, -30° , is chosen approximately, so a small reduction in vignetting can be achieved by optimizing this parameter.

The choice of fused silica as a material for lenses is only partly due to the excellent optical properties of this glass; many other types of glass are also suitable.

It is also worth noting that the cross-shaped optical scheme of the telescope makes it possible to realize a fairly compact design.

Evidently, replacing the two-lens corrector with a concave mirror will result in a three-mirror telescope of the type described long ago by Dimitroff and Baker (1945), although with dissimilar types of mirror surfaces (see also Wilson 1996, p. 223). In this way, it is possible to provide high-quality images on a spherical focal surface, but the linear obscuration of light in the system

risers to at least 0.25. The latter not only is undesirable in itself but also worsens the concentration of energy in a star's image.

The most obliging features of the proposed system are the curvature of the focal surface, the large size of the secondary mirror, and the significant asphericity of both mirrors with optical power.

The first point cannot now be regarded as a serious drawback of the optical layout (Section 1.3.2). On the other hand, it is possible to achieve a flat focal surface by increasing the number of lenses in the corrector to four, using suitable glass grades for them (say, from a list of Ohara recommendations) and slightly relaxing the restriction on the amount of distortion. As a result, the system becomes more complicated, so it is reasonable to ask about general priorities.

As for the second of the problems mentioned above, the significant size of the secondary mirror seems to be an unavoidable feature of this layout at a low focal ratio and a large field of view. Only because of this a two-mirror system, in essence, attains such a low vignetting of useful light in the absence of direct background illumination.

Finally, let us turn to the third point. According to Table 3.7 and to Eq. (C2) of Appendix C, the maximum asphericity gradient is $2.5 \mu\text{m}/\text{mm}$ and $3.0 \mu\text{m}/\text{mm}$ for the primary and secondary mirrors, respectively. These are noticeable values, but they are quite within the limits of modern technology.

The optical layout discussed here may be useful not only for space telescopes but also for ground-based versions.

3.3 Three-Mirror Paul Telescope with a Lens Corrector

Section 3.2.2 stated that the opinions of experts were divided regarding the ways to achieve the impressive goal of recording events on the entire celestial sphere to a stellar magnitude of at least 24 with an update time of the order of a few hours. The first path involves the mounting of several telescopes with a field of view of about 3° and an aperture of 1.5–2 m. at separate locations; the second way is based on the creation of a single telescope with approximately the same field of view but with an essentially larger effective aperture, say, of about 6.5 m. A representative of the former direction is the Pan-STARRS survey, described in Section 3.2.2, while the only example of the latter is the *Large Synoptic Survey Telescope* (LSST), which is currently in the final manufacturing stage (Fig. 3.11).

3.3.1 LSST project

The starting point for the LSST optical design was the *Dark Matter Telescope* proposed by Roger Angel, Michael Lesser, Roland Sarlot, and Edward Dunham (2000). Later, some details of the project were changed (in particular, the field increased from 3.0° to 3.5° , and it was decided to place the mirrors M_1 and M_3 on one blank), but the basis of the original project was preserved. The early stage of the project is described by Walker (2002).

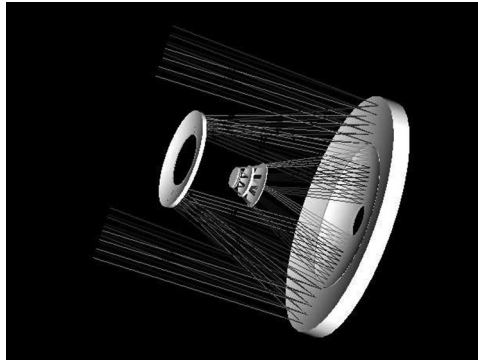


Figure 3.11 Optics of the Large Synoptic Survey Telescope with an entrance pupil diameter of 8.36 m, effective diameter of 6.68 m, and a flat field of 3.5° .

According to the *Astro2010* report,⁸ “Large Synoptic Survey Telescope (LSST) is a wide-field optical survey telescope that will transform observation of the variable universe and will address broad questions that range from indicating the nature of dark energy to determining whether there are objects that may collide with Earth.”

To perform these goals, the optical layout of a three-mirror Paul telescope was chosen (Fig. 2.13), supplemented with a three-lens field corrector at the tertiary focus (Allsman et al. 2006, Gressler 2009, Fig. 3.12). The need to provide a large effective aperture and a wide field of view under significant vignetting of light resulted in an increase of the entrance pupil diameter up to

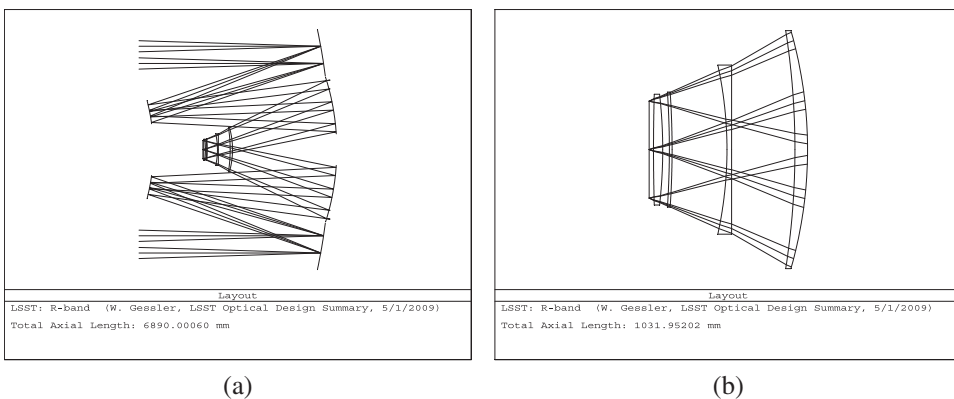


Figure 3.12 (a) Optical layout of the LSST, and (b) an enlarged LSST lens corrector. The curved filter is placed between the second and third lenses.

⁸ *Astro2010*, the current astronomy and astrophysics decadal survey, is the latest in a series of surveys that are produced every 10 years by the National Research Council of the National Academy of Sciences, U.S.A.

8.4 m. On the other hand, in order to match the optical resolution with that of modern detectors of light, the focal length of the telescope had to be made relatively short, 10.3 m, so that the LSST can be regarded as a huge and fast $f/1.23$ camera.

The telescope will be mounted on the Cerro Pachon peak in Chile. The construction of the dome began in 2011, and the scientific programs will begin towards the end of this decade. It is supposed that the telescope will give information on the southern sky up to 26^m-27^m , updated twice a week.

Let us give first a brief description of the telescope optics (Fig. 3.12). The 8.36-m primary and 5.0-m tertiary mirrors compose two zones of a single piece⁹ of a cast borosilicate glass; the 3.4-m secondary is made of Corning ULE material. The monolith M_1/M_3 mirror has been made by the University of Arizona's Steward Observatory Mirror Laboratory. The primary mirror and the concave surface of the middle lens in the corrector are even aspheres of sixth order, the secondary and tertiary mirrors are even aspheres of eighth order. All of the other surfaces, including curved filters, are of the standard type. The clear diameter of the largest lens is 1.55 m, and the flat image surface is 64 cm in diameter.

The expected star images in the six wavebands covering a wide wavelength range 0.32–1.06 μm are less than 10 μm , i.e., $0.2''$, taking into account the image scale 50 $\mu\text{m}/\text{arcsec}$. Thus, the 10- μm pixels are suitable to match the resolving powers of the optics and detector, thereby providing a high signal-to-noise ratio for faint objects. The image distortion is small, less than 0.1%. Obviously, the success of the project means just the stable realization of the designed image quality.

The detector is a 3.2-gigapixel mosaic with 10- μm pixels in $4\text{K} \times 4\text{K}$ sensor packages. The camera requires 6,400 channels of electronics to achieve 2-s read-out of each 15-s exposure. At such a high frame rate, nearly 120 TB of data will be acquired per night of observations.

It seems, nevertheless, that the basic obstacle in telescope development is not the handling of a huge stream of data but the stable implementation of tight tolerances for the large-scale $f/1.23$ optical system. Placing two mirrors on one substrate reduces the number of degrees of freedom and transfers the permanent difficulties of telescope operation to the unique manufacturing two coaxial large mirrors with smooth surfaces of the proper shape (at least three simultaneous conditions!).

Only the optical speed and the supposed pixel size result in shallow depth of focus: of about 10 μm . The tolerances on the spacing ($\sim 100 \mu\text{m}$), decenter ($\sim 50 \mu\text{m}$), and tilt ($\sim 7''$) of the optical elements are severe but workable. More demanding tolerances should be met for the shape of the mirror

⁹ Rumsey (1969) first pointed out the possibility of combining the primary and tertiary mirrors onto a single blank.

surfaces. Without going into details, we will mention only that the tolerances on the conic constants of the mirrors are of the order of 10^{-4} . The rigorous tolerances are also required for deviations of even aspheres from the standard surfaces.

There are five aspheric surfaces in the system, including one conic section and four even aspheres. The most steep of them are the primary and tertiary mirrors, as well as the concave surface of the middle lens; the corresponding gradients of asphericity are $2.85 \mu\text{m}/\text{mm}$, $1.40 \mu\text{m}/\text{mm}$, and $4.33 \mu\text{m}/\text{mm}$. These values are quite acceptable for modern technology (Appendix C). In this respect, the LSST favorably differs from some other existing wide-field systems, in which extremely high gradients were unreasonably allowed.

Tight tolerances required a new approach to the manufacture of complex optical systems (Seppala 2010). Unlike usual practice, where a system design is performed first and null tests for the optical components are determined later, the LSST itself and all necessary layouts of optical control have been designed in common. Seppala (2010) and Tuell et al. (2010) go into further detail about the various control schemes. The manufacture of mirrors M_1/M_3 on a single block of glass was carried out between 2008 and 2015.

Like all modern telescopes, the LSST includes the refined control systems of active optics. Indeed, in view of tight tolerances, it will not be easy to ensure the proper function of the numerous interconnected auxiliary systems during open-air observations.

At the same time, while the LSST will face serious technical challenges, there are significant positive factors that provide hope for the successful fulfillment of the project. According to Allsman et al. (2006), the most convincing of them is that “the telescope active optics, wave-front sensing, guiding, and observational monitoring systems are modern technologies with counterparts working in the field today.”

Returning to the dilemma outlined in Section 3.2.2 regarding the choice of a single very large telescope versus several smaller telescopes, it is difficult to avoid the impression that the second option would be closer to the optimum if one provide a reasonable optical layout of telescopes with apertures of the order of 2.5–4.5 m. Matching the optical system with the detector plays a key role in this problem. Undoubtedly, the highest productivity will reach *a hierarchical system of telescopes, each of which is designed as part of a general project*. The latter can proceed, for example, from the [Magnitude – Time] diagram, which sets the time for updating information (*cadence time*) concerning objects of a given stellar magnitude (see Section 1.1.4).

Chapter 4

Catadioptric Systems with a Full-Aperture Lens Corrector

Moving on to systems with the full-aperture lenses, we cannot hope to achieve large apertures; however, very wide fields of view of high quality often compensate the moderate apertures of such telescopes. As discussed earlier, the essential part of observations mentioned in the Introduction is at present carried out by means of catadioptric telescopes of 0.5–1.0 m in diameter and a field of up to about 10° . Moreover, even in the future relatively small telescopes with a wide field will be in demand for recording bright enough transient events in the sky.

All systems considered in this chapter proceed, in fact, from the ‘ideal’ telescope of Petzval–Vogel–Strehl and its embodiment in the form of the Schmidt camera, both of which were outlined in Section 1.3.3. Classical systems of this kind have been repeatedly discussed in the literature. It would seem that it is sufficient here to go directly to systems developed in the last couple of decades, but modern systems cannot be understood if their classical roots remain even a little unclear. Besides, the specific implementations of numerous designs of the type discussed are so diverse that a general look at the topic is required.

4.1 Singlet Full-Aperture Corrector

A decade after the pioneering Schmidt (1931) investigation, four patents for replacing a difficult-to-manufacture corrector plate with a single spherical lens were proposed almost simultaneously. D. Gabor (1941), A. Bouwers (1941), D. Maksutov (1941), and K. Penning (1941) relied on the fact that the meniscus—a lens, in which both surfaces have close radii of curvature of the same sign—can partly compensate for the spherical aberration of the spherical mirror.

As far as the author knows, the design proposed by Penning was not discussed in the open press.

The Bouwers system, studied in detail later (Bouwers 1946), was developed in connection with astronomical goals. The basic idea was to preserve the point symmetry of the Schmidt camera by making the meniscus surfaces concentric with a spherical mirror, whereas the position of the meniscus is markedly shifted from the aperture diaphragm to the mirror. The Bouwers system did not find practical application, because it leaves noticeable spherical aberration and introduces inadmissible longitudinal color. Due to symmetry, images of stars at various field angles remain the same but look equally bad. For example, a concentric $f/2.5$ telescope, optimized in the spectral range 0.40–0.85 μm with an aperture of 0.5 m (the meniscus is made of fused silica), provides images with an RMS spot size of 114 μm (19") throughout a 3° curved field. The width of the chromatic focal shift curve is more than 1 mm at all pupil zones, i.e., the system is severely affected by longitudinal color. All of these characteristics are an order of magnitude worse than those provided by an $f/2$ Schmidt camera with a 10° field (see Section 4.1.1 below).

The Gabor scheme was designed to project images formed by a cathode-ray tube. Little information about the system is contained in the Maxwell (1972) monograph; a more detailed description is given by Shafer (2017). According to the latter, the idea of the Gabor system is that the first surface of the correcting lens is concentric with the center of the entrance pupil, whereas the second surface of the lens is aplanatic for axial rays—it slightly changes the direction of the chief ray so that it falls on the spherical mirror normally. The mirror is concentric about the shifted (due to second lens surface) pupil. Shafer notes that, in view of the greater optical power of the lens, the Gabor system suffers more from longitudinal color than the design of Bouwers and therefore requires achromatization with the aid of an additional lens.

As for the fourth of the systems mentioned above, a more detailed description appeared shortly after its advent (Maksutov 1942, 1944, 1946).¹ The articles of 1942 and 1944 were the first open publications on meniscus telescopes, but Maksutov's priority is not based only on this fact. The crucial step was the proposal of a new type of lens: the *achromatic meniscus*. This is a meniscus on the surfaces of which the longitudinal color has approximately the same absolute value but the opposite sign.² It was this feature that ensured the paradoxical feasibility of a telescope with a single full-aperture spherical lens.

1 A corresponding prototype with a diameter of 100 mm was successfully tested in 1941. It is stored in the museum of the Pulkovo Observatory.

2 The totalities of concentric and achromatic menisci do not intersect. As noted by Wynne (1956, p. 321), "Another form of meniscus lens corrector for a spherical mirror which is superficially similar to the monocentric meniscus and has been confused with it, but has quite different aberration characteristics, was first described in English by Maksutov in 1944." However, such confusion can be found even in modern literature.

We only briefly cover numerous modifications of the classical Schmidt system with a singlet aspheric corrector, because this topic has been repeatedly discussed in the literature (see, e.g., Köhler 1948, Linfoot 1955, and Bowen 1967). Besides, this direction has largely lost its relevance since modern all-spherical systems with two full-aperture lenses achieve the goal more simply.

4.1.1 Classical Schmidt camera

As stated in Section 1.3.3, in order to eliminate spherical aberration of an ordinary (not Mangin) spherical mirror, Schmidt inserted a corrector plate of complex shape into the entrance pupil of the system (Fig. 1.4). To find out the shape of the plate’s surface, Schmidt resorted to an approximate analytical solution. With the help of powerful modern programs of optical calculations, it is not difficult to get an optimal design of Schmidt’s system given a set of integral parameters. Figure 4.1 shows an example of such a design for a Schmidt telescope with an aperture 0.5 m in diameter and a field of view of 10°. The performance of the system is given in Table 4.1.

As expected, the main feature of the Schmidt system—the location of the corrector plate at the center of the curvature of the spherical mirror—provides nearly the same image quality throughout the very large field. Since the Schmidt system has approximate point symmetry, the focal surface has a spherical shape and is located in the middle of the corrector and the mirror. A small shift of the focal surface relative to the exact average position (the ‘focal gap’) is important; we shall discuss this feature below. The design has a noticeable longitudinal color (Fig. 4.2), but chromaticity still remains acceptable. The lateral color is negligible for the same reason as the other off-axis aberrations.

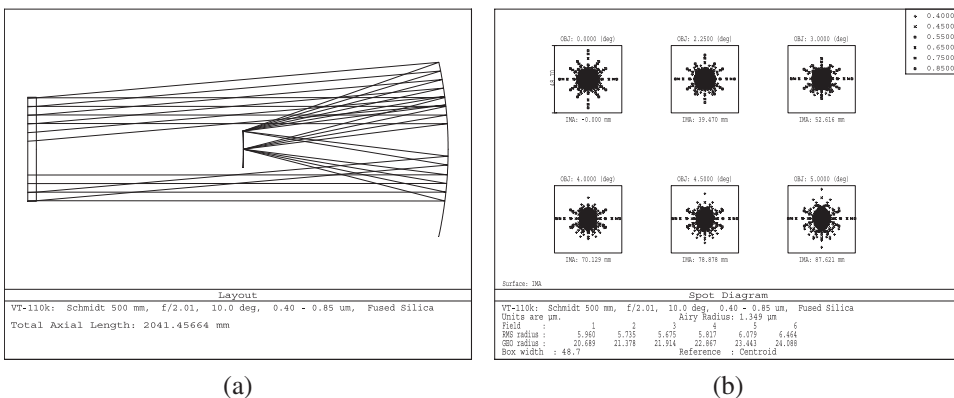


Figure 4.1 (a) Optical layout of the Schmidt system (VT-110k design). (b) Corresponding spot diagrams in the curved focal surface for the integral waveband 0.40–0.85 μm; the box width is 48.7 μm (10'').

Table 4.1 Performance of the 500-mm Schmidt telescope with a 10° field (design VT-110k).

Parameter	Value
Entrance pupil diameter	500 mm
System focal length	1005.42 mm
System focal ratio	2.01
Spectral range	0.40–0.85 μm
Angular field of view	10.0°
Mirror curvature radius	−2000.0 mm
Meniscus maximum asphericity gradient	1.39 μm/mm
Back focal length	−994.638 mm
Focal gap	5.36 mm
Image curvature radius	−1000.22 mm
RMS spot size	11.6–13.2 μm (2.4″–2.7″)
D_{80} image diameter	13.2–17.4 μm (2.7″–3.6″)
Total system length	2041.5 mm

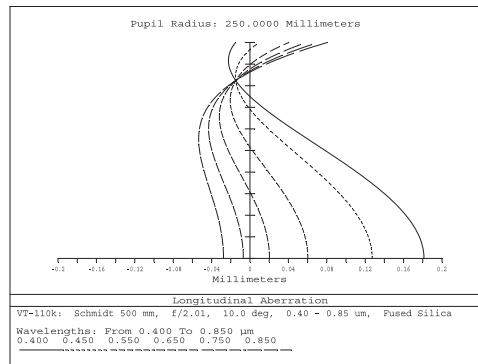


Figure 4.2 Longitudinal color in the VT-110k design. The horizontal axis shows focal displacements (μm) for different wavelengths, the height (mm) of the zone at the entrance pupil is given along the vertical axis. Horizontal sections are the usual chromatic focal shift curves for each zone.

Let us turn to the ‘heart’ of Schmidt’s system: the corrector plate. It is assumed in our design that the plate is made of fused silica. Both sides have an infinitely large radius of curvature; the front surface is really flat, whereas the asphericity is superimposed on the rear surface in the form of a so-called *even asphere*. The sag of such a surface is described by Eq. (1.12), which in a case of infinite radius of curvature takes the following form:

$$z(x, y) = \alpha_1 r^2 + \alpha_2 r^4 + \dots + \alpha_N r^{2N}, \quad r = \sqrt{x^2 + y^2}. \quad (4.1)$$

In the model under consideration, we limit this polynomial with only two terms, so that the relief of the second surface is given by

$$z = \alpha_1 r^2 + \alpha_2 r^4, \tag{4.2}$$

where the design coefficients optimized by numerical calculations are

$$\alpha_1^{(opt)} = -5.863 \cdot 10^{-6} \text{ mm}^{-1}, \quad \alpha_2^{(opt)} = 6.908 \cdot 10^{-11} \text{ mm}^{-3}. \tag{4.3}$$

In order to understand the Schmidt system, we should explain, at least approximately, these values. Fortunately, it is very simple to do this.

Suppose that a parallel beam of monochromatic light falls on a system including the lens corrector with a refractive index n and a spherical mirror of radius R (Fig. 4.3). Two elements of the system are located at a distance R from each other. The front surface of the corrector of thickness $h(y)$ in the plane $x=0$ is flat, whereas the rear surface has some profile $z = t(y)$. We have to find the profile at a given height $t(y) \equiv h(y) - h_0$, which provides the best image at the system focus F .

The idea is that the correction plate should compensate for the difference between the spherical mirror S and the imaginary paraboloid P , which is free of spherical aberration.

First, one needs to find the distance $\delta z(y)$ between S and P at some height y . We write down the approximate equation of the circle of radius $R > 0$ in the form

$$z = -R \left[1 - \sqrt{1 - (y/R)^2} \right] \approx -\frac{y^2}{2R} - \frac{y^4}{8R^3}, \tag{4.4}$$

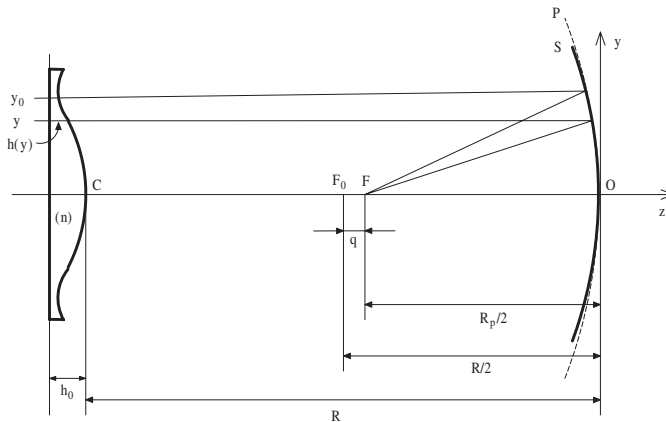


Figure 4.3 Schematic representation of a Schmidt system. The following notations are accepted: C – center of curvature of the spherical mirror S of radius R ; F_0 – the paraxial focus of the mirror; F – focus of the system; $h(y)$ – thickness of correction plate at a height y , which can be more or less than its central thickness h_0 ; and $R_p/2$ – focal length of the auxiliary paraboloid P . The values R , $h(y)$, h_0 , and R_p are assumed to be positive.

whereas the exact equation of the parabola of paraxial curvature radius $R_p > 0$ is

$$z_p = -\frac{y^2}{2R_p}. \quad (4.5)$$

Thus,

$$\delta z(y) \equiv z - z_p \approx \frac{y^2}{2} \left(\frac{1}{R_p} - \frac{1}{R} \right) - \frac{y^4}{8R^3}. \quad (4.6)$$

We assume that R_p is slightly less than R , i.e., $R - R_p \ll R$. Let us choose the paraxial radius of the paraboloid so that the latter intersects the sphere at some height $y_0 \geq 0$ (generally speaking, y_0 can exceed the aperture radius $D/2$). It follows from the equation $\delta z(y_0) = 0$ that

$$y_0^2 = 4R^3 \left(\frac{1}{R_p} - \frac{1}{R} \right), \quad (4.7)$$

so that Eq. (4.6) can be written in the form

$$\delta z(y) = \frac{y_0^2 y^2 - y^4}{8R^3}. \quad (4.8)$$

This deviation causes a relative temporal advance of the light wave upon reflection from the sphere, equal to $2\delta z(y)/c$, where c is the speed of light in air. It is precisely such a retardation that a correction plate must make to compensate for the difference of the sphere from the paraboloid. Since the velocity of light in the glass is c/n , a layer of glass of thickness $h(y)$ at height y introduces a delay $[h_0 - h(y)](n - 1)/c$ in comparison with the axial beam. Equating the two time intervals, we find

$$t(y) = \frac{-y_0^2 y^2 + y^4}{4(n - 1)R^3}, \quad (4.9)$$

where $t(y) \equiv h(y) - h_0$ is the desired profile of the correction plate. For convenience, we rewrite the last equation in the form adopted for aspheric surfaces:

$$t(y) = \alpha_1 y^2 + \alpha_2 y^4, \quad (4.10)$$

where

$$\alpha_1 = -\frac{y_0^2}{4(n-1)R^3} = -\frac{2q}{(n-1)R^2}, \quad \alpha_2 = \frac{1}{4(n-1)R^3}, \quad (4.11)$$

and

$$q \simeq \frac{y_0^2}{8R} \quad (4.12)$$

is the length of the segment F_0F between the foci of the sphere and the paraboloid (Fig. 4.3). The last relation follows from Eq. (4.7).

The *focal gap* q (or y_0) remains a free parameter in a frame of the consideration based on accounting for only the longitudinal spherical aberration. It is worth recalling in this connection that the latter is $D^2/16R$ for a spherical mirror of diameter D and of radius R . The optimum choice of q allows one to change the shape of the aspheric surface in the desired way to get a trade-off between the image quality and complexity of the corrector surface. In particular, according to Linfoot (1949, 1955), the minimum chromaticity of the corrector plate is attained at a q value equal to

$$q_* = \frac{3}{64} \frac{D^2}{R}, \quad (4.13)$$

i.e., almost reaching the longitudinal spherical aberration of the mirror.

Thus, we come just to Eq. (4.2) for the shape of the corrector's surface, which was found by numerical calculations. It remains only to check the proximity of the analytical approximation given by Eq. (4.11) to the optimized values of the model parameters according to Eq. (4.3). Let us take the average wavelength $\lambda_c = 0.625 \mu\text{m}$ in the considered waveband; the corresponding refractive index $n(\lambda_c) = 1.4572$ for the fused silica. After setting the mirror curvature radius $R = 2000.0 \text{ mm}$ and the focal gap $q = 5.362 \text{ mm}$ (see Table 4.1), we get the following from Eq. (4.11):

$$\alpha_1 \simeq -5.864 \cdot 10^{-6} \text{ mm}^{-1}, \quad \alpha_2 = 6.835 \cdot 10^{-11} \text{ mm}^{-3}. \quad (4.14)$$

Taking into account the high speed of the system and simplifications adopted, the agreement with Eq. (4.3) should be considered very good. This shows that the analytical approach under consideration grasps the essence of the matter, although with more rigorous analysis it is necessary also to consider other aberrations (in particular, spherochromatism) and to increase the order of the series expansions. For example, aberrations of the fifth order can be eliminated by adding a term of the sixth power into Eq. (4.2); the subsequent terms are of little importance, and therefore they are usually neglected.

It is indicative that the presence of a quadratic term in the profile Eq. (4.10) is ensured only by the nonzero focal gap q , with the signs of the two terms being opposite. At $q=0$, the aspheric component would look like a smooth valley with a flat bottom unfolded at its edges to the mirror. In the opposite case, the profile is more complicated, as illustrated in Fig. 4.4. The figure proceeds from the dimensionless form of Eq. (4.10), namely,

$$t/A = Y^2 (Y^2 - Y_0^2), \quad Y \equiv y/H, \quad Y_0 \equiv y_0/H, \quad (4.15)$$

where the height of the ray is normalized by the radius of the aperture $H \equiv D/2$, and

$$A \equiv \frac{D^4}{64(n-1)R^3}. \quad (4.16)$$

Here, D is the diameter of the correction plate, and R is the radius of the spherical mirror. Since the mirror is usually substantially larger than the plate, the use in Eq. (4.16) of a focal ratio can lead to misunderstandings.

In order to give an idea of the real profile scale of the corrector plate, we write out several numerical values concerning the VT-110k design shown in Fig. 4.1. The constant $A = 267 \mu\text{m}$; the maximum depth of the aspheric relief is $-125.8 \mu\text{m}$, which is reached at a distance 207.1 mm from the optical axis. As can be seen, the relief of the corrector plate is not only complicated but also deep enough in the wavelength scale. Recall that in order to correct

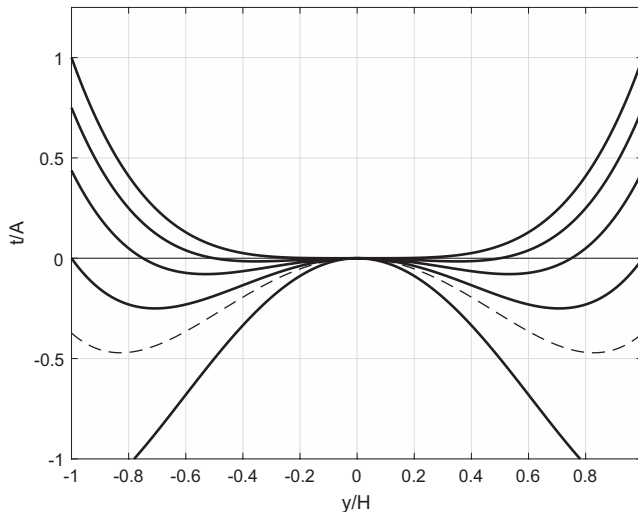


Figure 4.4 Solid lines, from top to bottom: Profiles of the corrector plate according to Eq. (4.15) for $Y_0 = 0, 0.50, 0.75, 1.0$, and 1.5 . The dashed line corresponds to the VT-110k design.

spherical aberration of the mirror (see Fig. 1.5), the central part of the plate must act as a positive lens, while the outer part acts as a negative lens.

The Schmidt system realizes, albeit in a complex way, a deep theoretical concept in its pure form and therefore remains unique. It is very likely that the achievements of modern technology allow one to level the difficulties of manufacturing a corrector plate, so that the Schmidt camera will receive a second life. The laconism of this system is particularly attractive for space research. This is evidenced, e.g., by the success of the recent Kepler mission, which used a Schmidt camera with a diameter of 95 cm and a field of 115 square degrees.

4.1.2 Modifications of Schmidt camera

Providing a good field of view of about 10° in diameter with the use of a minimum number of optical elements, the Schmidt camera is not devoid of some features that can be considered disadvantages. The most significant of them are

- The curvature of the focal surface;
- An excessive length of the optical assembly, which is twice the focal length;
- The longitudinal chromatic aberration caused by the corrector plate; and
- The complexity of the relief of the corrector plate.

At the same time, these features are due to the very idea of the system, so the rejection of the point symmetry underlying the Schmidt camera must inevitably lead to a decrease in the field of view. Therefore, the frequently used term ‘modified Schmidt camera’ means simply that certain characteristics of the telescope that are of special interest, including those mentioned in the above list, are achieved at the cost of reducing the field. Apparently, the term ‘version of a Schmidt camera’ is more adequate in such cases.

4.1.2.1 Adding a field flattener and direct shortening

The first modifications were made by Schmidt himself. In particular, he suggested the addition a field flattener in the form of a single Piazzì–Smith plano-convex lens to the original camera design. This step is more useful because it entails the need to bring the corrector slightly closer to the mirror.

The direct reduction of length of the original system, when only two optical elements are retained, has been investigated by Wright (1935) and Väisälä (1936). They showed analytically that doubling the aspherics on the corrector plate and turning the mirror into an oblate ellipsoid are necessary for a significant reduction in length. In this case, the focal surface becomes either flat or slightly curved. We have to pay for all this by doubling of

longitudinal color and, eventually, the most attractive property of Schmidt's camera: the size of its field of view.

In subsequent years, a few Wright–Väisälä (WV) telescopes were manufactured, until Charles Wynne (1977) found that "...A system consisting of an aspheric plate, a spherical mirror and a self-achromatic lens some distance in front of the focus can be corrected for spherical aberration, coma, astigmatism, field curvature and chromatic difference of focus over a wide spectral range. Compared with a Schmidt camera of the same focal length, these systems have an overall length that is considerably shorter, by an amount that can be controlled in the design." Naturally, modern versions of a Schmidt camera follow Wynne's approach.

In order to show more clearly the difference in approaches, we first designed a pure $f/2.0$ Wright–Väisälä model with the same diameter of 500 mm as the Schmidt model VT-110k discussed in the previous paragraph but shortened to 1500 mm from previous 2042 mm (Table 4.1); the curvature of the focal surface remained free. The result should be considered disappointing. The field of view had to be reduced from 10° to 2.5° with the worst image quality (RMS spot size $3.3''$ – $5.6''$), the mirror became a prolate ellipsoid with a conic constant of 0.3525, as required the WV theory, and the depth of the aspheric relief on the corrector plate increased significantly, also in accordance with the WV theory.

As recommended by Wynne, the alternative model was Schmidt's initial system, to which we added a three-lens corrector in front of the focal surface to make this surface flat and to shorten the system's length to 1500 mm. The $f/2.05$ design VT-110f (Fig. 4.5) obtained in this way has a flat field of 7.5° (134.5 mm) in diameter and image quality $D_{80} = 1.6''$ – $2.2''$ in the integral

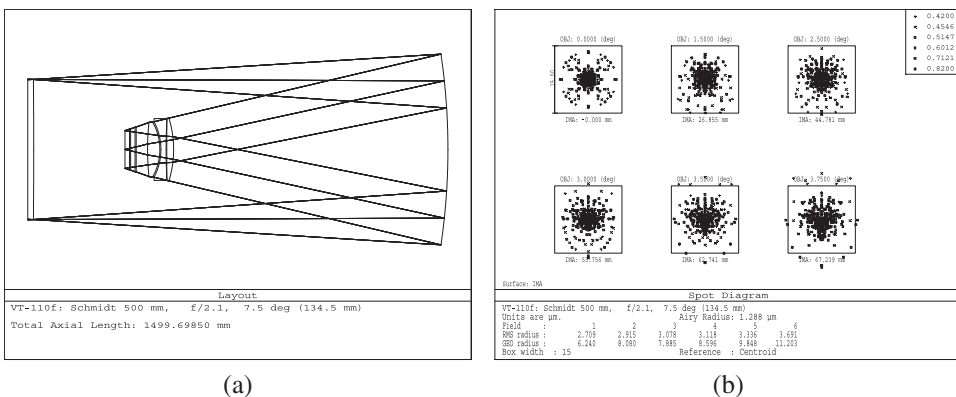


Figure 4.5 (a) Optical layout of a 500-mm compact Schmidt system with a 7.5° flat field (VT-110f design). (b) Corresponding spot diagrams for the integral waveband 0.42 – $0.82 \mu\text{m}$; the box width is $15 \mu\text{m}$ ($3''$).

spectral range of 0.42–0.82 μm . Standard but rather expensive grades of glass were used for the prefocal lenses. It should not be overlooked that the compactness of the telescope is largely due to the high asphericity gradient of the corrector, its maximum value is 7.48 $\mu\text{m}/\text{mm}$ (Appendix C). A complete description of the system VT-110f, along with data for the alternative all-spherical systems, is provided by Terebizh (2016b).

Although the example above shows the possibility of achieving acceptable image quality in a sufficiently wide field, it seems that the latest all-spherical designs are easier to achieve the goal.

4.1.2.2 Schmidt–Cassegrain design

An attractive way to shorten the Schmidt camera and simultaneously flatten the focal surface assumes adding a second, now convex, mirror and moving the focus by the Cassegrainian method. There are a number of options here related to the spherical or aspheric shape of the mirrors, as well as to the position of their centers of curvature. Initial studies of all these directions were made by Baker (1940), Burch (1942), and Linfoot (1943, 1944, 1955). Several practical decisions of a small size are given by Rutten and van Venrooij (1999). Since an exhaustive analytical study is presented in Linfoot (1955), Wilson (1996), and Schroeder (2000), we confine the discussion to general remarks and a numerical example.

The equality of the radii of curvature of two mirrors may be efficient due to the known Petzval's theorem on the curvature of a focal surface (Born and Wolf 1999, Section 5.5.3). On the other hand, it seems attractive to make both mirrors concentric to maintain the point symmetry of the design. The first of these options helps to flatten the focal surface, while the second one preserves the size of the field of view. In addition, the spherical shape of one or both mirrors can be important in terms of their manufacture or expansion of the field. However, these considerations are quite speculative, because the inevitable addition of a multi-lens corrector in front of the focus essentially influences the appearance of a larger optics.

It seems that the possibilities of analytical investigation within the framework of the third-order theory of aberrations are insufficient to find the optimal layout for such a complex telescope. We used the capabilities of the ZEMAX program for this purpose.

All our trial designs had a 500-mm entrance pupil and a flat field of view 4.0° in diameter. It was assumed that the corrector plate is made of fused silica, its rear surface is a two-term even asphere given by Eq. (4.2), and the three lenses of the output corrector have spherical surfaces and are made of the standard (recommended) grades of Schott and Ohara glass. The optimization was carried out for the same spectral range 0.42–0.82 μm , which was adopted for the VT-110f design shown in Fig. 4.5.

It immediately became clear that fast systems with a focal ratio ϕ of less than ~ 3 , based on all combinations of spherical and aspheric mirrors, require a too high asphericity gradient (Appendix C). Of the slower models, we chose the $f/3.3$ design VT-110p (Fig. 4.6). On the side, the Baker's 81-cm version of a Schmidt–Cassegrain camera that was realized in the ADC telescope (Bloemfontein, S. Africa) has the same focal ratio and a field with a diameter of 4.6° (24 cm).

Table 4.2 gives the main characteristics of the VT-110p design. We add that the primary mirror has a spherical shape with a radius of curvature of -2127.45 mm, whereas the secondary mirror is a hyperboloid with a paraxial radius of curvature of -2313.91 mm and a conic constant of -4.945 . Thus, the mirrors are far from concentric, but their radii of curvature are close: the first option discussed above is implemented. The whole system is compact

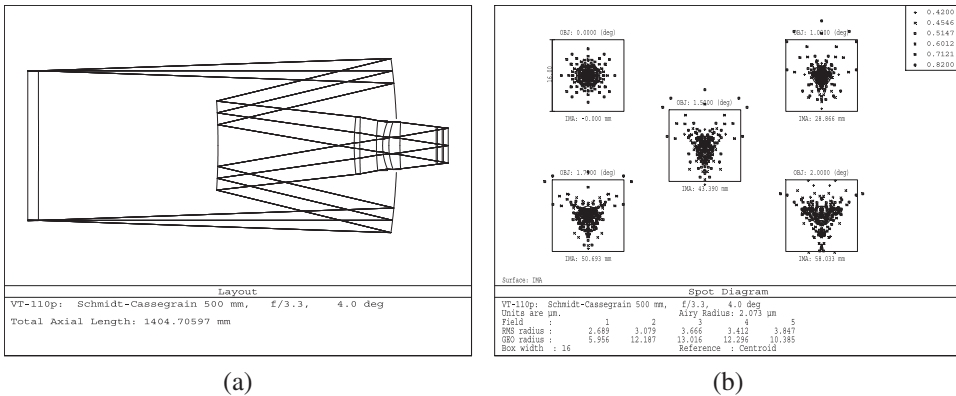


Figure 4.6 (a) Optical layout of a 500-mm Schmidt–Cassegrain $f/3.3$ system with a 4° flat field (VT-110p design). (b) Corresponding spot diagrams for the integral waveband $0.42\text{--}0.82\ \mu\text{m}$; the box width is $16\ \mu\text{m}$ ($2''$).

Table 4.2 Performance of the 500-mm Schmidt–Cassegrain $f/3.3$ telescope with a 4° field (design VT-110p).

Parameter	Value
Entrance pupil diameter	500 mm
System focal length	1651.1 mm
Scale in the focal plane	$8.0\ \mu\text{m}/\text{arcsec}$
Spectral range	$0.42\text{--}0.82\ \mu\text{m}$
Angular field of view	4.0°
Linear obscuration	0.64 across the field
Corrector maximum asphericity gradient	$1.24\ \mu\text{m}/\text{mm}$
Back focal length	159 mm
RMS spot size	$5.4\text{--}7.7\ \mu\text{m}$ ($0.67''\text{--}0.96''$)
D_{80} image diameter	$12.9\text{--}16.4\ \mu\text{m}$ ($1.6''\text{--}2.1''$)
Total system length	1405 mm

enough, well fixed for chromaticity, and provides good images throughout the flat field. The asphericity gradient is still acceptable.

The most significant shortcoming of the Schmidt–Cassegrain camera is the large vignetting of light. This time, the fraction of unvignetted rays is 0.59 throughout the field (the linear obscuration is 0.64), so the effective aperture of the design is only 384 mm. Ultimately, this is because of the inability to move the correction plate closer to the primary mirror.

4.1.2.3 Achromatization of the Schmidt camera

Of the four points listed at the beginning of Section 4.1.2, we have not yet discussed the chromaticity due to the correction plate. Since the plate is located at the entrance pupil, it does not introduce lateral color, but it still introduces longitudinal color (Fig. 4.2) and, most importantly, the dependence of the spherical aberration on the wavelength (spherochromatism). The latter becomes especially large when the focal ratio $\phi < 3$. For example, in the design VT-110k discussed in Section 4.1.1, the RMS wavefront error of the axial beam due to the spherochromaticity changes by 0.7 wavelengths in the transition from the blue part of the range to the red part. At the edge of the field, this error exceeds one wavelength.

For simplicity, we assumed above that one of the surfaces of the correction plate is absolutely flat. It was mentioned in the literature that giving it a spherical shape with a finite radius of curvature reduces the chromaticity. Of course, this complicates the manufacture of the corrector plate, but not radically. The corresponding check on the example VT-110k design discussed in Section 4.1.1 showed that the gain from this step is insignificant.

The minor image enhancement can be achieved by slightly moving the aperture stop from the aspheric surface inside the telescope (by 24.5 mm in the case of system VT-110k).

Baker (1940) and Bouwers (1946) studied a more effective, historical way to overcome chromaticity by applying a full-aperture double-plate corrector made of different glass. More precisely, this option transforms the original longitudinal color of the singlet into the secondary color of the achromatic pair of glasses. The first implementation of this approach was carried out by Wynne (1981) when creating the United Kingdom Schmidt Telescope at Siding Spring, Australia, in 1977. This telescope is a near duplicate of the famous 48-inch Schmidt camera of the Palomar Observatory (known as the *Samuel Oschin Telescope* since 1987), which was upgraded similarly in 1984. The theoretical aspect of the Schmidt camera with a double corrector is well covered by Schroeder (2000, Section 7.4); G. Smith (1998, Section B.6.6) did the same for numerical optimization using ZEMAX.

Perhaps doubling the corrector plate is an appropriate way if the Schmidt camera is not provided with a Wynne's multi-lens prefocal corrector-flattener, which looks simpler.

4.1.3 Maksutov telescope

A solution of practical interest to the problem of simultaneous correction of chromaticity and spherical aberration with one spherical lens was found by Dmitry Maksutov (1941, 1942, 1944). Concerning the significance of this achievement, Maxwell (1972, p. 27) wrote: “As all real systems are used over a finite bandwidth, it is not usually possible to use the unachromatized concentric meniscus, which means that some form of achromatic solution must be sought. Maksutov’s meniscus shines out as the most desirable solution under these (the usual) circumstances. Not only is it a single piece of glass, but it is capable of providing a better axial chromatic correction than the doublet achromatic meniscus, which suffers from the usual crown-flint secondary spectrum.”

In general, the Maksutov system does not reach such a high speed and wide field as the Schmidt camera (Belorossova et al. 1963, Mikhel’son 1976). The focal ratio for the first of them is usually more than 3–4; however, images are still acceptable at $\phi = 2.5$, as shown in Fig. 4.7 with the example VT-114b (the meniscus is assumed to be made of fused silica).

To achieve the goal, Maksutov had to combine two facts. The first was that there is a singlet lens that introduces very small chromaticity into the parallel light beam. This lens is a special kind of meniscus, and therefore he called it the *achromatic meniscus*. The second fact is that the achromatic meniscus can reduce the spherical aberration of a spherical mirror located further along the path of the rays.

Let us denote the radii of curvature of the meniscus surfaces by R_1 and R_2 , while its thickness and the refractive index of the glass will be denoted by t and n , respectively. Both R_1 and R_2 are values of the same sign for the meniscus, whereas $t \geq 0$ and $n \geq 1$ are assumed. According to Maksutov (1944), the condition that distinguishes the achromatic meniscus is

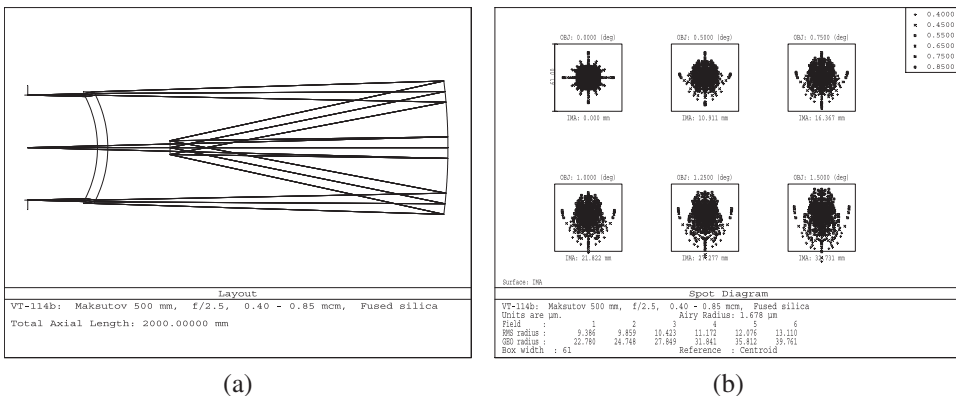


Figure 4.7 (a) Optical layout of the basic Maksutov system (VT-114b design with a 0.5-m aperture and a 3° field). (b) Corresponding spot diagrams for the integrated waveband 0.40–0.85 μm ; the box width is 61 μm (10”).

$$\frac{R_1 - R_2}{t} = 1 - \frac{1}{n^2}. \quad (4.17)$$

More specifically, if this condition is met, the chromatic aberrations on both surfaces of the lens are close in absolute value and have opposite signs. Note that, at a minimum, condition $R_1 > R_2$ must be met.

Equation (4.17) will be derived below, but for now, note that the left side depends only on the geometric characteristics of the lens, whereas the right side is determined only by its material. Assuming a typical value of $n \simeq 1.5$, we get about 0.56 for the right side. Thus, being both positive or both negative, the radii of the achromatic meniscus surfaces should be close to each other. For example, the right side of Eq. (4.17) equals 0.529 for the fused silica at the central wavelength $0.625 \mu\text{m}$ of the waveband $0.40\text{--}0.85 \mu\text{m}$ accepted in the VT-114b model discussed above.

But what is the situation for the other wavelengths that enter the Eq. (4.17) through the refractive index $n(\lambda)$? It is important that the changes along the spectrum are rather small: from 0.537 for the blue edge to 0.526 for the red. In practice, Eq. (4.17) slightly retreats from the exact performance for better chromatic balancing, e.g., the left side of this condition is 0.560 in the example VT-114b.

The achromaticity condition follows directly from the well-known expression for the focal length f of an arbitrary thick lens (see, e.g., Hecht 1998, Eq. (6.2)):

$$\frac{1}{f} = (n - 1) \left(\frac{1}{R_1} - \frac{1}{R_2} \right) + \frac{(n - 1)^2}{n} \frac{t}{R_1 R_2}. \quad (4.18)$$

The dependence of the focal length on the wavelength λ is due to the dispersion of light; it enters only via the refractive index $n(\lambda)$. Hence, the extremum of $f(\lambda)$ can be found from a requirement $\partial f / \partial n = 0$. Differentiating Eq. (4.18) with respect to n , we get

$$-\frac{1}{f^2} \frac{\partial f}{\partial n} = \frac{1}{R_1} - \frac{1}{R_2} + \left(1 - \frac{1}{n^2} \right) \frac{t}{R_1 R_2}. \quad (4.19)$$

To obtain Eq. (4.17), it only remains to equate the right side of the last equation to zero.

Finally, we can find the optical power of the achromatic meniscus ('AM') by substituting Eq. (4.17) into Eq. (4.18):

$$\frac{1}{f_{AM}} = -\frac{t}{R_1 R_2} \left(1 - \frac{1}{n} \right)^2 = \frac{n - 1}{n + 1} \left(\frac{1}{R_1} - \frac{1}{R_2} \right). \quad (4.20)$$

These formulas show that the achromatic meniscus is a negative lens. Since the thickness of the meniscus is usually much smaller than the absolute value of the radii of curvature of the surfaces, the optical power of the meniscus is small.

In itself, the achromaticity condition provides only a negligible longitudinal color, but it is important that Eq. (4.17) entails the *negative* longitudinal spherical aberration of the meniscus, while that is positive for a spherical mirror. Thus, the meniscus can substantially compensate for the spherical aberration of the spherical mirror, practically without introducing its own longitudinal color.

It is important also that slight movements of the meniscus along the optical axis can noticeably reduce coma of the meniscus telescope, so that in the end we get not only an achromatic telescope but also a nearly aplanatic system with a rather wide field of view.

Figure 4.7 gives an idea of the simplest form of the Maksutov telescope, when a concave meniscus with negative radii of curvature is located in front of the spherical mirror. As Maksutov (1946) noted, the achromatic meniscus can be turned with a convex side to the object, but then, to reduce coma, it will have to be moved further away from the mirror.

The main shortcomings of the basic Maksutov system are due to its departure from the point symmetry about the center of curvature of the mirror. In particular, the displacement of the meniscus from the aperture stop and the change in the thickness of the meniscus from its center to the edge lead to the appearance of lateral color (Section 1.3.4). Indeed, the light beams emerging from the stop at different field angles fall on different parts of the meniscus. The closer the working zone of the meniscus shifts to its edge, the more the shape of the zone approaches the prism, which stretches the image into a small spectrum directed toward the optical axis. For the VT-114b example under consideration, the length of the spectrum reaches $\sim 20 \mu\text{m}$ ($3.3''$) at the edge of the field.

To suppress chromaticity, Maksutov (1946) proposed the application of two menisci, deployed next to each other either by concave or convex sides. Such a two-meniscus telescope, AZT-16, with a diameter of 70 cm and a 5° field was installed in 1967 on Mt. Sierra Roble in Chile. The telescope provides $1.5''$ (RMS) image quality in the integral band $0.40\text{--}0.66 \mu\text{m}$ throughout the field.

A system with one meniscus located in front of the aperture stop and facing the concave side to the spherical mirror can be considered. In this case, chromaticity is so great for both the achromatic meniscus and, especially, for its concentric version that it is not possible to achieve good images.

Another difficulty of the Maksutov system is due to the rigidity of the tolerances on the design parameters. The optical power of the Schmidt corrector is close to zero, so it can be shifted and tilted within fairly wide limits. On the

contrary, the achromatic meniscus is required to have some optical power, so the tolerances for it are tougher. They are especially tight for the alignment of the two surfaces of the meniscus and its edge thickness (a clinoid shape). Fortunately, the Maksutov telescope allows for various types of retouching, suggesting light deviations from the spherical shape of the corrector and mirror.

In its pure form, the Maksutov system demonstrates a fine and fragile compromise between the simplicity of surfaces and the accuracy of manufacturing the entire optics. Its real significance lies in the fact that the achromatic meniscus serves as an important element of more complex systems, both in implicit and explicit forms, for example, in the Wynne and the Hawkins–Linfoot designs with a 30° field of view that are discussed in the next two sections.

4.2 Doublet Full-Aperture Corrector

The one-lens correctors considered in the previous section show an obvious lack of degrees of freedom. That's why we had to use surfaces of complex shape and tight tolerances for optical parameters. Designs with two lenses in an input corrector allow one to significantly alleviate both of the above difficulties. Although the mass of optical elements increases, as well as the mass of the mechanical design, this factor is often not very important for background telescopes of a moderate size.

4.2.1 Richter–Slevogt system

Robert Richter and Hermann Slevogt (Richter and Slevogt 1941, 1954) proposed an elegant way to implement a common desire to replace the essentially aspheric Schmidt plate with spherical elements, namely, a nearly afocal double-lens corrector made of a single type of glass.³

The sense of the system is that a one-glass corrector made of positive and negative lenses of equal optical power is practically equivalent to a flat plate, and therefore, it introduces only minimal longitudinal color, whereas the emergence of three additional free parameters allows one to compensate for the spherical aberration of the mirror and partly eliminate off-axis aberrations of the system. Moreover, the all-spherical corrector of almost zero optical power has much milder tolerances for parameters than the meniscus. As a result, we get a simple and efficient all-spherical system whose natural development provides a flat field of more than 5° in diameter.

Figure 4.8 depicts the $f/1.4$ Richter–Slevogt (RS) telescope with a 643-mm aperture, which is the scaled *Abb. 1* design of their patent of 1941. This telescope was made by Carl Zeiss at the beginning of the 1940s and was removed to the

³ A similar system was proposed one year later by James Houghton (1942, 1944).

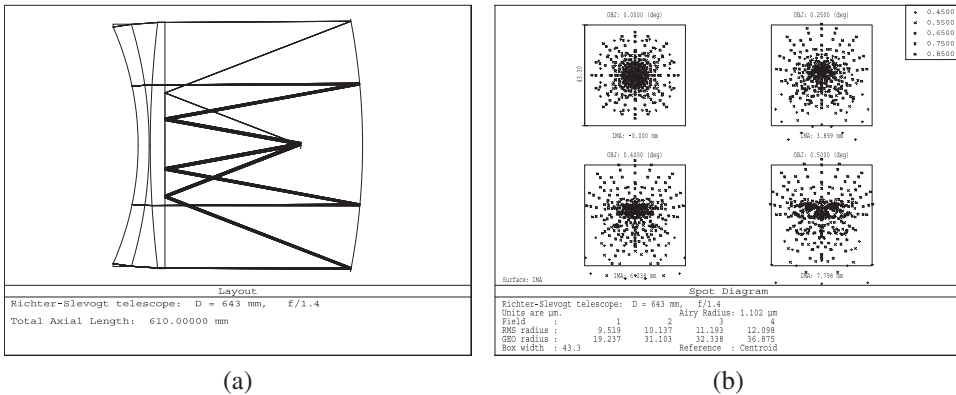


Figure 4.8 (a) Optical layout of the operating Richter–Slevogt 643-mm, $f/1.4$ telescope. (b) Corresponding spot diagrams for the integral waveband $0.45\text{--}0.85\ \mu\text{m}$ in a flat 1° field; the box width is $43.3\ \mu\text{m}$ ($10''$).

Crimean Astrophysical Observatory at the end of World War II. At such a size of the system, it is possible to leave the focus inside a tube. A reflective coating is put on the flat back surface of the corrector's rear lens. Three other versions of this camera, presented in said patent of Richter and Slevogt, include both internal and external focus positions. In 2010, the telescope shown in Fig. 4.8 was supplied with a three-lens field corrector of the author's design, which improved the image quality and expanded the field up to 3° .

Modification of the RS system, which has been studied by Terebizh (2001b), involves a significant increase in the distance between the corrector lenses, the optimal placement of the aperture stop, and the installation of a two-lens output corrector. In the issue, it was possible to substantially compensate for monochromatic aberrations, including the astigmatism and field curvature, thereby having increased the field of view diameter by an order of magnitude. The paper mentioned above also includes an extensive numerical comparison of tolerances for a set of Maksutov and RS designs of similar general performance. The significant advantage of the RS system is evident in this regard.

Figure 4.9 shows an example of a modified Richter–Slevogt design (see Terebizh 2016b for a complete description). The position of the aperture stop on the rear surface of a lens, where the secondary mirror is located, helps to reduce the vignetting of light. The linear diameter of a flat field, $134.5\ \text{mm}$, coincides with the diagonal length of the frequently used STA1600 CCD from Semiconductor Technology Associates. The pixel size of $9\ \mu\text{m}$ of this CCD corresponds to $1.2''$. Finally, the spot D_{80} size is $10.4\text{--}13.9\ \mu\text{m}$ ($1.4''\text{--}1.8''$), so the sampling factor χ defined by Eq. (1.21) is 1.8, an adequate value for exploration observations.

During the last decade, a number of telescopes of this kind have been made with an aperture from $25\ \text{cm}$ to $70\ \text{cm}$ and a field of view up to 10° .

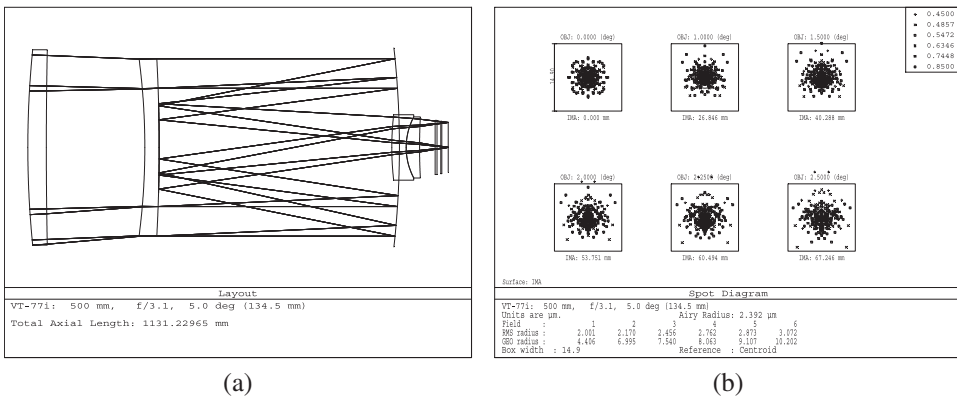


Figure 4.9 (a) The VT-077i, $f/3.1$ design with a diameter of 50 cm and a 5° (134.5 mm) flat field. (b) Corresponding spot diagrams for the integral waveband $0.45\text{--}0.85\ \mu\text{m}$; the box width is $14.9\ \mu\text{m}$ ($2''$).

Modifications of the original RS optical layout that do not involve a substantial increase in the spacing of two entering lenses also have been created. In particular, the astrometric URAT system of 85 cm in diameter provides a 4.5° field (Zacharias et al. 2006). A valuable feature of this study is connected with the comparative analysis of several alternative optical schemes, including a purely refractive system. URAT had successful first light on 2011.

4.2.2 Symmetrical corrector

The correctors of Schmidt, Maksutov, and Richter–Slevogt, used together with a spherical mirror, can achieve an angular field of view in the range of $5^\circ\text{--}10^\circ$. Further progress is hampered by their inherent drawback—breaking the strict point symmetry of an ‘ideal telescope’ of Strehl (Section 1.3.3). Therefore, it is not surprising that several researchers at about the same time proposed a corrector almost symmetric with respect to the aperture stop. The basic ‘building element’ in all cases was Maksutov’s achromatic meniscus; it is also important that in a system with two meniscuses facing each other with concave sides, chromatic aberration is substantially compensated (Section 4.1.3). The concrete embodiment goes back to Dyson (1944), Bennett (1945), Maksutov (1946), and Bouwers (1946); the advanced approach was proposed by Wynne (1947a, 1947b, 1950).

Figure 4.10 depicts a scaled and slightly optimized design discussed in the patent by Wynne (1950).⁴ All of the optical surfaces and the focal surface have a spherical shape, the corrector lenses are of one simple glass. The inner and

4 Wynne was the leader in the use of numerical methods in optics, but computational facilities were so scarce in the mid-20th century that designers rarely achieved feasible—in the modern sense—images. So, we assumed the responsibility to optimize some of the old designs a little to show their essence.

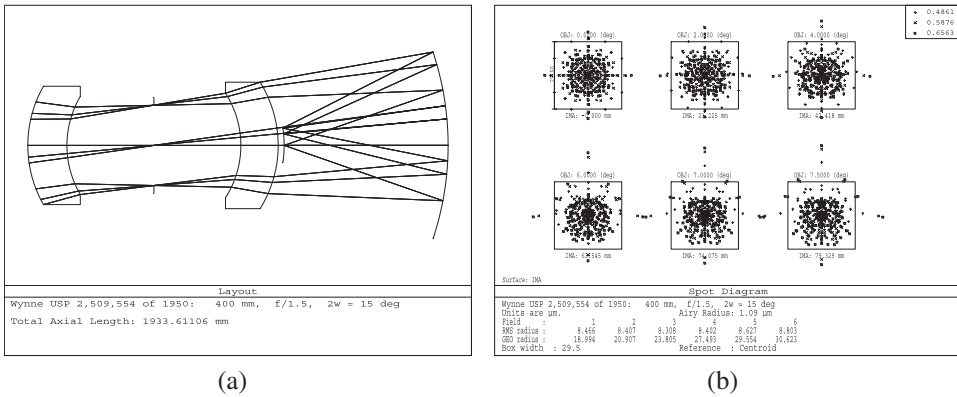


Figure 4.10 (a) Wynne (1950) $f/1.5$ design with a diameter of 40 cm and a 15° spherical field of view. (b) Corresponding spot diagrams for the integral waveband $0.48\text{--}0.65 \mu\text{m}$; the box width is $29.5 \mu\text{m}$ ($10''$).

outer surfaces of these lenses have the same radii of curvature; the second lens is slightly thinner than the first one (the quality of images is preserved even if the lens thickness is equalized). The aperture stop is located exactly in the middle between the lenses.

With regard to image quality, the RMS spot diameter is $16.9\text{--}17.6 \mu\text{m}$ ($5.7''\text{--}6.0''$) from the center of field to its edge. Given the not-too-wide spectral range, the Fraunhofer F-C lines, it is not high enough, but in this case it is important that the quality is constant across the field. The field can be noticeably expanded, so that the general principle underlying the system is productive.

Indeed, the system of the same type presented in Fig. 4.11 has twice the diameter of the field of view with better quality of images, $16.1\text{--}16.3 \mu\text{m}$

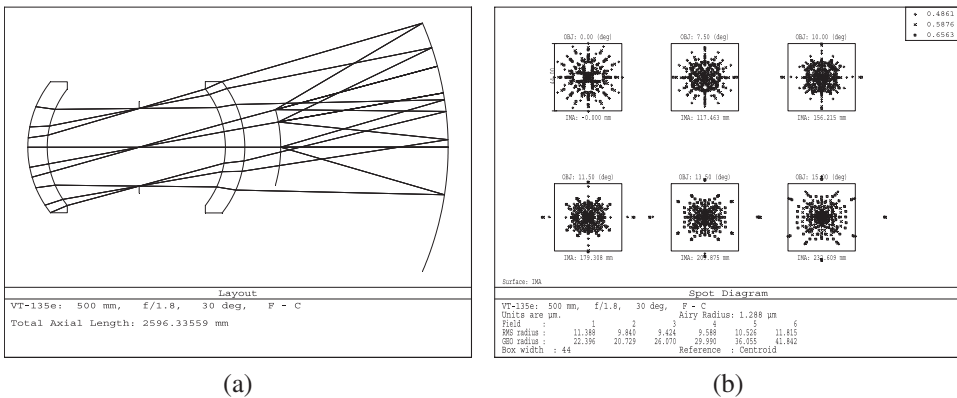


Figure 4.11 (a) VT-135e $f/1.8$ design of a Wynne-type telescope with a diameter of 500 mm and a 30° spherical field. (b) Corresponding spot diagrams for the integral waveband $0.48\text{--}0.65 \mu\text{m}$; the box width is $44 \mu\text{m}$ ($10''$).

(4.1"–4.2"), in a wider integrated range of the spectrum. This all-spherical design was created by optimizing for all variables. Note that the thicknesses of lenses are exactly equal to each other, whereas their distances to the stop are slightly different. Generally speaking, the lenses could be made absolutely identical, but then their position relative to the stop would become somewhat more asymmetric.

The almost exact point symmetry of the corrector relative to the aperture stop provides here the width of the field of view, while the mirror symmetry of the lenses compensates for the longitudinal color of the corrector. Spherical aberration of the primary mirror is well compensated by a slight difference in the shape of the two lenses or by their shift with respect to the diaphragm. At the same time, one would like to achieve even better compensation for spherical aberration and thereby improve images. We will turn to this in Sections 4.3.2 and 4.4.

An important conclusion to be made in connection with the subsequent description of much more complex aspheric systems that also use the refined glass: *a fully spherical telescope with a two-lens corrector made of one glass provides a curved field with a diameter of about 30° with an image quality of about 4", or 16 μm, adequate to resolve the photographic emulsion.* The real historical path in this area may be considered as more evidence that science and technology often do not develop in a consistent manner.

4.2.3 Hamiltonian telescopes

Until now, we have discussed systems with the usual, not Mangin, mirrors. Meanwhile, the latter have very attractive properties, discovered by Newton (Turnbull 1959, Whiteside 1969; Section 1.3.4) and Hamilton (1814). The essence of the matter is that the longitudinal color of a Mangin mirror has the opposite sign to that of a single lens (Fig. 1.6). Therefore, by combining only two large optical elements, a lens and a Mangin mirror, one can get an achromatic all-spherical wide-field system (Fig. 4.12). In addition, the parameters of the Mangin mirror can be coordinated in such a way that its spherical aberration becomes noticeably less than that for a simple mirror of close f -number.

A different look at this system is also helpful. In the original layout of Richter and Slevogt (Fig. 4.8), the longitudinal color due to a front lens is compensated by the second corrector lens, which is located close to the front lens. The subsequent modification of this scheme (Fig. 4.9) attains correction of color and, partly, monochromatic aberrations with a remote component of the corrector. In principle, we may move the rear lens further away until it merges with the mirror, so the whole system will consist of only two optical elements.

The prime focus seems to be preferable for such systems of large apertures. Figure 4.12 shows the resulting all-spherical system with a flat field (Terebizh 2007b). A few similar telescopes have been made over the past decade.

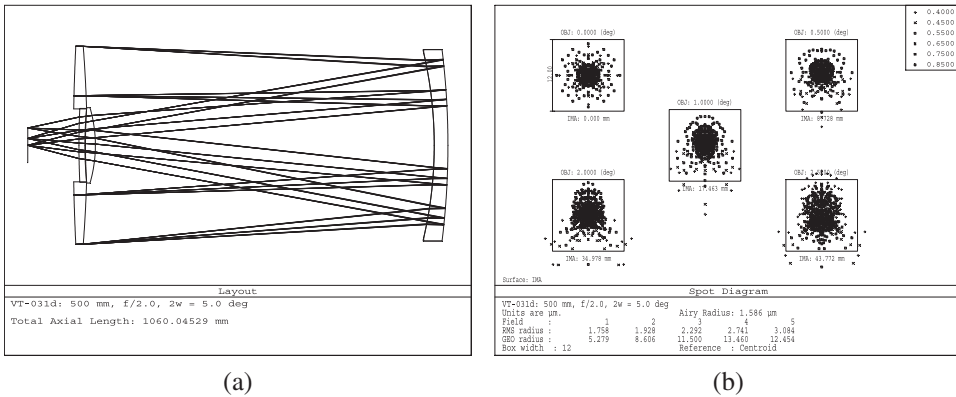


Figure 4.12 (a) VT-031d $f/2.0$ all-spherical design with an aperture of 500 mm and a flat field of 5° (88 mm). (b) Corresponding spot diagrams for the integrated waveband 0.40–0.85 μm ; the box width is 12 μm ($2.5''$).

The creation of a Mangin mirror has specific requirements compared to the creation of a common lens or a simple mirror of the same size (see Section 1.3.4). For this reason, the Mangin mirror should be made of glass with a low coefficient of thermal expansion, for example, fused silica, as is assumed in the design shown in Fig. 4.12.

4.2.4 The Ω_2 design

The external arrangement of the focal plane in a Hamiltonian system makes the detector more accessible and facilitates the removal of heat. On the other hand, this requires an opening in the lens and significantly increases vignetting. Both defects can be mitigated by allowing the light reflected from the mirror to pass through the front lens a second time. It will also allow one to use the lens as an element of the output corrector and thus achieve better performance. The corresponding design, called Ω_2 , was proposed by Terebizh (2007c, 2011).

Figure 4.13 depicts an all-spherical design of the Ω_2 type with a 7° flat field (Terebizh 2016b). Pay attention to the external location of the aperture stop. Both large elements are supposed to be made of fused silica. The system is compact: its total axial length is only 1207 mm.

For the image quality D_{80} in the range of $1.5''$ – $1.6''$ across the 7° field, the design VT-102j is an efficient instrument of survey observations. Its sky survey rate $\Gamma = 0.87$ herschels (Section 1.1.3). Figure 4.14 shows the relevant survey speed S and the limiting magnitude m_{lim} versus the exposure time T (Section 1.1.4). For example, the expected $m_{lim} \simeq 20.5$, and $S \simeq 1 \text{ deg}^2/\text{s}$ at $T = 20 \text{ s}$, so a sky area of 10^4 deg^2 will be registered in 3 hours.

At will, the fraction of unvignetted rays U in the telescope is unusually high, $U = 0.791$, for such a wide field of view. We also assumed in these

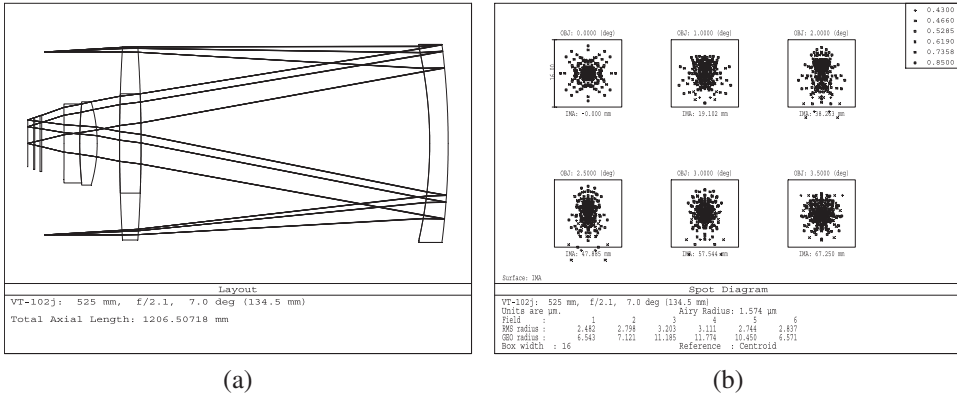


Figure 4.13 (a) VT-102j $f/2.2$ all-spherical design of the Ω_2 type with an aperture of 525 mm and a field of 7° (134.5 mm). (b) Corresponding spot diagrams for the integrated waveband $0.43\text{--}0.85 \mu\text{m}$; the box width is $16 \mu\text{m}$ ($3.0''$).

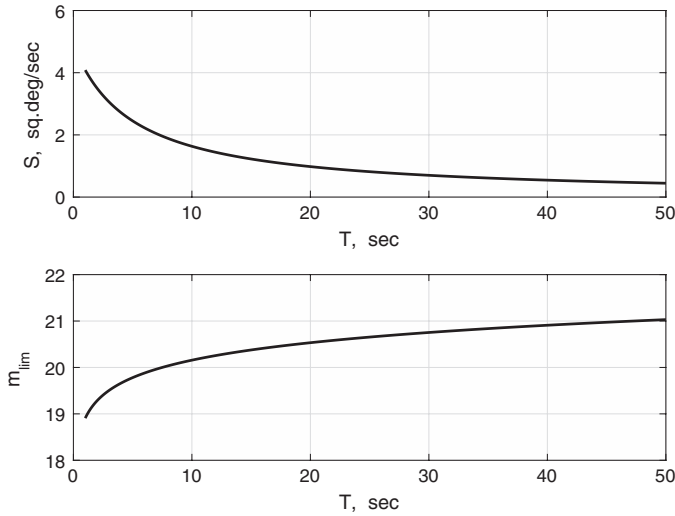


Figure 4.14 Survey speed S (deg^2/s) and limiting stellar magnitude m_{lim} as functions of the exposure time T (seconds) for the VT-102j design.

calculations that the telescope transparency $q_t = 0.75$ and the corresponding image size $\theta_{\text{tel}} = 1.6''$. The STA1600 detector is assumed with the pixel size of $9 \mu\text{m}$ and the quantum efficiency $\epsilon = 0.87$. The atmosphere blurring $\theta_{\text{atm}} = 1.5''$, the sky background is $20''/\text{arcsec}^2$, the object zenith angle is 30° , the bandwidth is $0.5 \mu\text{m}$, the dead time is 5 s, and the threshold signal-to-noise ratio $S/N = 7$.

We gave in Section 1.1.4 similar data for the 1-m telescope with a field of 3.5° . At the same exposure time of 20 s, objects of 2 stellar magnitudes weaker are attained with the 1-m telescope, but the survey speed is 4 times lower.

This once again demonstrates the need to create a unified set of instruments, designed as a whole to maximize the efficiency of deep wide-field sky observations.

It is necessary to mention that there is an extensive family of telescopes with two mirrors of the Mangin type, both primary and secondary, starting with the Flügge (1941) system and the closely related designs of Weidemann (1981) and Canzek (1985). All of these designs use a Cassegrainian placement of the focal surface, which causes the severe vignetting of light (Kohler 1948, Bass 1995). This shortcoming is minimized, as far as possible, in the systems described above.

4.3 Triplet Full-Aperture Corrector

Generally speaking, the two-lens corrector in the Richter–Slevogt family of telescopes meets all of the conditions that have been set in Section 1.3.4, namely, it reduces monochromatic aberrations of the spherical primary mirror without introducing its own chromaticity. Why add a third large lens? The answers are different for cases with a flat or curved focal surface.

In the first case, the extra lens provides a sufficiently large back focal length and further reduces the chromatic aberration. In the second case, if we agree to use a curved focal surface, an additional lens can noticeably increase the angular field of view—up to a couple dozen of degrees, as the following examples show. Thus, sometimes it is necessary to recognize the validity of the step being discussed, although it entails excess weight and complexity of the mechanical design.

4.3.1 Schmidt–Houghton systems

Realizing that only a few opticians can cope with the manufacture of a complex aspheric surface of the corrector plate, Schmidt designed in 1934 a system in which an aspheric corrector plate was replaced by two spherical lenses, and then made and tested in sky observations a model with three spherical lenses.⁵ Only the premature death of Bernhard Schmidt in 1935 delayed the spread of a completely spherical wide-field system. As stated previously, a two-lens system of this kind was proposed by Richter and Slevogt (1941), whereas a three-lens all-spherical system was proposed by James Houghton (1942, 1944).

Figure 4.15 shows that three-lens designs of Schmidt and Houghton are very similar. The RMS spot sizes within a 5° field are also approximately the same; they are about $25''$ on a curved focal surface in a rather narrow integral range of F-C Fraunhofer lines.

⁵ The model is stored in the Schmidt Museum of the Hamburg-Bergedorf Observatory, Germany. See a recent investigation by Busch, Ceragioli, and Stephani (2013).

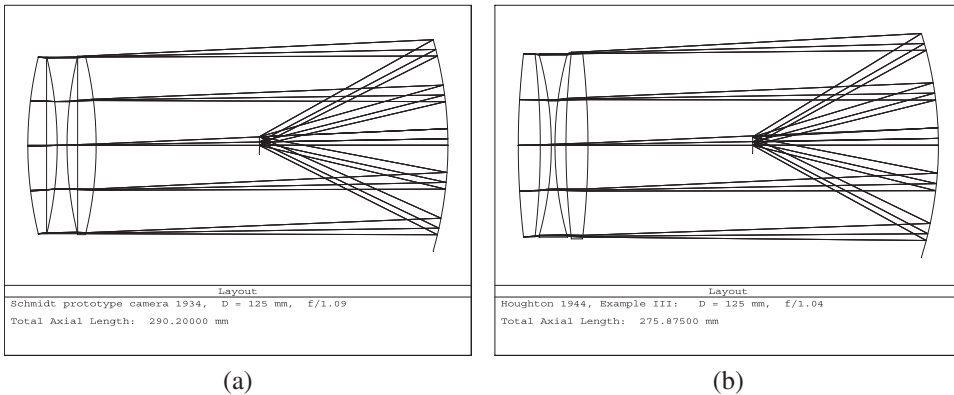


Figure 4.15 (a) Optical layout of the Schmidt, 1934, prototype $f/1.1$ model with a diameter of 125 mm according to measurements by Busch, Ceragioli, and Stephani (2013). (b) Houghton (1944) $f/1.04$ example III with a diameter of 125 mm according to US Patent 2,350,112.

In subsequent years, opticians and astronomers have rarely turned to all-spherical Schmidt–Houghton systems. One of the most frequently mentioned studies in this direction was performed by Shenker (1966), but his design differs little from those presented in Fig. 4.15 (see Fig. 22 in Terebizh 2011). More successful were the designs of Maxwell (1972) and Laikin (1995). The latter author enlarged the flat field of view up to 9° . His $f/1.2$ design of 206.5 mm in diameter includes only spherical lenses made of one type of glass; the RMS diameter of a star images in the wavelengths range 0.486–0.656 μm is 15–35 μm ($12''$ – $28''$).

A deep study, the importance of which was revealed only recently, was performed by Wynne (1950). He assumed the division of the achromatic front meniscus of the system shown in Fig. 4.10 into two parts, each of which is no longer an achromatic meniscus, while together they correct not only the longitudinal color, but also the lateral color. This study did not find continuation. The mainstream has gone to the systems with several highly aspheric surfaces (Section 4.3.2), although modified, purely spherical three-lens designs can provide a flat field of high-quality images with a diameter of up to 10° and a curved field of even larger size (but not as good).

The first of these possibilities, directly extending the line of Schmidt–Houghton, is illustrated by the VT-078e design shown in Fig. 4.16 (Terebizh 2016b). Three large lenses are made of the most simple and reliable Schott N-BK7 glass; if desired, it can be replaced by fused silica. The linear dimensions of the field correspond to the diagonal of the STA1600 CCD. The RMS spot size in the integral light is less than $1.7''$ across the 10° field.

Among the produced telescopes of this type, there is the TEC-VT300mm (VT-099c) $f/1.44$ design with a diameter of 300 mm and a 7° field, intended for a visual waveband and a detector with a diagonal of 52.1 mm. Two copies of

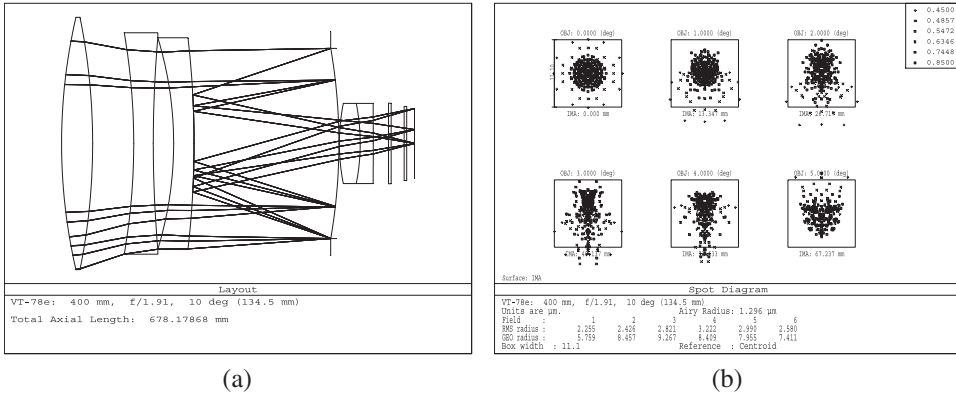


Figure 4.16 (a) Optical layout of the 400-mm, $f/1.9$ all-spherical telescope VT-078e with a flat field 10° (134.5 mm) in diameter. (b) Corresponding spot diagrams in the integral waveband 0.45–0.85 μm ; the box side is 11.1 μm (3.0").

the telescope were manufactured by the Telescope Engineering Company (TEC). One of them enters a dual system Panoptes-1AB, which is installed by the Polish SST consortium in Australia (Konacki et al. 2017). The second specimen used in the *Gattini-IR* project for Antarctic observations up to the J-band (Moore et al. 2016)—the TEC-VT300mm retains good image quality in the infrared region.

The another direction, namely, systems with a curved field, is illustrated by an $f/1.8$ design VT-119w with a diameter of 500 mm and a field of view of 30° (Fig. 4.17). Lenses can be made of simple glass grades; in this instance, they are all made of Schott N-BK7 and fused silica. The RMS spot diameter varies across the field from 9.2 μm (2.2") up to 14.6 μm (3.4") in the integral waveband of Fraunhofer F-C lines.

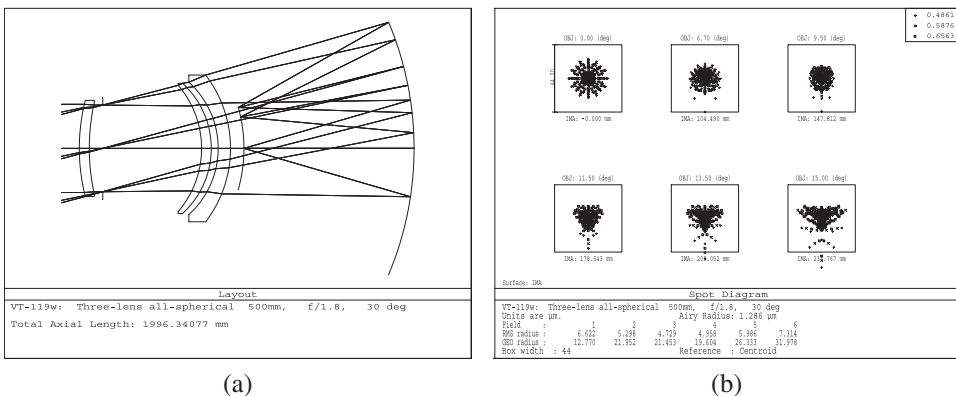


Figure 4.17 (a) Optical layout of the 500-mm, $f/1.8$ all-spherical telescope VT-119w with a spherical field 30° in diameter. (b) Corresponding spot diagrams in the integral waveband 0.48–0.66 μm ; the box width is 44 μm (10").

A deeper understanding of systems with a field of tens of degrees can be achieved by comparing the above design VT-119w with the VT-135e design discussed in Section 4.2 (Fig. 4.11). Both systems were optimized for the same speed, field size, and spectral range. It would seem that adding one lens and permission for different types of glass will improve the image quality, but it turned out to not be radical. The addition of the third lens inevitably worsens the point symmetry relative to the center of curvature of the mirror, so the benefits and losses are mutually compensated here.

In themselves, images with a three-lens asymmetric corrector can already be considered acceptable for a number of problems, so one can choose a simple system of the type VT-119w. But if better, nearly-diffraction-limited image quality is required in a wider field of view, we should turn to the all-spherical system with a four-lens symmetric corrector considered in Section 4.4. Thus, the symmetry of systems with an even number of lenses relative to the aperture stop and the mirror's center of curvature is more important than the total number of lenses in the corrector.

4.3.2 Baker–Nunn and Super-Schmidt cameras

4.3.2.1 Baker–Nunn camera

In the middle of the last century, a dozen Baker–Nunn $f/1.0$ cameras (Fig. 4.18) with an aperture of 0.5 m were made for satellite tracking.⁶ The general description of the operating telescope can be found in Henize (1957).

The design specifications required a field with a diameter of 20° at a spot size of not more than 20 microns. As in the Schmidt and Houghton systems (Fig. 4.15), the three-lens corrector of the Baker–Nunn camera is placed at the

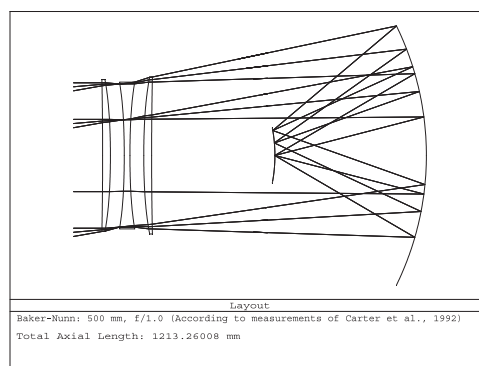


Figure 4.18 Optical layout of the Baker-Nunn camera with a 500-mm aperture and a spherical field 20° in diameter.

⁶ James Baker (1962) designed the optics of the camera, and Joseph Nunn designed its mechanics.

center of curvature of a spherical mirror, but unlike the systems mentioned, the four inner surfaces of the corrector are even aspheres of sixth and eighth orders. To achieve chromatic correction, Schott KzFS2 and SK14 glasses were used. The camera provides a field strip of $30^\circ \times 5^\circ$ formed at a curved focal surface with a radius of about the focal length of the primary mirror. The telescope is compact: its length from the first to the last optical surface is nearly 1.2 m.

The Baker–Nunn cameras have survived until now, and Carter et al. (1992) published a complete description of the optics of one of them. The authors relied on private information supplied by J. Baker and on their own careful measurements. The optical layout shown in Fig. 4.18 corresponds to the prescription given in Table 1 of Carter et al. The original design provides images of the RMS diameter 50–90 μm (20"–38") in the integral waveband of 0.48–0.68 μm ; if we additionally optimize the curvature of focal surface and the spacing between the lens corrector and mirror, the spot size will decrease to about 35 μm (15").

It is useful to compare the Baker–Nunn camera with the Wynne three-lens design, which we discussed in the previous paragraph. In particular, the $f/1.8$ modification VT-119w of the original Wynne (1950) system was shown there with a diameter of 0.5 m and a field of 30° . In that design, all optical surfaces are spheres, and all lenses are made of the simplest sorts of glass, whereas the spot size is in the range 2.2"–3.4" across a field. However, the length of the VT-119w design is almost 2 m, so one have to give weights to such characteristics as the compactness of the telescope, the complexity of its optics, and the image quality.

Over the past years, a few projects were initiated to refurbish some Baker–Nunn cameras that were not in use for a long time. Perhaps, Carter et al. (1992) made the first such step. They took into account the effects of filters, changed the front lens surface, and inserted a field-flattener lens, enabling a system to produce a 5° field with spot sizes of 15–40 μm . Law et al. (2002) describe a similar effort at the U.S. Air Force Maui Optical and Supercomputing Site (AMOS) on the Hawaiian island of Maui. The resulting flat field of the renewed telescope named *Phoenix* is 9.6° in diameter. A similar Indian project, ARIES, provides a flat field of size $4^\circ \times 4^\circ$ by installing a field flattener lens inside the CCD camera and adding a large meniscus lens (Mondal et al. 2009). Finally, a Spanish project aims to reach a $5^\circ \times 5^\circ$ flat field (Fors et al. 2011).

Apparently, the installation of additional optical elements into the existing highly complicated system can be considered as a satisfactory solution only with respect to the low cost of the project.

4.3.2.2 Baker Super-Schmidt camera

Over the years, it became clear that three areas of research related to the names of Schmidt, Maksutov, and Wynne have proved to be productive in creating

wide-field systems. The main efforts in these areas are associated, respectively, with a single-lens aspheric corrector, a single-lens achromatic corrector of a spherical shape, and a two-lens symmetric spherical corrector. It is natural that various combinations of these three ideas were soon studied. In particular, the Baker (1945) *Super-Schmidt camera* assumes the placement of an aspheric plate near the aperture stop of symmetric corrector (Fig. 4.19); another difference with the Wynne design is the double passage of light through the inner meniscus.

In fact, the camera is even more complicated: the aspheric plate is a two-layer lens with slightly curved surfaces, one of which is also an even asphere of the sixth order. The combination of Schott glasses F2/SK2 almost completely eliminates the longitudinal color. All other surfaces of the system are spherical. The RMS spot size is nearly 14 μm (4.8") across the 30° field. The total length of the optical system is 2.0 m.

The comparison of the Super-Schmidt camera with the all-spherical modification of the Wynne system shown in Fig. 4.17 is even more in favor of the latter. It is superior in all respects, including the simplicity of surfaces and glass, the image quality, and the total length of the telescope.

4.3.3 Meniscus Schmidt design of Hawkins and Linfoot; VAU telescope

A more attractive conjunction of directions, outlined in the previous Section, was studied by Hawkins and Linfoot (1945). Here is how the authors describe their design: “We consider what can be achieved by combining the two ideas of Maksutov and of Schmidt, and show that it is possible to design a system whose performance at a speed of $f/1.2$ is much superior to that of both the Schmidt and of the meniscus system with spherical surfaces. We shall refer to this system as a meniscus Schmidt.”

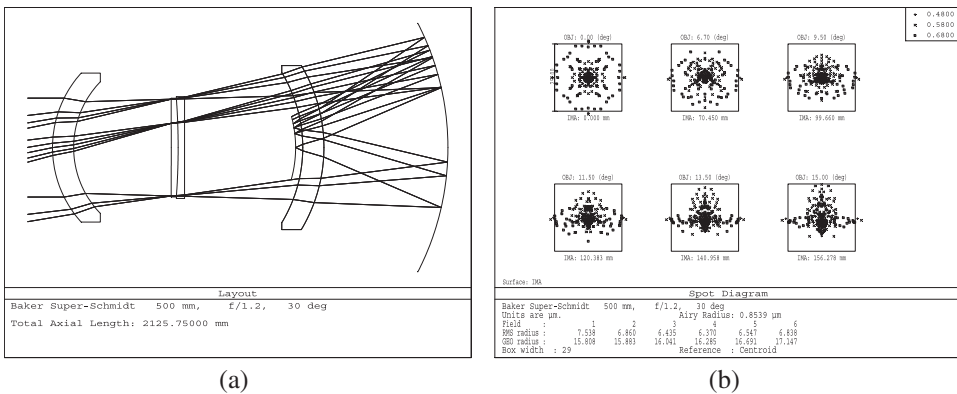


Figure 4.19 (a) Optical layout of the 500-mm, $f/1.2$ Baker Super-Schmidt camera with a curved field 30° in diameter. (b) Corresponding spot diagrams in the integral waveband 0.48–0.68 μm ; the box width is 29 μm (10").

The initial system in the Hawkins and Linfoot analysis was a design in which both surfaces of the meniscus are concentric with the mirror (see the similar design in Fig. 4.20). Evidently, if the common center of curvature coincides with the aperture stop, then the ‘monocentric meniscus’ system has small off-axis aberrations, but it suffers from both spherical and chromatic aberrations. These aberrations are nearly compensated by a double corrector plate, the asphericity of which is much less than that in a classical Schmidt telescope. As expected, the system provides a very wide but inevitably curved field.

The original layout of the Hawkins–Linfoot (HL) telescope is described in the literature more than once, so we prefer to show a lesser-known version, a VAU camera, created by D. Maksutov and M. Sosnina in the early 1960s (unpublished, Fig. 4.20). The aspheric surface of the double corrector plate is now of the eighth order. A strip of sky $30^\circ \times 5^\circ$ is imaged by the camera onto a curved focal surface. The RMS spot size is $10\text{--}28\ \mu\text{m}$ ($2.9''\text{--}8.2''$). The total length of the optical system, 1.6 m, can be considered moderate.

Although the performance of the Hawkins–Linfoot system is close to that of the Super-Schmidt camera, the former has a few advantages in the constructive respect. Namely, there is only one large lens in the HL camera, which is also used in one passage of light. The same property makes the HL system shorter than the Super-Schmidt camera.

4.3.4 Family of Sonnefeld cameras; the Ω_3 system

The modification in question (Fig. 4.21) can be interpreted either as the addition a large lens to the Hamilton camera corrector (Fig. 4.12) or as a replacement for a simple mirror in the Richter–Slevogt system (Fig. 4.8) with

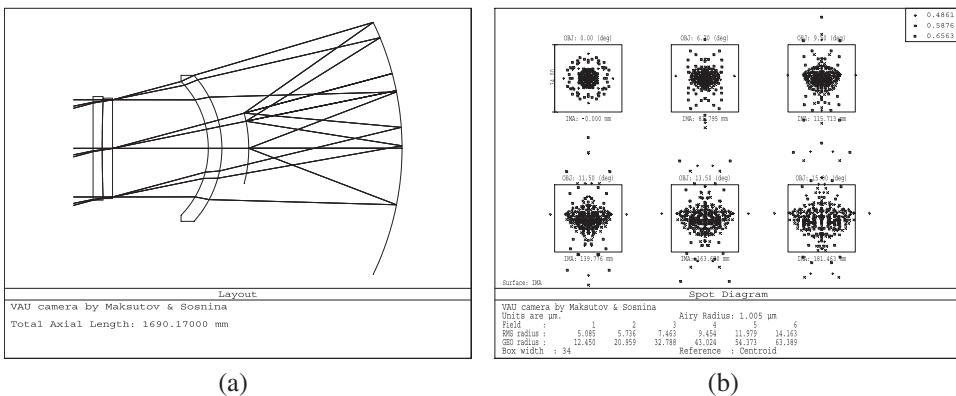


Figure 4.20 (a) Meniscus Schmidt system of Hawkins and Linfoot, as it was implemented by Maksutov and Sosnina in the $f/1.4$ VAU camera with a 500-mm aperture and of 30° curved field. (b) Corresponding spot diagrams in the integral waveband $0.48\text{--}0.66\ \mu\text{m}$; the box width is $34\ \mu\text{m}$ ($10''$).

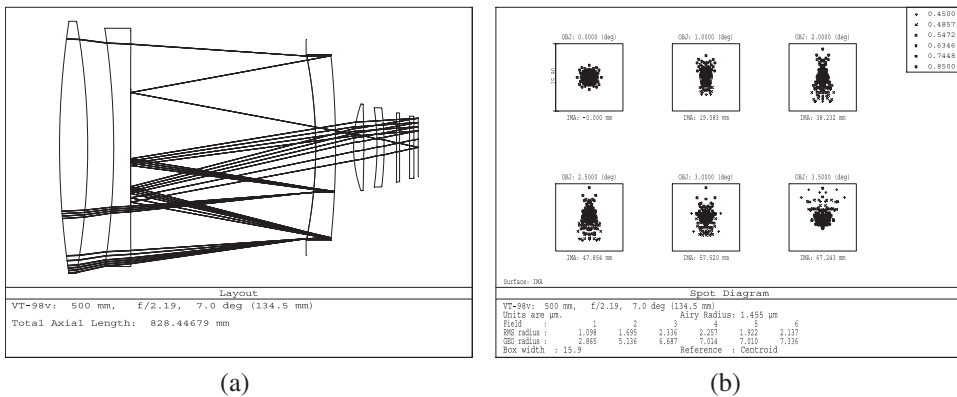


Figure 4.21 (a) Optical layout of the 500-mm, $f/2.2$ VT-098v design with a flat field 7.0° in diameter. (b) Corresponding spot diagrams in the integral waveband $0.45\text{--}0.85\ \mu\text{m}$; the box width is $15.9\ \mu\text{m}$ ($3.0''$).

a Mangin mirror. Probably, the latter is more consistent with the meaning of the system. This optical layout (with inner focus) was proposed by August Sonnefeld (1936) even before the Richter–Slevogt (1941) patent. In this way, Sonnefeld achieved a feasible field of view at a very high speed of $f/0.5$. The Sonnefeld design finds applications as a camera for spectrographs.

Much later, Amon, Rosin, and Jackson (1971) implemented the Cassegrainian focus position by reducing the speed of the system (see also Amon 1973). In the 1971 article, a successful $f/1.5$ working model was described with a diameter of 230 mm and a field of 6.5° . The authors found that substituting a Mangin version for the primary mirror has several advantages: it gives additional degrees of freedom, permits the correction of most of the spherical aberration of the primary mirror at the mirror itself, and significantly reduces the coma.

A modern example of this system is shown in Fig. 4.21; see Terebizh (2016b) for the complete description.

Figure 4.22 gives an idea of the Ω_3 model proposed by Terebizh (2007c). The VT-060q system differs from the Ω_2 system VT-102j (Fig. 4.13) by an additional full-aperture dual-light lens, which allows one to double the aperture diameter with a significantly wider field of view. All optical surfaces of the VT-060q are spheres; three large elements are assumed to be made of fused silica. It is also possible to make large two lenses of a simple glass Schott N-BK7 (Ohara S-BSL7), but fused silica remains preferred in the manufacture of the Mangin mirror (see Section 1.3.4). For the base model, in which we consider VT-060q, three smaller lenses are assumed to be made of N-BK7 and fused silica; somewhat better images can be obtained by expanding glass grades. The last lens is an optically powered dewar window of the Piazz-Smyth type. Note that the original Ω_3 systems described by Terebizh (2007c, 2016) did not contain this lens.

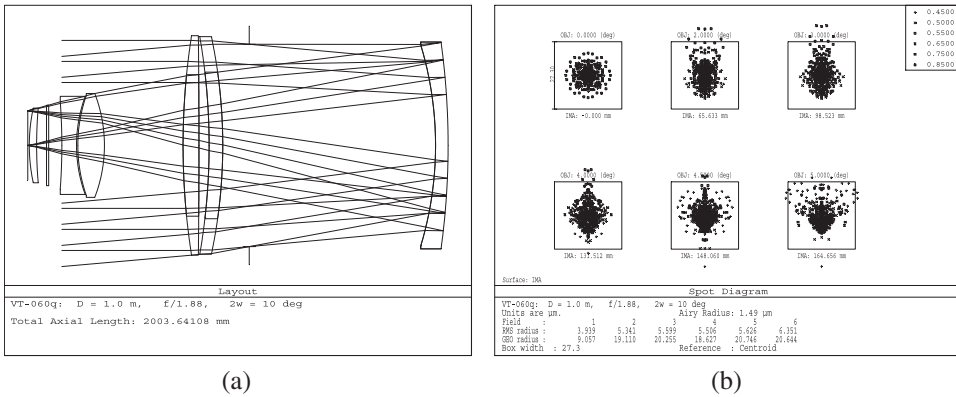


Figure 4.22 (a) Optical layout of the 1-m, $f/1.88$ design VT-060q with a flat field of 10° in diameter (Ω_3 type). (b) Corresponding spot diagrams in the integral waveband $0.45\text{--}0.85\ \mu\text{m}$; the box width is $27.3\ \mu\text{m}$ ($3.0''$).

Comparison of the Ω_3 system (Fig. 4.22) with the modified Sonnfeld camera (Fig. 4.21) allows to see one of two main reasons for using double light passing through the input corrector. Both of the designs are all-spherical, both were designed for the same spectral range and have a similar image quality—not worse than $2''$ across the field. However, the need to put the focus of VT-098v in a Cassegrainian way does not allow one to expand the field because of significant vignetting. Indeed, the fraction of unvignetted rays changes in the VT-098v from 0.68 on the optical axis down to 0.56 at the edge of the 7° field, whereas it is 0.73 over the entire 10° field in VT-060q. Thus, the effective aperture diameter of the VT-098v varies from 412 mm in the center of a field down to 374 mm at its edge, while it is 854 mm across the full field in VT-060q.

Of interest is also the fraction of unvignetted rays for the VT-110k design of the classical Schmidt system shown in Fig. 4.1: it is 0.875 throughout the field. Such a high value is achieved at the cost of a large length of the Schmidt camera and the position of the focus inside the tube.

The second reason for the utility of additional light passing through the lens is that it makes it easier to achieve a large flat focal surface. Indeed, the fundamental Petzval condition requires that the sum of the reciprocals of the radii of curvature of the surfaces and the corresponding refractive indices be equal to zero (Born and Wolf 1999, Section 5.5.3, Eq. 20). This condition cannot be met in extremely laconic systems such as the Schmidt camera, but the introduction of additional light transmissions while maintaining the number of optical elements opens up this possibility.

In connection with the need for a large flat field, it is appropriate to recall the fruitful Palomar Observatory Sky Survey with a 48-inch Schmidt camera. The survey utilized square photographic plates, covering about $6^\circ \times 6^\circ$ of sky. In the middle of the last century, photographic plates had to be bent according

to the curvature of the focal surface, but there were serious problems during the transition to modern flat detectors. Nevertheless, sequential complications of the camera's optical system provided efficient sky surveys aimed mainly at studying transient objects.

The last upgrade was made in connection with the *Zwicky Transient Facility* project (Bellm et al. 2019). To achieve a flat field with a 7.8° effective angular diameter, three large aspheric plates, the meniscus dewar window, and an aggregate of field flattener lenses above each detector were used. Such complexity is not surprising in view of Petzval's condition on the curvature of a focal surface. On the other hand, the flattening of the focal surface does not necessarily include aspheres. This is exactly what an Ω_3 system implements, in addition to a feasible color correction and radical reduction of the telescope length (about 2 m for VT-060q).

It seems that the simple Ω_3 system can serve as a basic design for future survey telescopes with a flat field of about 10° .

4.4 All-Spherical System with an Extremely Large Field

4.4.1 Statement of the problem

Not all survey observations can be done with the help of flat-field telescopes, such as those discussed in this chapter. Sometimes, when the goal is to quickly register a field with dimensions of about 40° , too many flat-field cameras are needed. Let us mention, in this regard, the watching of fast transient events, e.g., optical counterparts of sources of gravitational waves or of powerful x-ray flares. It seems that the better way in this case is the creation of a single telescope with an extremely wide angular field, even at a spherical focal surface.

Just this way was chosen in the second half of the last century, when the Baker–Nunn (Section 4.3.2), Hawkins–Linfoot, and Maksutov–Sosnina (Section 4.3.3) cameras were put into operation. Their angular field attained 20° – 30° , whereas the vignetting of light and curvature of the focal surface were taken into account by application of narrow emulsion tape. These cameras required substantially aspheric optical surfaces and demanding sorts of glass, and yet did not provide image quality of about a few angular seconds.

In view of what has been said, it was somewhat surprising that an all-spherical system made of the simplest types of glass provides nearly diffraction-limited polychromatic images in the field of the order of several tens of degrees in diameter (Terebizh 2016a).

4.4.2 Examples of designs with an ultra-wide field of view

The VT-119g design shown in Fig. 4.23 has been optimized for the 30° field and the waveband 0.45 – $0.85 \mu\text{m}$. All four lenses of the corrector can be made of the same material; we prefer fused silica because of its stability and

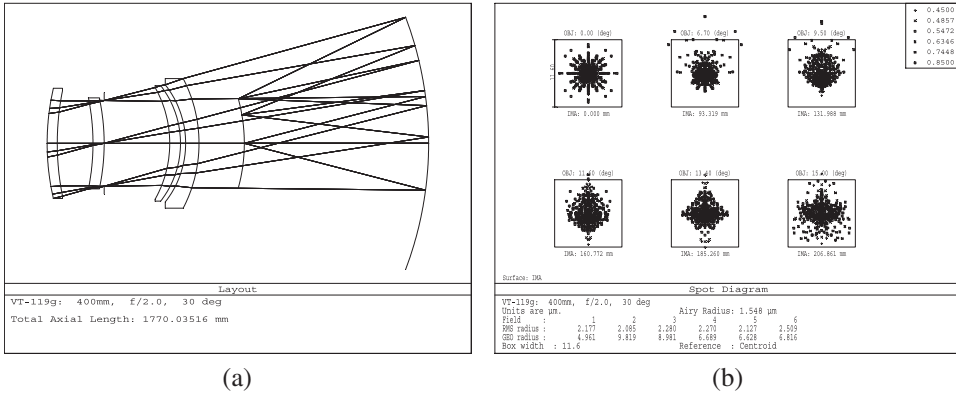


Figure 4.23 (a) Optical layout of the 400-mm, $f/2.0$ design VT-119g with a spherical field 30° in diameter. (b) Corresponding spot diagrams in the integral waveband $0.45\text{--}0.85\ \mu\text{m}$; the box width is $11.6\ \mu\text{m}$ ($3''$).

excellent optical properties, in particular, high UV transparency. As one can see, the image quality is nearly constant across the field. More specifically, the D_{80} diameter of a star image in the polychromatic light varies from $5.4\ \mu\text{m}$ ($1.4''$) on the optical axis to $7.3\ \mu\text{m}$ ($1.9''$) on the edge of the field.

The optical system under discussion proceeds from the symmetrical two-lens all-spherical design by Wynne (1950), which was described in Section 4.2.2 (Fig. 4.10). Wynne showed that the symmetrization of the input corrector to a spherical mirror makes it possible to significantly expand the field in comparison with that in the classical Schmidt camera, but at the cost of poorer image quality (Fig. 4.11). The addition of the third spherical lens gives only a moderate gain both in the image quality and in the field size (Fig. 4.17), although in itself such a system is already of practical interest. The reason for the insufficient progress is the violation of the point symmetry of the corrector with an odd number of spherical lenses. Wynne (1950) also considered a four-lens spherical corrector made of one kind of glass, but a significant hole in the last lens made the system only quasi-symmetrical and thus limited the field of view to about 10° with a RMS spot size $\sim 300''$ in the range of F-C Fraunhofer lines (we optimized additionally the back focal length, the radius of the focal surface, and the aperture stop position).

It seems natural to achieve a truly wide field of view of arcsecond images in integral light by placing a four-lens spherical corrector symmetrically, in the optical sense, relative to the stop at the center of the curvature of the spherical mirror. Hence, the point symmetry is limited now only by the inevitable vignetting on the aperture stop.

The second feature of the system, which provides almost complete absence of chromatic aberration, is the afocality of the four-lens corrector: it operates in the VT-119g at a focal ratio of $f/61$.

Finally, the third property necessary for ensuring wide field is the close proximity of the entrance pupil to the aperture stop; their separation is only 24 mm in this design.

As an another example, we give a 45° design VT-119j (Fig. 4.24) from the article of Terebizh (2016b). The D_{80} image diameter in polychromatic light varies here in the range 8.2–9.5 μm (1.2''–1.4''), whereas the diameter of the diffraction Airy disk is 0.64''. The drastic extension of the angular field of high image quality is due to the transition to purely spherical optics. The lens corrector works in the VT-119j at a speed of $f/87$, and the distance between the aperture stop and the curvature center of the mirror is only 31 mm.

Since the requirements for the system are simple, it is scalable in a wide range. Terebizh (2016a) provides an example of scaling the VT-119g design to a twice-larger aperture of 800 mm while preserving image quality. Unfortunately, not optics itself but practical limitations on the lens size limit further scaling. In particular, the diameter of the last lens in the scaled system is about 1.2 m, which is already not far from the size reached by modern technology based on the use of glass. Because of mild tolerances, some plastic materials may be promising for lenses. For example, the replacement of fused silica in the scaled system with acrylic reduces the weight of the lens corrector twice at the same image quality and transparency in a wide spectral range. Perhaps further research will produce more stable lenses made of plastic materials, especially with a simple spherical shape.

The maximum angular size of the field of view is still unknown for the symmetrical four-lens system. Trial calculations show the possibility of getting images of about 2'' on the edge of a field with a diameter of 60°. In this respect, we are again limited by the dimensions of lenses.

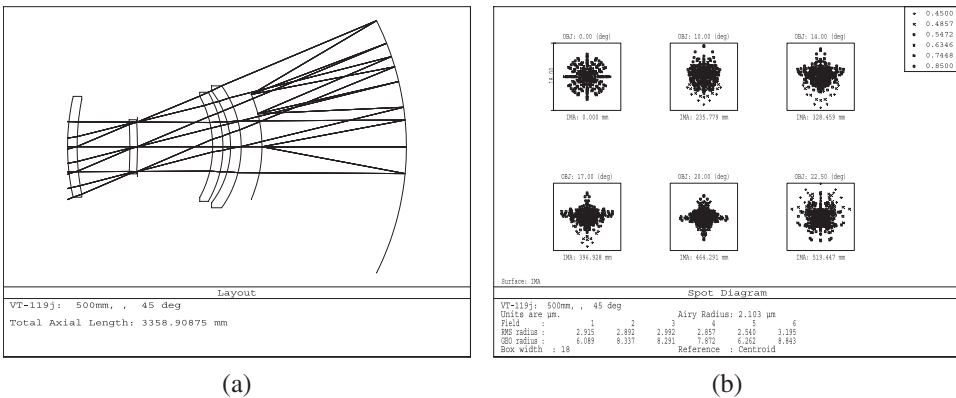


Figure 4.24 (a) Optical layout of the 500-mm, $f/2.72$ design VT-119j with a spherical field 45° in diameter. (b) Corresponding spot diagrams in the integral waveband 0.45–0.85 μm ; the box width is 18 μm (2.7'').

Some tasks, for example, protecting against asteroids, require continuous monitoring of the entire celestial hemisphere visible from the surface of the Earth. In this regard, numerous all-sky systems have been proposed. Unfortunately, the diameter of the entrance pupil in these systems is usually only a few millimeters, reaching values a little more than 10 mm in some cases. Meanwhile, several simultaneously operating cameras of the type described here solve this problem with an incomparably deeper brightness limit.

It seems likely that further research will expand the scope of the proposed optical layout. In particular, applications in spectroscopy, physics of cosmic rays, geophysics, and tomography are especially promising.

Afterword

During the four centuries of the evolution of telescopes, so many different optical systems have been proposed that they are not even easy to systematize. This diversity reflects the essence of the matter; the choice of a suitable optical layout depends largely on the variety of observational and technological problems. Recall the analogy that we used in Section 1.2.2: just as the navy cannot be restricted to aircraft carriers only, in a survey case it is reasonable to distribute tasks between instruments of various apertures and field sizes. We may only hope that the above discussion will contribute to the choice of a proper optical design for particular circumstances.

In our presentation, we analyze the performance of various optical systems but do not discuss *how* the final result was achieved, that is, the optimization technique in multidimensional ‘optical’ space. This is because the goal of the book is to help with *understanding* the various optical systems of telescopes, which is the primary tool for conditions where a formal design algorithm is not known. There are good guides focusing also on technical work using modern optical programs, in particular, ZEMAX. The fundamental monographs of G. H. Smith *Practical Computer-Aided Lens Design* and J. M. Geary *Introduction to Lens Design with Practical ZEMAX Examples* seem to be most suitable in our case. It is only necessary to add that, in view of the existence of numerous local minima of the quality function, the search cannot be limited to the choice of the final design from a scarce sample, no matter how attractive it looks, but one should build a ‘tree’ of all acceptable solutions and then select the best design. As often happens, there is no formal sign indicating the achievement of the best solution. The beauty of the design most likely testifies to this: it seems that any change in the optical system only worsens it.

The reader could get the impression that the author unconditionally prefers spherical surfaces to all other forms. This is only partly true. The fact is that for wide-field systems the spherical shape is advantageous, because it is the same for rays in a wide range of directions; it provides the softest tolerances (since its slopes and transverse displacements can mutually compensate each other); the spheres are the most simple to manufacture and reliable in operation; spheres are easy to make as smooth as you like; and

finally, they significantly reduce the cost of a telescope. This is supported by numerous examples of systems that are discussed in Chapters 3 and 4. However, the concept of ‘simplicity’ is not limited to the use of spherical surfaces. For example, the Schmidt camera with a substantially aspheric surface of the corrector is the optimal solution for a space telescope with a hard mass limitation. Obviously, spherical surfaces should be preferred in those situations where they allow one to achieve the goal, *ceteris paribus*. As Einstein noted, “Everything should be done as simple as possible, but not simpler.”

In a concise discussion of the topic, we were able to provide only cursory historical reminiscences. With an eye to move further, we have to reconsider more carefully the classical heritage. When one reads the works of Karl Schwarzschild, Bernhard Schmidt, Maurice Paul, Dmitry Maksutov, or Charles Wynne, it is no accident that deep reflections by Max Herzberger (1966) come to mind: “Historical knowledge is important because it stimulates creative thinking. The man, who first struggled with an idea, trying to find a law, looked at the situation with different eyes than do we who accept the law as a matter of course. He considered alternatives to the law, and different interpretations, and some of these alternatives and interpretations may still be stimulating and worth thinking about.” In this respect, the publication by Daniel Schroeder of *Selected Papers on Astronomical Optics* (SPIE Milestone Series, V. 73, 1993) was invaluable, to which we refer the reader.

Appendices

Appendix A

Limiting Stellar Magnitude and Sky Survey Rate

Suppose that a star with a monochromatic magnitude of m is observed with a telescope of an effective aperture D_e (cm) for a time T (s). The average number of photo-counts registered by the detector in the waveband $\Delta\lambda$ (μm) can be written as follows:

$$N_* = N_0 \cdot 10^{-0.4m} \cdot q \cdot \frac{\pi D_e^2}{4} \cdot \Delta\lambda \cdot \epsilon \cdot T \quad \text{counts}, \quad (\text{A1})$$

where N_0 (photons/s $\text{cm}^2 \mu\text{m}$) is the photon flux from a star of zeroth magnitude, $q = q_{atm} \cdot q_{tel}$ is the total transparency, including atmosphere and the telescope, and ϵ (photo-events/photon) is the quantum efficiency of the detector.

The average number of photo-counts due to the sky background registered during the same time is

$$N_b = N_0 \cdot 10^{-0.4\mu} \cdot q \cdot \frac{\pi D_e^2}{4} \cdot \Delta\lambda \cdot \epsilon \cdot T \cdot \frac{\pi(\theta'')^2}{4} \quad \text{counts}, \quad (\text{A2})$$

where μ (magnitude/square arcsec) is the sky surface brightness, and θ'' (arcsec) is the *delivered image quality* defined by Eq. (1.5).

Assuming that the statistics of photo-counts obeys to the Poisson distribution, the signal-to-noise ratio is

$$S/N = N_*/(N_* + N_b)^{1/2}. \quad (\text{A3})$$

For a weak star near the limit of visibility, we can accept $N_* \ll N_b$, so

$$S/N \simeq N_*/N_b^{1/2}. \quad (\text{A4})$$

Substituting here expressions (A1) and (A2), and solving the resulting equality with respect to m , we find for a limiting stellar magnitude:

$$m_{lim} = \mu/2 + 1.25 \log_{10}(N_0 \cdot q \cdot U \cdot \delta\lambda \cdot \epsilon \cdot T) + 2.5 \log_{10}(D/(\theta'' \cdot S/N), \quad (\text{A5})$$

where we used the definition of the effective diameter $D_e = D \cdot U^{1/2}$ in terms of the physical diameter D and the fraction of unvignetted rays in the telescope U .

Evidently, the S/N in Eq. (A5) should be considered as the threshold signal-to-noise ratio adapted for observations. Its value depends on the specific task and the detector of light.

Let us turn to the justification of Eq. (1.4) for the *sky survey rate* Γ . It follows from Eqs. (A1)–(A4) that

$$S/N \propto \frac{D_e}{\theta} \sqrt{T} 10^{-0.4m}. \quad (\text{A6})$$

It is clear from this equation that the exposure time T , required to observe an object of a given brightness at a fixed signal-to-noise ratio, is proportional to $(\theta/D_e)^2$. Hence, the sky survey rate Γ , defined as a ratio of the registered solid angle πw^2 to the exposure time T , is proportional to $(wD_e/\theta)^2$. Taking into account the definition of the *étendue*, $E \equiv \pi w^2 \times \pi D_e^2/4$, we see that $\Gamma \propto E/\theta^2$. To retain a simple connection of the sky survey rate Γ with the conventional parameter E , we put a constant multiplier equal to 1, so $\Gamma = E/\theta^2$, or

$$\Gamma \equiv \frac{\pi w^2 \times \pi D_e^2}{4\theta^2}. \quad (\text{A7})$$

As was noted in Section 1.1.3, Γ is approximately equal to the number of elements resolved in the investigated region of the sky.

Appendix B

Schwarzschild Aplanats

Schwarzschild's (1905) approach to aplanatic two-mirror telescopes has been described in Section 2.2.4. Below we write out the strict and approximate formulas, which describe the shape of surfaces of the primary and secondary mirrors according to Terebizh (2005a). These equations are given in a form that is valid for an arbitrary two-mirror system in the Maksutov (q, β) plane (Section 2.2.1).

B1. Basic Formulas

The relations, it is said, have a parametric form. They connect the ordinates of the light ray (Y_1, Y_2) at the points of its intersection with the mirror surfaces and the mirror sags (S_1, S_2) corresponding to these points with a free parameter

$$t = \sin^2(U/2), \quad 0 \leq t \leq t_{\max}, \quad (\text{B1})$$

where U is an arbitrary aperture angle (see Fig. B1 below and Fig. 2.2 in the main text).

The Schwarzschild theory proceeds from a *sine condition* for the infinitely far object:

$$Y_1/\sin U = F = \text{const} \quad (\text{B2})$$

for all of the incident ray heights Y_1 and aperture angles U . This condition and the evident inequality $|Y_1| \leq D/2$ yield the maximum aperture angle:

$$U_{\max} = \arcsin (2\phi)^{-1}. \quad (\text{B3})$$

Substituting this value into Eq. (B1) yields

$$t_{\max} = \frac{1}{2} \left[1 - \sqrt{1 - (2\phi)^{-2}} \right]. \quad (\text{B4})$$

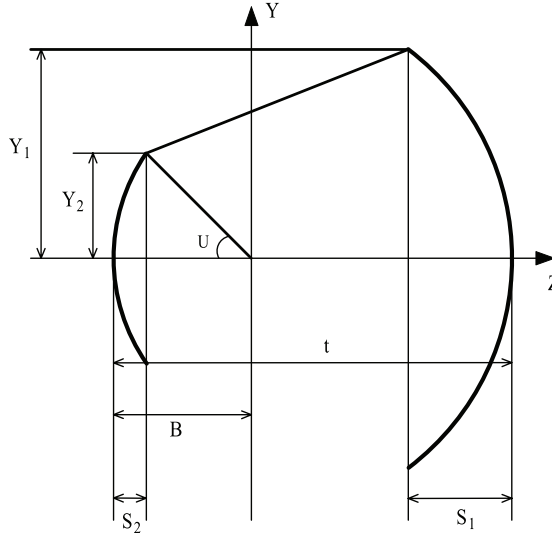


Figure B1 Basic notation for a conditional optical layout.

Usually, t_{\max} is small; even for a fast system with a focal ratio of $\phi = 1$, we have $t_{\max} \simeq 0.067$.

Let us also define two indexes

$$\delta \equiv (1 - q)\beta; \quad \gamma \equiv (1 - \delta)^{-1}, \quad \text{for } \delta \neq 1. \quad (\text{B5})$$

Then, the formulas that specify the primary mirror profile can be written as

$$Y_1/|F| = 2\sqrt{t(1-t)}, \quad (\text{B6}')$$

$$S_1/F = \begin{cases} q[1 - (1-t)^\gamma |1 - t/\delta|^{2-\gamma}] - t(1-t)/\delta, & \delta \neq 1, \\ q[1 - (1-t)^2 e^{t/(1-t)}] - t(1-t), & \delta = 1. \end{cases} \quad (\text{B6}'')$$

The analogous relations for the secondary mirror are

$$Y_2/|F| = 2\sqrt{t(1-t)}/\Theta(t), \quad (\text{B7}')$$

$$S_2/F = q - (1 - 2t)/\Theta(t), \quad (\text{B7}'')$$

where the auxiliary function

$$\Theta(t) = \begin{cases} t/\delta + q^{-1}(1-t)^{1-\gamma}|1 - t/\delta|^\gamma, & \delta \neq 1, \\ t + q^{-1}(1-t)e^{-t/(1-t)}, & \delta = 1. \end{cases} \quad (\text{B8})$$

Note that the results for $\delta=1$ can be obtained both by repeating calculations similar to Schwarzschild's original calculations and by passing to

the limit $\delta \rightarrow 1$. According to Eq. (B5), $\beta = (1 - q)^{-1}$ in the case under consideration, and we get

$$t = -F, \quad R_1 = -\frac{2}{1 - q}F, \quad R_2 = 2F, \quad \text{for } \delta = 1. \quad (\text{B9})$$

Thus, assigning values from the interval $[0, t_{\max}]$ to the free parameter t , we find the profile of the mirror surfaces from Eqs. (B6)–(B8), which ensure the absence of paraxial spherical aberration and coma in an arbitrary two-mirror telescope.

B2. Slow Systems

According to Eq. (B4), the upper boundary of the free parameter t_{\max} is less than 0.01 at $\phi = 2.6$, and at an even slower focal ratio, we have

$$t_{\max} \simeq (4\phi)^{-2} \ll 1. \quad (\text{B10})$$

For this case, Schwarzschild (1905) expanded the exact formulas in a power series of the normalized ray heights $y_1 \equiv Y_1/F$ and $y_2 \equiv Y_2/F$, the first terms of which, in our notation, are

$$S_1/F = -\frac{1 - q}{4\delta}y_1^2 + \frac{q}{32\delta}y_1^4 + q\frac{1 + 4\delta}{384\delta^2}y_1^6 + q\frac{2 + 11\delta + 30\delta^2}{6144\delta^3}y_1^8 + \dots, \quad (\text{B11})$$

$$S_2/F = -\frac{1 - q - \delta}{4q\delta}y_2^2 + \frac{2 - \delta - 4q + 2q^2 + 2q\delta}{32q^3\delta^2}y_2^4 + \dots \quad (\text{B12})$$

The expansions are also valid for $\delta = 1$.

The sag of an arbitrary conic section S_c is known to be

$$S_c/F = \frac{y^2}{r} \left[1 + \sqrt{1 - (1 - \epsilon^2)(y/r)^2} \right]^{-1}, \quad (\text{B13})$$

where $r = R/F$ is the dimensionless radius of curvature at the vertex, and ϵ is the surface eccentricity. Hence, one can easily obtain the expansion

$$S_c/F = \frac{1}{2r}y^2 + \frac{1 - \epsilon^2}{8r^3}y^4 + \frac{(1 - \epsilon^2)^2}{16r^5}y^6 + \dots \quad (\text{B14})$$

Its comparison with Eq. (B11) and Eq. (B12) allows the approximation of exact aplanatic surfaces by conicoids for slow systems to be elucidated.

For the primary mirror, the first two expansion terms give the following expressions for the radius of curvature and the square of the eccentricity:

$$r_1 = -\frac{2\delta}{1-q}, \quad \epsilon_1^2 = 1 + \frac{2q\delta^2}{(1-q)^3}. \quad (\text{B15})$$

Accounting for the definition of the constant δ in Eq. (B5), we see that the former expression is identical to that in Eq. (2.8), while it follows from the latter expression that

$$\epsilon_1^2 = 1 + \frac{2q\beta^2}{1-q}. \quad (\text{B16})$$

Just as above, we obtain for the secondary mirror

$$r_2 = -\frac{2q\delta}{1-q-\delta}, \quad \epsilon_2^2 = \left(\frac{1-q+\delta}{1-q-\delta}\right)^2 + \frac{2\delta^2}{(1-q-\delta)^3}. \quad (\text{B17})$$

The expression for r_2 is identical to that in Eq. (2.9), while the square of the eccentricity of the secondary mirror expressed in terms of the basic variables (q, β) can be written as

$$\epsilon_2^2 = \left(\frac{1+\beta}{1-\beta}\right)^2 + \frac{2\beta^2}{(1-q)(1-\beta)^3}. \quad (\text{B18})$$

Equations (B16) and (B18) form the basis for the theory of systems aplanatic in the third order of the aberration theory (see, e.g., Schroeder 2000, Section 6.2.b, and Eq. (2.16) above).

B3. Schwarzschild Surfaces in ZEMAX

Ascertaining the image quality in exact Schwarzschild aplanats requires either developing a special program for calculating the ray path in such systems or extending the class of surfaces in one of the existing optical programs. We chose the second way (Terebizh 2005a), especially since the powerful ZEMAX optical program allows it to be implemented with relative ease. This requires writing the additional programs in the C/C++ language, in which the new surfaces [Eqs. (B6)–(B8)] and the optics based on them are described, and then compiling these programs and dynamically linking them with the main program. Thus, we can use the extensive set of tools to study the properties of optical systems provided by ZEMAX.

In this way, we created the files *ksp.dll* and *kss.dll* (from **K**arl **S**chwarzschild **p**rimary/**s**econdary) that define, respectively, the primary and secondary mirrors of an arbitrary aplanat. The quantities $\{D, F, q, \beta\}$ defined in Section 2.2.1 should be specified as additional parameters when calling a surface.

Appendix C

The Complexity of Optical Surfaces

The advance of powerful computers and software for optical system design has drastically accelerated progress in the calculation and manufacture of fine optical systems, but, at the same time, there emerged the temptation to reach performance goals by using arbitrarily complex surfaces.

Usually, an aspheric surface is called complex if it deviates significantly from a nearest sphere. Modern technology for grinding mirrors allows even deviations of about a few millimeters to be realized, but there is a more serious problem connected with a large *gradient of asphericity* G : the *local speed of deviation* of the surface from the nearest sphere.

According to Terebizh (2011), for a not-excessively-fast conic surface of diameter D , paraxial radius of curvature R_0 , and conic constant $b \equiv -\epsilon^2$, the maximum absolute value of G is

$$G_{\max} \simeq 31.25 |b| (D/|R_0|)^3 \text{ } \mu\text{m/mm.} \quad (\text{C1})$$

For mirrors, the equivalent formula is more suitable:

$$G_{\max} \simeq 3.906 |b| \phi^{-3}, \text{ } \mu\text{m/mm,} \quad (\text{C2})$$

where $\phi \equiv |R_0|/(2D)$ is the focal ratio. For example, $G_{\max} \approx 0.54 \text{ } \mu\text{m/mm}$ for a secondary mirror of the Hubble Space Telescope (see Table 2.2), i.e., the deviation of its surface from the nearest sphere increases by $0.54 \text{ } \mu\text{m}$ with an increasing distance from the mirror's center by 1 mm—a perceptible quantity by the standards of optics.

The above equations allow one to feel the nature of the problem, namely, *the asphericity gradient* G is proportional to the conic constant $|b|$ and inversely proportional to the third power of the speed ϕ . Exact calculations should be performed instead of using Eq. (C1) in the case of fast or non-standard aspheric surfaces. The above equations relate only to the radial gradient, whereas some transverse asphericity gradient also takes place.

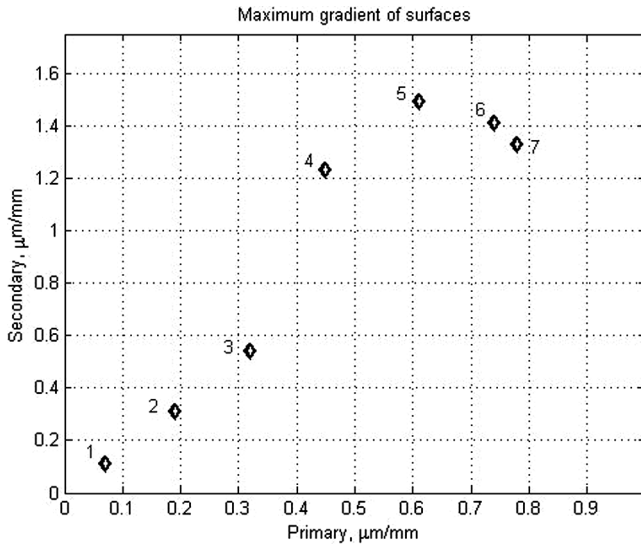


Figure C1 Maximum asphericity gradient ($\mu\text{m}/\text{mm}$) for the primary and secondary mirrors of the Cassegrain telescopes: (1) 2.6-m G. A. Shain, (2) 3.8-m Mayall of KPNO, (3) 2.4-m Hubble Space Telescope, (4) 2.5-m SDSS, (5) 1.8-m Pan-STARRS, (6) 3.5-m WIYN, and (7) 2.6-m VST.

Figure C1 depicts relevant data for a few existing and under-construction two-mirror telescopes. Not shown are many classical telescopes that have a small G . As can be seen, telescopes reach wider fields of view due to both the lens correctors and the high steepness of the mirrors.

According to data provided by Hill and Salinari (1998), $G_{\text{max}} = 2.65 \mu\text{m}/\text{mm}$ for the 8.4-m, $f/1.142$ primary mirror of the Large Binocular Telescope. Within a decade and a half, the highest values of the asphericity gradient were for the 1.8-m Vatican Advanced Technology Telescope (West et al. 1997), which was put into operation in 1993. Its primary and secondary mirrors have a G_{max} of $3.9 \mu\text{m}/\text{mm}$ and $3.6 \mu\text{m}/\text{mm}$, respectively. Both mentioned telescopes were designed according to the Gregorian layout. As we saw in Sections 3.1.3–3.1.4, the asphericity gradient in some modern designs reaches tens of microns per millimeter.

There are two main reasons why the use of too steep optical surfaces, say, with $G_{\text{max}} > 10 \mu\text{m}/\text{mm}$, is undesirable if an alternative solution with smoother surfaces can be attained.

First of all, tolerances for all parameters of the optical system are much tighter if aspherics are used. An inaccurate slope of the spherical surface and its transverse displacement can mutually compensate each other, which is impossible for aspheres. Meanwhile, it is the tolerances that determine the cost and reliability of a telescope, both in its manufacture and, more importantly, in the subsequent operation.

The second point is that the manufacture of steep surfaces entails the use of polishing tools of small size, and this leads to the appearance of a *ripple* with a characteristic scale of about the size of the polishing pad. The nature of the latter is not so important, be it a small solid device, a so-called ‘smart pad,’ or an ion beam; all of which generate irregular ripples on a material as fragile as glass. Oddly enough, the effect of ripple on the optical surface is often underestimated.

The foundations of the general theory concerning the effect of random wave-front errors on image quality were laid down by O’Neill (1963, Chapter 6); a clear discussion of the related issues is given by Schroeder (2000, Sections 11.1.c and 18.1.c). Special studies conducted in several USA institutions before the launch of the Hubble Space Telescope have shown the severity of the problem (Wetherell 1980, 1982). This prompted the opticians to make the surfaces of the HST mirrors unprecedentedly smooth, so that the RMS wavefront deviations for the primary and secondary mirrors are, respectively, $\lambda/64$ and $\lambda/96$ at $\lambda = 0.6328 \mu\text{m}$ (Barrows 1990).

Figure C2(a) illustrates the ‘subsidence’ of the Modulation transfer function (MTF) at a ripple amplitude of $\lambda/14$ and a characteristic transverse dimension of 6 cm (author’s calculations). The first value is chosen equal to the well-known *Mareschal’s limit*, which provides the diffraction quality of images for large-scale wavefront aberrations (Born and Wolf 1999, Section 9.3). It is not difficult to go over from the standard representation of MTF as a function of the spatial frequency f (cycles/mm) to the angular scale in arc seconds:

$$\alpha'' = \frac{206265}{F_{mm} f_{c/mm}}. \tag{C3}$$

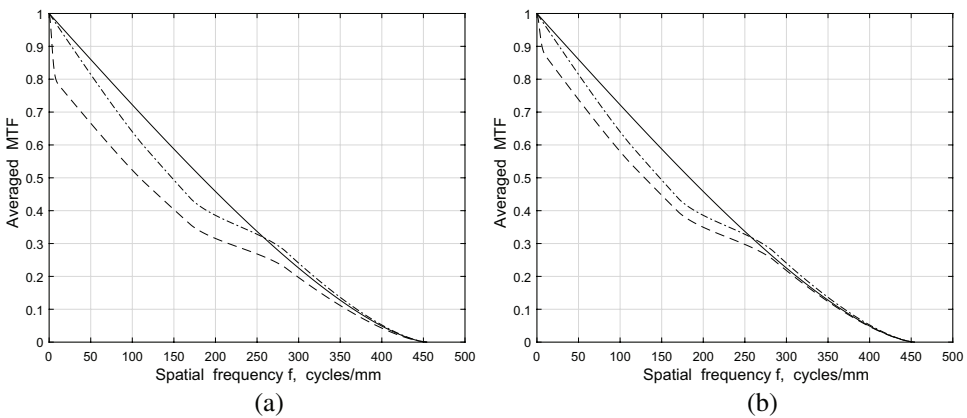


Figure C2 (a) Modulation transfer function of a 3-m, $f/4$ telescope in monochromatic light of $0.55 \mu\text{m}$. Solid line – perfect optics; bar-dotted line – obscuration of 0.25 aperture; dashed line – ripples on the wavefront with the RMS amplitude of $\lambda/14$ and correlation length of 6 cm. (b) The same but with an RMS amplitude of $\lambda/20$.

In this case, details with an angular size of less than $1.5''$ correspond to a frequency range of more than 11.5 c/mm, in which the image contrast drops by almost 20%. Even with a ripple amplitude of $\lambda/20$ [Fig. C2(b)], the contrast drop is about 10%, which is noticeably superior to the effect of light vignetting. The dependence of the MTF on the average transverse size of the ripples is weaker (Wetherell 1980).

Appendix D

Base Prime-Focus Lens Corrector with a 2.5° Field

This appendix, which is viewed as a continuation of the discussion in Section 3.1.2, provides a complete description of the basic model VT-014j of a 4-m telescope with a 2.5° prime-focus lens corrector.

The primary mirror has the shape of a paraboloid with a focal ratio of 2.60, which is slightly less than the focal ratio of the telescope, 2.875. The corrector consists of six spherical lenses made of fused silica (one can use other types of glass, e.g., Schott N-BK7, but fused silica has perceptible advantages). As is often the case now, the last lens is also a detector window. The total axial length of the telescope is 10551 mm, and the length of the corrector alone is 2202 mm. The light diameter of the first corrector lens is 1.10 m, the total mass of the corrector glass within the luminous flux is about 390 kg. Table D1 gives a complete description of the optical scheme of the telescope; Fig. D1 depicts the corrector optical layout and the image quality in the integral light.

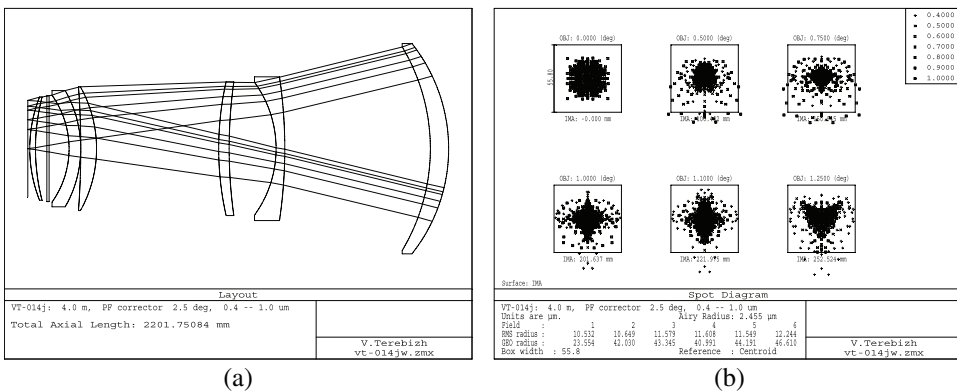


Figure D1 (a) Optical layout of the all-spherical corrector with a flat field 2.5° in diameter (VT-014j design). (b) Corresponding spot diagrams in the integral waveband 0.4–1.0 μm; the box width is 55.8 μm (1.0'').

Table D1 Design data for the VT-014j system.

Surface number	Comments	Radius of curvature, mm	Thickness, mm	Glass	Clear aperture, mm
1	Screen	∞	8253.06	–	1100.00
2	Aperture stop	∞	96.225	–	4000.00
3	Primary*	–20784.6	–8349.28	Mirror	4000.00
4	L1	–883.918	–95.623	FS	1099.97
5		–1036.45	–761.666	–	1064.72
6	L2	–2553.03	–45.511	FS	752.174
7		–591.968	–245.596	–	696.284
8	L3	2515.67	–54.784	FS	696.574
9		1598.01	–639.078	–	700.130
10	L4	–662.780	–82.550	FS	647.458
11		–4360.13	–0.250	–	643.562
12	L5	–609.035	–61.000	FS	608.170
13		–482.700	–104.400	–	559.695
14	Filter	∞	–12.000	N-BK7	553.654
15		∞	–59.294	–	550.533
16	L6 (Window)	1081.85	–30.000	FS	540.464
17		738.660	–10.000	–	539.165
18	Detector	∞			505.090

*The primary mirror is assumed to be parabolic (conic constant $b = -1.00$).

The flat light detector has a diameter of 505 mm. With a system effective focal distance of 11497 mm, the scale in the focal plane is 55.74 $\mu\text{m}/\text{mm}$. Thus, the RMS linear spot sizes along the field radius of 21.0–24.5 μm correspond to 0.38''–0.44''. The D_{80} diameter of images varies in the range of 0.42''–0.54'' along the field. As usual, the quality of images in narrow spectral bands is noticeably better than in integral light.

In terms of telescope optics, the characteristic feature of the corrector is the use of two lens doublets, L2/L3 and L4/L5, each of which is an effective coma compensator. It is this feature that maintains the stability of the corrector's structure with changes in the parameters of the entire system. The importance of the spherical shape of optical surfaces (in particular, the ability to compensate images for atmospheric dispersion) was discussed in Section 3.1.2.

The conic constant of the primary mirror was not fixed in advance, but it was naturally aiming to -1.0 in the course of optimization, so the difference in the shape of the mirror from the paraboloid was eventually negligible. It would be interesting to find out the optimal shape of the mirror for other integral conditions, in particular, with an increase in the field of view size.

The VT-014j model is useful not only as an initial design when searching for specific solutions but also is of independent interest because of the large enough flat field of view achieved with simple optics.

Appendix E

List of Referenced VT Designs

Descriptions of telescopes that can be found in the literature are far from always sufficient for a detailed discussion of their optical systems, so we have provided information about more than two dozen of our own designs. For convenience, the following Table E1 presents the general characteristics of these systems. The Index gives relevant references to the main text.

Table E1 List of VT designs.

Name VT-	D (m)	$ F $ (m)	ϕ	$2w$ (deg)	Optical system
014d	4.0	11.5	2.92	2.12 F	Blanco-R prime focus corrector
014e	4.0	11.4	2.90	2.4 F	Blanco-S prime focus corrector
014f	4.0	11.5	2.92	3.0 F	Blanco-T prime focus corrector
014j	4.0	11.5	2.88	2.5 F	Base prime focus corrector
031d	0.5	1.00	2.00	5.0 F	Hamiltonian telescope
050k	6.0	15.8	2.64	2.0 F	Corrected Gregorian
050m	6.0	12.3	2.05	2.0 F	Corrected Gregorian
056y	1.0	2.19	2.19	3.5 F	Prime focus corrector
060q	1.0	1.88	1.88	10.0 F	Terebizh Ω_3 design
061b	3.5	4.38	1.25	3.5 F	Three-mirror Paul system
077i	0.5	1.54	3.08	5.0 F	Modified Richter–Slevogt
078e	0.4	0.764	1.91	10.0 F	Modified Schmidt–Houghton
090j	1.5	2.98	1.99	2.5 F	Three-mirror Paul system
098v	0.5	1.09	2.19	7.0 F	Modified Sonnefeld camera
099c	0.3	0.425	1.42	7.0 F	Modified Schmidt–Houghton
102j	0.525	1.09	2.08	7.0 F	Terebizh Ω_2 design
110f	0.5	1.03	2.05	7.5 F	Schmidt–Wynne camera
110k	0.5	1.01	2.01	10.0 S	Schmidt camera
110p	0.5	1.65	3.30	4.0 F	Schmidt–Cassegrain camera
114b	0.5	1.25	2.50	3.0 S	Maksutov telescope
119g	0.4	0.80	2.00	30.0 S	Terebizh symmetrical camera
119j	0.5	1.36	2.72	45.0 S	Terebizh symmetrical camera
119w	0.5	0.895	1.79	30.0 S	Modified Schmidt–Houghton
133c	0.4	1.20	3.00	3.0 S	Corrected Gregory–Maksutov
135e	0.5	0.90	1.80	30.0 S	Wynne symmetrical camera
137d	2.5	9.50	3.80	3.0 F	Corrected Cassegrain
137q	3.6	10.8	3.00	2.5 F	Corrected Cassegrain

The designations are as follows: D – the entrance pupil diameter; F – the effective focal length; $\phi \equiv |F|/D$ – the effective focal ratio; $2w$ – the angular field of view, with the addition of ‘F’ if the focal surface is flat or ‘S’ if it has a spherical shape.

Appendix F

New Algorithm for Calculating Anastigmatic Three-Mirror Telescopes

This appendix refers to three-mirror telescopes in which the basic two-mirror system is of the Cassegrain type, that is, it combines a concave primary mirror with a convex secondary mirror (Fig. F1). The tertiary mirror is supposed to be concave. An example of such a system with a positive effective focal length F is the reflective component of the LSST [Figs. 3.11 and 3.12(a)]; an example of a telescope with a negative F is the SNAP [Fig. 2.14(a)]. A distinctive feature of systems with different signs of F is the presence of an intermediate image at $F < 0$.

The purpose of the proposed algorithm is to provide, according to given input characteristics, a complete set of parameters of a three-mirror system with conic surfaces, which is corrected for third-order aberrations, namely, spherical aberration, coma, astigmatism, and field curvature. Such optical systems are called anastigmats. In this case, we get a telescope with all standard surfaces, which provides a subsecond-quality field of the order of several degrees on a flat focal surface. The input parameters mentioned above are: the value of F , mirror diameters, and the distance between the secondary and tertiary mirrors. Such a choice of input parameters is determined by the convenience and stability of the algorithm.

The calculations consider an axial light beam coming from an infinitely distant point source (see Fig. F1). It is assumed that the aperture stop is located at the primary mirror. Specifically, the following design parameters are assumed to be set:

1. The primary mirror diameter $D > 0$;
2. The effective focal length of the telescope $F \neq 0$;
3. The diameter of the secondary mirror $D_2 > 0$;
4. The diameter of the tertiary mirror $D_3 > 0$;
5. The secondary-tertiary spacing $T_2 > 0$.

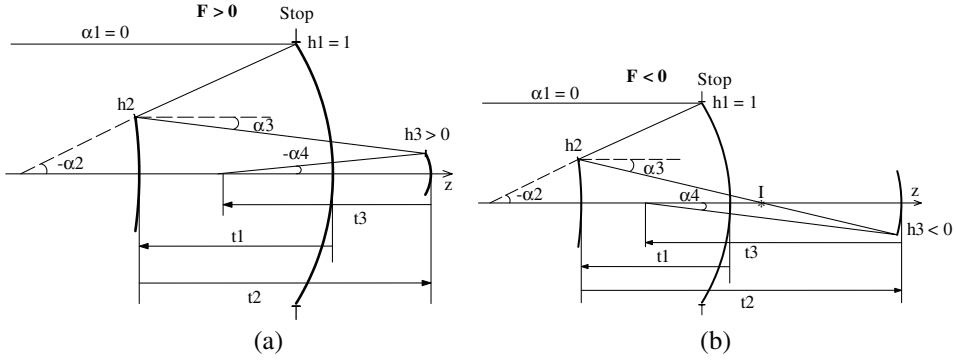


Figure F1 (a) Schematic optical layout of a three-mirror telescope for the case when the effective focal length $F > 0$. (b) Schematic optical layout of a three-mirror telescope for the case when $F < 0$. Point I corresponds to the intermediate image.

One must find the following: the radii of curvature of the mirrors at the vertex, $R_1 < 0$, $R_2 < 0$, and $R_3 < 0$; the distance between the primary and secondary mirrors, $T_1 < 0$; the distance from the tertiary mirror to the focal plane (the back focal length), $T_3 < 0$; and the mirror conic constants of any sign, σ_1 , σ_2 , and σ_3 .

As usual in the design of optics, we introduce the normalization value $H \equiv D/2$ and the following dimensionless parameters:

$$\phi \equiv |F|/D, \quad f \equiv F/H, \quad r_k \equiv R_k/H, \quad t_k \equiv T_k/H; \quad k = 1, 2, 3. \quad (\text{F1})$$

Evidently, $f = \pm 2\phi$, depending on the sign of F . The set of $[\alpha_1 = 0, \alpha_2, \alpha_3, \alpha_4]$ includes the tangents of the corresponding angles indicated in Fig. F1. By definition of the effective focal length, we can write $\alpha_4 = -H/F = -1/f$ for the last angle.

The calculation algorithm consists of the following sequential steps:

$$h_2 = D_2/D; \quad h_3 = \text{sign}(F) \cdot D_3/D; \quad (\text{F2})$$

$$\alpha_3 = (h_2 - h_3)/t_2; \quad (\text{F3})$$

$$\alpha_2 = \frac{t_2 \alpha_3^2 + h_2 \alpha_4}{(1 - h_2)h_3}; \quad (\text{F4})$$

$$t_1 = (1 - h_2)/\alpha_2; \quad t_3 = h_3/\alpha_4; \quad (\text{F5})$$

$$r_1 = \frac{2}{\alpha_2}; \quad r_2 = \frac{2h_2}{\alpha_2 + \alpha_3}; \quad r_3 = \frac{2h_3}{\alpha_3 + \alpha_4}; \quad (\text{F6})$$

$$\sigma_1 = -1 + 2h_2 \alpha_4 \frac{2h_2 + t_2 \alpha_4}{t_1(t_2 - h_3 t_1) \alpha_3^3}; \quad (\text{F7})$$

$$\sigma_2 = -\left(\frac{\alpha_2 - \alpha_3}{\alpha_2 + \alpha_3}\right)^2 + 2\alpha_4 \frac{2h_2 + (t_2 - h_3 t_1)\alpha_4}{t_1 t_2 (\alpha_2 + \alpha_3)^3}; \quad (\text{F8})$$

$$\sigma_3 = -\left(\frac{\alpha_3 - \alpha_4}{\alpha_3 + \alpha_4}\right)^2 - 2h_2 \alpha_4 \frac{2h_2 + (2t_2 - h_3 t_1)\alpha_4}{t_2 (t_2 - h_3 t_1) (\alpha_3 + \alpha_4)^3}. \quad (\text{F9})$$

These equations allow us to find all the necessary parameters, but we still need to clarify the range of initial values of the diameter of the tertiary mirror D_3 that lead to negative radii of curvature. If $F < 0$, then such restrictions arise only when considering obscuration of light by mirrors. If F is positive, the requirement $R_1 < 0$ leads to a condition

$$|D_2 - D_3| < (D_2 T_2 / \phi)^{1/2} \quad (\text{F10})$$

that should be inserted immediately after setting Eq. (F1). The conditions $R_2 < 0$ and $R_3 < 0$ lead to inequality

$$D_3^{\min} < D_3 < D_3^{\max}, \quad (\text{F11})$$

where

$$\begin{cases} D_3^{\min} = D h_3^{\max}, D_3^{\max} = D h_3^{\min}, \\ h_3^{\min} = \max(0, h_2 - \tau), \\ h_3^{\max} = h_2 + (\tau h_2)^{1/2}, \\ \tau = T_2 / F. \end{cases} \quad (\text{F12})$$

This condition should be checked after Eq. (F4).

The system generated according to the algorithm should be evaluated with respect to light shielding and focal ratios of mirrors, which may be inconvenient to manufacture. These focal ratios are given by the following formulas:

$$\phi_1 = |r_1|/4, \quad \phi_2 = |r_2|/(4h_2), \quad \phi_3 = |r_3|/(4|h_3|). \quad (\text{F13})$$

We illustrate the algorithm with the example of the SNAP system described in Section 2.3.2. Table F1 includes both the original design parameters according to Lampton et al. (2002) and the results obtained using the described algorithm. In the calculations, the above five parameters of the original model were used. As can be seen from Table F1, the calculated parameters are close to the original parameters, although this is not necessary due to the different origin of the models. The necessary property is that any model should provide high-quality images within a wide, flat field of view. The algorithm achieves this; the RMS diameter of the images varies from a

Table F1. Parameters of the SNAP three-mirror telescope and the results obtained using the algorithm. All linear dimensions are given in millimeters.

Parameter	SNAP	Algorithm
D	2000	The same
F	-21445.5	The same
D_2	372.0721	The same
D_3	165.0453	The same
R_1	-4908.057	-4840.285
R_2	-1098.949	-1087.443
R_3	-1405.998	-1402.546
T_1	-1999.996	-1969.909
T_2	3780.087	The same
T_3	-1770.085	-1769.739
σ_1	-0.981128	-0.981076
σ_2	-1.847493	-1.833956
σ_3	-0.599000	-0.601330

diffraction-limited value on the optical axis to $0.25''$ at the edge of a flat field with a diameter of 1.5° .

Direct numerical optimization and the analytical approach should not be opposed to each other. The first method requires the formulation of a number of restrictions that provide the optimal solution under the given conditions, but not necessarily the theoretically best system, because it can be outside the given domain of the parametric space. The second method immediately gives the best solution but only within the framework of the theory of third-order aberrations. A reasonable approach, apparently, uses an analytical solution in the first stage, followed by light numerical optimization in the second stage.

In Section 2.3.2, we touched on the difficulties characteristic of analytical solutions by Korsch (1972), Robb (1978), and Lee and Yu (2009). The algorithm proposed here requires the assignment of simple natural input data and, no less important, is stable with respect to small variations of the latter. Like the authors mentioned, we also used the third-order theory of aberrations; however, our path was different, both in interpreting the Petzval condition and in the analytical representation of primary aberrations. Appropriate calculations are very cumbersome; surprisingly, Eqs. (F7) – (F9) are simple. Full calculations are forthcoming.

Bibliography

- [1] T. Abbott, F. Abdalla, S. Allam, et al., “The dark energy survey data release 1”, *arXiv:1801.03181v1* [astro-ph.IM] 9 Jan (2018).
- [2] M. Ackermann, J. McGraw, and P. Zimmer, “Are curved focal planes necessary for wide-field survey telescopes?”, *Proc. SPIE* **6267**, 626740-1-10 (2006).
- [3] M. Ackermann, J. McGraw, and P. Zimmer, “An overview of wide-field-of-view optical designs for survey telescopes”, *Proc. AMOS Conf.* **E41**, 1–19 (2010).
- [4] C. Akerlof, R. Kehoe, T. McKay, et al., “The ROTSE-III robotic telescope system”, *PASP* **115**, 132–140 (2003).
- [5] R. Allsman, W. Althouse, S. Aronson, et al., “The Large Synoptic Survey Telescope (LSST)”, Proposal for LSST (2006).
- [6] M. Amon, U.S. Patent 3,711,184 (1973).
- [7] M. Amon, S. Rosin, and B. Jackson, “Large objective for night observation”, *Appl. Opt.* **10**, 490–493 (1971).
- [8] J. Angel, N. Woolf, and H. Epps, “A 1.8-m three mirror telescope proposal for survey with CCDs”, *Proc. SPIE* **332**, 134–142 (1982).
- [9] J. Angel, M. Lesser, R. Sarlot, and T. Dunham, “Design for an 8-m telescope with a 3 degree field at $f/1.25$: the Dark Matter Telescope”, *ASP Conf. Ser.* **195**, 81–93 (2000).
- [10] J. Baker, “A family of flat-field cameras, equivalent in performance to the Schmidt camera”, *Proc. Amer. Phil. Soc.* **82**(3), 339–349 (1940).
- [11] J. Baker, U.S. Patent 2,458,132 (1945).
- [12] J. Baker, “The catadioptric refractor”, *Astron. J.* **59**, 74–83 (1954).
- [13] J. Baker, U.S. Patent 3,022,708 (1962).
- [14] J. Baker, “On improving the effectiveness of large telescopes”, *IEEE Trans. Aerosp. Electron. Syst.* **5**, 261–272 (1969).
- [15] J. Barbe, G. Cerutti-Maori, and J.-P. Roselot, “Large field-of-view telescope for deep surveys”, *Proc. SPIE* **2871**, 150–158 (1997).
- [16] M. Bass (ed.), *Handbook of Optics*, **II**, McGraw-Hill, New York (1995).
- [17] E. Bellm, S. Kulkarni, M. Graham, et al., “The Zwicky Transient Facility: system overview, performance, and first results”, *arXiv:1902.01932v1* [astro-ph.IM], 5 Feb 2019.

- [18] T. Belorossova, D. Maksutov, N. Merman, and M. Sosnina, “700-mm meniscus astrometric telescope” (in Russian), *Trans. of the 15th Astrometric Conf.*, Leningrad, 215–219 (1963).
- [19] N. Benitez, E. Gaztañaga, R. Miquel, et al., “Measuring baryon acoustic oscillations along the line of sight with photometric redshifts: the PAU survey”, *Astroph. J.* **691**, 241–280 (2009).
- [20] H. Bennett, US Patent 2,571,657 (1945).
- [21] T. Blake, E. Pearce, J. Gregory, et al., “Utilization of a curved focal surface array in a 3.5-m wide field of view telescope”, *Proc. AMOS Conf.*, 256–265 (2013).
- [22] M. Born and E. Wolf, *Principles of Optics*, 7th Ed., Cambridge Univ. Press (1999).
- [23] A. Bouwers, Netherlands Patent 102,016 (1941).
- [24] A. Bouwers, *Achievements in Optics*, Elsevier, Amsterdam (1946).
- [25] I. Bowen, “Astronomical Optics”, in *Annual Rev. Astron. and Astrophys.* **5**, 45–66 (1967).
- [26] R. Buchroeder, “Application of aspherics for weight reduction in selected catadioptric lenses”, *Opt. Sci. Center, Univ. of Arizona, Techn. Rep.* **69** 1–13 (1971).
- [27] A. Buffington, “Very-wide-angle optical systems suitable for spaceborne photometric measurements”, *Appl. Opt.*, **37**, 4284–4293 (1998).
- [28] C. Burch, “On the optical see-saw diagram”, *Monthly Notices of RAS* **102**, 159–165 (1942).
- [29] C. Burrows, “Hubble Space Telescope. Optical Telescope Assembly Handbook”, Vers. 1, STSI (1990).
- [30] W. Busch, R. Ceragioli, and W. Stephani, “A little-known 3-lens catadioptric camera by Bernhard Schmidt”, *Journ. of Astron. History and Heritage*, **16**(2), 107–126 (2013).
- [31] L. Canzek, U.S. Patent 4,547,045 (1945).
- [32] B. Carter, M. Ashley, Y-S. Sun, and J. Storey, “Redesigning a Baker-Nunn camera for CCD imaging”, *Proc. ASA* **10**(1), 74–76 (1992).
- [33] A. Cenarro, M. Moles, D. Cristóbal-Hornillos, et al., “The Javalambre Astro-physical Observatory project”, *Proc. SPIE* **7738**, 0V–1 (2010).
- [34] Z. Challita, T. Agycs, E. Hugot, et al., “Design and development of a freeform active mirror for an astronomy application”, *Opt. Eng.* **53**(3), 031311 (2014).
- [35] K. Chambers, E. Magnier, N. Metcalfe, et al., “The Pan-STARRS1 Surveys”, *arXiv:1612.05560* [astro-ph.IM] (2016).
- [36] H. Chrétien, “Le telescope de Newton et le telescope aplanétique”, *Rev. d’Opt. Theor. et Instrum.* **1**, 13–22, 49–64 (1922).
- [37] A. Couder, *C.R. Acad. Sci. Paris*, **183** (II), 1276 (1926).
- [38] X. Cui, D. Su, and Y. Wang, “Progress in the LAMOST optical system”, *Proc. SPIE* **4003**, 347–354 (2000).

- [39] J. Daley, *Amateur Construction of Schupmann Medial Telescopes* (1984).
- [40] A. Danjon and A. Couder, *Lunettes et Telescopes*, Edition De La Revue D'optique Théorique et Instrumentale (1935). Re-issued: Blanchard, Paris (1983).
- [41] G. Dimitroff and J. Baker, *Telescopes and Accessories*, Blakiston, Philadelphia (1945).
- [42] S. Djorgovski, A. Mahabal, A. Drake, et al., "Sky Surveys", in *Astronomical Techniques, Software, and Data*, H. Bond, Ed., Springer (2012).
- [43] P. Doel, T. Abbott, M. Antonik, et al., "Design and status of the optical corrector for the DES survey instrument", *Proc. SPIE* **7014**, 70141V (2008).
- [44] A. Drake, S. Djorgovski, A. Mahabal, et al., "First results from the Catalina Real-Time Transient Survey", *Astroph. J.*, **696**, 870–884 (2009).
- [45] J. Dyson, British patent 586,851 (1944).
- [46] H. Epps and D. Fabricant, "Field correctors for wide-field CCD imaging with Ritchey-Chrétien telescopes", *Astron. J.*, **113**, 439–445 (1997).
- [47] L. Epstein, "All-reflecting Schmidt camera", *PASP*, **79**, 132–135 (1967).
- [48] L. Epstein, "Improved geometry for the all reflecting Schmidt telescope", *Appl. Optics*, **12**, 926 (1973).
- [49] E. Etedgui-Atad and S. Worswick, "Optical design concept of the 4-m visible and infrared survey telescope for astronomy", *Proc. SPIE*, **4842**, 95–105 (2003).
- [50] B. Flaugher, H. Diehl, K. Honscheid, et al., "The Dark Energy Camera". *Astron. J.*, **150**, 150–193 (2015).
- [51] J. Flugge, "Neue spiegelobjektive", *Z. für Instrumentenkunde*, **61**, 175 (1941).
- [52] O. Fors, F. Montojo, J. Nunez, et al., "Status of telescope Fabra ROA at Montsec: optical observations for space surveillance and tracking", *arXiv:1109.5903v1 [astro-ph.EP]*1–6 (2011).
- [53] D. Gabor, British Patent 544,694 (1941).
- [54] J. Gardner, J. Mather, M. Clampin, et al., "The James Webb Space Telescope", *Space Science Reviews* **123**, 485–606 (2006).
- [55] J. Geary, *Introduction to Lens Design With Practical ZEMAX Examples*, Willmann-Bell, Richmond (2002).
- [56] J. Gonzalez, "SPM-Twin telescopes: project overview", *RevMexAA (SC)*, **28**, 39–48 (2007).
- [57] J. Gonzalez and V. Orlov, "Relevant optical issues of the SPM-Twin telescopes", *RevMexAA (SC)* **28**, 60–66 (2007).
- [58] T. Grayson, "Curved focal plane wide-field-of-view telescope design", *Proc. SPIE* **4849**, 269–274 (2002).
- [59] W. Gressler, "LSST optical design summary", 5/1 (2009).
- [60] W. Hamilton, English Patent 3781 (1814).

- [61] C. Harmer, C. Claver, and G. Jakoby, “The optical design of the WIYN one degree imager (ODI)”, *Proc. SPIE* **4836**, 260–270 (2002).
- [62] C. Harmer and C. Wynne, “A simple wide-field Cassegrain telescope”, *Monthly Notices of RAS*, **177**, 25P–30P (1976).
- [63] D. Hawkins and E. Linfoot, “An improved type of Schmidt camera”, *Monthly Notices of RAS* **105**, 334–344 (1945).
- [64] E. Hecht, *Optics*, 3rd Ed., Addison-Wesley, Reading (1998).
- [65] K. Henize, “The Baker-Nunn satellite-tracking camera”, *Sky and Telescope*, 108–111, Jan. (1957).
- [66] M. Herzberger, “Optics from Euclid to Huygens”, *Appl. Optics* **5**, 1383–1393 (1966).
- [67] J. Hill and P. Salinari, “Large Binocular Telescope project”, *Proc. SPIE* **3352**, 23–33 (1998).
- [68] K. Hodapp, N. Kaiser, H. Aussel, et al., “Design of the Pan-STARRS telescopes”, *Astron. Nachr.* **325**, 636–642 (2004).
- [69] J. Houghton, British Patent 546,307 (1942).
- [70] J. Houghton, U.S. Patent 2,350,112 (1944).
- [71] S. Howell, *Handbook of CCD Astronomy*, Cambridge Univ. Press (2000).
- [72] E. Hugot, Xin Wang, D. Valls-Gabaud, et al., “A freeform-based, fast, wide-field, and distortion-free camera for ultralow surface brightness surveys”, *Proc. SPIE* **9143**, 91434X (2014).
- [73] Z. Ivezić, S. Kahn, J. Tyson, et al., “LSST: from science drivers to reference design and anticipated data products”, *arXiv:0805.2366* (2008).
- [74] O. Iwert and B. Delabre, “The challenge of highly curved monolithic imaging detectors”, *Proc. SPIE* **7742**, 27–35 (2010).
- [75] O. Iwert, D. Ouelette, M. Lesser, and B. Delabre, “First results from a novel curving process for large area scientific imagers”, *Proc. SPIE* **8453**, 1–15 (2012).
- [76] W. Jeas and R. Anctil, “The Ground-based Electro-Optical Deep Space Surveillance /GEODSS/ system”, *Military Electronics/Countermeasures*, **7**, 47–51 (1981).
- [77] D. Jones, “Wide-field prime focus corrector for the Anglo-Australian telescope”, *Appl. Optics* **33**, 7362–7366 (1994).
- [78] N. Kaiser, H. Aussel, B. Burke, et al., “Pan-STARRS: a large synoptic survey telescope array”, *Proc. SPIE* **4836**, 154–164 (2002).
- [79] S. Kent, R. Bernstein, T. Abbott, et al., “Preliminary optical design for a 2.2 degree diameter prime focus corrector for the Blanco 4 meter telescope”, *Proc. SPIE*, **6269**, 37–47 (2006).
- [80] S.-L. Kim, B.-G. Park, C.-U. Lee, et al., “Technical specifications of the KMT-Net observation system”, *Proc. SPIE*, **7733-3F** (2010).
- [81] S.-L. Kim, B.-G. Park, C.-U. Lee, et al., “Wide-field telescope design for the KMTNet project”, *Proc. SPIE*, **8151-1B** (2011).
- [82] H. King, *The History of the Telescope*, Griffin, London (1955).

- [83] H. Köhler, “Die entwicklung der aplanatischen spiegelsysteme”, *Astron. Nachr.* **278**, 1–23 (1948).
- [84] M. Konacki, P. Lejba, P. Sybilski, et al., “The Solaris-Panoptes global network of robotic telescopes and the Borowiec Satellite Laser Ranging System for SST: a progress report”, *Proc. AMOS Conf.* (2017).
- [85] Y. Komiyama, H. Aihara, H. Fujimori, et al., “Hyper Supreme-Cam: camera design”, *Proc. SPIE* **7735**, 77353F-1-12 (2010).
- [86] D. Korsch, “Closed form solution for three-mirror telescopes, corrected for spherical aberration, coma, astigmatism, and field curvature”, *Appl. Optics* **11**, 2986–2987 (1972).
- [87] D. Korsch, “Reflective Schmidt corrector”, *Appl. Optics* **13**, 2005–2006 (1974).
- [88] D. Korsch, “Anastigmatic three-mirror telescope”, *Appl. Optics* **16**, 2074–2077 (1977).
- [89] D. Korsch, “Design and optimization technique for three-mirror telescopes”, *Appl. Optics* **19**, 3640–3645 (1980).
- [90] D. Korsch, *Reflective Optics*, Academic Press, San Diego (1991).
- [91] H. Kramer, *Observation of the Earth and its Environment: Survey of Missions and Sensors*, 4th ed., Springer (2002).
- [92] M. Laikin, *Lens Design*, Dekker, New York (1995).
- [93] M. Lampton, C. Akerlof, G. Aldering, et al., “SNAP telescope”, *Proc. SPIE*, **4849**, 215–226 (2002).
- [94] C. Lanczos, *Applied Analysis*, Dover, New York (1988).
- [95] B. Law, J. Africano, K. Hamada, et al., “Phoenix telescope at AMOS: return of the Baker-Nunn camera”, *Proc. SPIE* **4836**, 119–128 (2002).
- [96] N. Law, S. Kulkarni, R. Dekany, et al., “The Palomar Transient Factory: system overview, performance, and first results”, *PASP*, **121**, 1395–1408 (2009).
- [97] N. Law, S. Sivanandam, R. Carlberg, et al., “New transiting planet surveys in the high Canadian Arctic”, *AAS Meeting 219*, id.125.04 (2012).
- [98] N. Law, O. Fors, J. Ratzloff, et al., “Evryscope science: exploring the potential of all-sky gigapixel-scale telescopes”, *arXiv:1501.03162v1* 13 Jan (2015).
- [99] J.-U. Lee and S.-M. Yu, “Analytic design procedure of three-mirror telescope corrected for spherical aberration, coma, astigmatism, and Petzval field curvature”, *J. of the Opt. Soc. of Korea*, **13**, 184–192 (2009).
- [100] G. Lemaitre, “Reflective Schmidt anastigmat telescopes and pseudo-flat made by elasticity”, *J. Opt. Soc. Am.* **66**, 1334–1340 (1976).
- [101] G. Lemaitre, *Astronomical Optics and Elasticity Theory. Active Optics Methods*, Springer (2009).
- [102] E. Linfoot, “On some optical systems employing aspherical surfaces”, *Monthly Notices of RAS* **103**, 210–221 (1943).

- [103] E. Linfoot, “The Schmidt-Cassegrain systems and their application to astronomical photography”, *Monthly Notices of RAS* **104**, 48–64 (1944).
- [104] E. Linfoot, “On the optics of the Schmidt Camera”, *Monthly Notices of RAS* **109**, 279–297 (1949).
- [105] E. Linfoot, *Recent Advances in Optics*, Oxford (1955).
- [106] D. Lynden-Bell, “Exact optics: a unification of optical telescope design”, *Monthly Notices of RAS* **334**, 787–796 (2002).
- [107] D. Lynden-Bell and R. Willstrop, “Exact optics – IV. Small ‘trumpet’ correctors for large spheres”, *Monthly Notices of RAS* **351**, 317–323 (2004).
- [108] M. MacFarlane and E. Dunham, “Simplifying the prime focus corrector of the Discovery Channel Telescope”, *Proc. SPIE* **6269**, 29–36 (2006).
- [109] D. Maksutov, “Anaberration reflecting surfaces and systems, and new ways to test them”, *Trans. of the State Opt. Inst. (GOI)*, **86**, 1–119 (1932).
- [110] D. Maksutov, USSR Patent No. 65007, 42h, 10₀₁ (1941).
- [111] D. Maksutov, “New catadioptric systems”, *Trans. USSR Academy* **37**, No. **4**, 147 (1942).
- [112] D. Maksutov, “New catadioptric meniscus systems”, *J. Opt. Soc. Am.* **34**, 270–284 (1944).
- [113] D. Maksutov, *Astronomical Optics* (in Russian), Gostechizdat (1946).
- [114] D. Mancini, G. Sedmak, M. Brescia, et al., “VST project: technical overview”, *Proc. SPIE* **4004**, 79–90 (2000).
- [115] P. Martini, S. Bailey, R. Besuner, et al., “Overview of the Dark Energy Spectroscopic instrument”, *Proc. SPIE* **10702**, 1–11 (2018).
- [116] T. Matsuda, US Patent 2015/0070496 A1 (2015).
- [117] J. Maxwell, *Catadioptric Imaging Systems*, American Elsevier, New York (1972).
- [118] M. Mersenne, *L’Harmonie Universelle: de la nature des sons*, Paris (1636).
- [119] N. Mikhel’son, *Optical Telescopes. Theory and Framework* (in Russian), Moscow, Nauka (1976).
- [120] N. Mikhel’son, “Three-mirror telescope anastigmats”, *Optica Acta* **29**, 979–983 (1980).
- [121] T. Miller, R. Besuner, M. Levi, et al., “Fabrication of the DESI corrector lenses”, *Proc. SPIE* **10706**, id. 107060X 9 pp. (2018).
- [122] S. Miyazaki, Yu. Komiyama, S. Kawanomoto, et al., *Publ. Astron. Soc. Japan* **70** (SP1), 1–26 (2018).
- [123] S. Mondal, K. Gupta, S. Lata, et al., “Development of ARIES Baker-Nunn camera to a wide-field imaging telescope with CCD”, *arXiv:0905.0361v1* 4 May (2009).

- [124] A. Moore, M. Kasliwal, C. Gelino, et al., “Unveiling the dynamic infrared sky with Gattini-IR”, *Proc. SPIE* **9906**, id. 99062C 12 pp (2016).
- [125] J. Morgan and W. Burgett, “System/Subsystem specification for the Pan-STARRS PS4 telescopes”, *PSDC-350-002* (2009).
- [126] P. Muursepp and Y. Weismann, *Bernhard Schmidt* (in Russian), Leningrad, Nauka (1984).
- [127] E. O’Neill, *Introduction to Statistical Optics*, Addison-Wesley (1963).
- [128] D. Osterbrock, *Getting the picture: wide-field astronomical photography from Barnard to the achromatic Schmidt, 1888-1992*, *Journ. for the History of Astronomy*, **XXV**, 1–14 (1994).
- [129] R. Owen, “Easily fabricated wide angle telescope”, *Proc. SPIE* **1354430**–433 (1990).
- [130] M. Paul, “Systemes correcteurs pour reflecteurs astronomiques”, *Rev. Opt. Theor. Instrum.* **14**, 169–202 (1935).
- [131] K. Penning, German Pat. No. P 82 128 IX a/42h (1941).
- [132] H. Plummer, “On the images formed by a parabolic mirror. I. The geometrical theory”, *Monthly Notices of RAS* **62**, 352–370 (1902).
- [133] W. Press, S. Teukolsky, W. Wetterling, and B. Flannery, *Numerical Recipes*, Cambridge Univ. Press (1992).
- [134] A. Rakich, M. Blundell, G. Pentland, et al., “The SkyMapper wide field telescope”, *Proc. SPIE* **6267**, 62670E (2006).
- [135] A. Rakich and N. Rumsey, *Adv. Opt. Techn.* **2**(1), 111–116 (2013).
- [136] R. Richter and H. Slevogt, Deutsche Patentanmeldung (Zeiss) Z 26 592 IXa 42h, 5.9.1941 (1941).
- [137] R. Richter and H. Slevogt, Deutsches Patentamt, Patentschrift No. 904 602, Z 615 IXa/42h (1954).
- [138] G. Ritchey and H. Chrétien, “Présentation du premier modèle de télescope aplanétique”, *C.R. Acad. Sci. Paris* **185**, 266–268 (1927).
- [139] P. Robb, “Three-mirror telescopes: design and optimization”, *Appl. Opt.* **17**, 2677–2685 (1978).
- [140] F. Ross, “Lens systems for correcting coma of mirrors”, *Astroph. J.* **81**, 156–172 (1935).
- [141] F. Roy, “The One-Metre Initiative: an update”, *Journ. of the Royal Soc. of Canada* **104**, 16–23, 2010.
- [142] N. Rumsey, “A compact three-reflection astronomical camera”, in *Optical Instruments and Techniques*, Oriel Press, 514–520 (1969).
- [143] M. Rusinov, *Non-spherical Surfaces in Optics*, Nedra, Moscow (in Russian) (1973).
- [144] M. Rusinov, *Technical Optics*, Mashinostroenie, Leningrad (in Russian) (1979).
- [145] H. Rutten and M. van Venrooij, *Telescope Optics*, Willmann-Bell, Richmond (1999).

- [146] R. Sampson, *Phil. Trans. Roy. Soc. (London)* **213**, 27–66 (1913a).
- [147] R. Sampson, “On correcting the field of a Newtonian telescope”, *Monthly Notices of RAS* **73**, 524–527 (1913b).
- [148] W. Saunders, P. Gillingham, G. Smith, et al., “Prime focus wide-field corrector designs with lossless atmospheric dispersion correction”, *Proc. SPIE* **9151**, 91511M (2014).
- [149] B. Schmidt, “Ein lichstarkes komafreies spiegelsystem”, *Centr. Ztg. f. Opt. u. Mech.* **52**, 25–26 (1931). Reprinted in *Selected Papers on Astronomical Optics*, D. Schroeder, Ed., SPIE Milestone Series **73**, 165–168 (1993).
- [150] D. Schroeder, “All-reflecting Baker-Schmidt flat-field telescopes”, *Appl. Optics* **17**, 141–144 (1978).
- [151] D. Schroeder, Ed., *Selected Papers on Astronomical Optics*, SPIE Milestone Series, V. MS **73**, SPIE Optical Engineering Press (1993).
- [152] D. Schroeder, *Astronomical Optics*, Academic Press, San Diego (2000).
- [153] L. Schupmann, *Die Medial-Fernrohre*, B.G. Teubner, Leipzig (1899).
- [154] K. Schwarzschild, “Untersuchungen zur geometrischen optik. II”, *Astronomische Mittheilungen der Königlichen Sternwarte zu Göttingen*, **10**, 3–28 (1905). Reprinted in *Selected Papers on Astronomical Optics*, D. Schroeder, Ed., SPIE Milestone Series **73**, 3–23 (1993).
- [155] G. Sedmak, S. Carozza, and G. Marra, “Numerical characterization of the observed point spread function of the VST wide-field telescope”, in *6th Livio Scarsi Int. Workshop on Data Analysis in Astronomy*, Erice 15-22 April, 134–140 (2007).
- [156] G. Sedmak, D. Mancini, D. Ferruzzi, et al., *VST: preliminary design review*, Osserv. Astr. Napoli (1999).
- [157] L. Seppala, “Simultaneous design of an optical system and null tests of the components: examples and results from the Large-aperture Synoptic Survey Telescope”, *Proc. SPIE* **7652**, 76520I (2010).
- [158] D. Shafer, 2017, “Catadioptric optically compensated zooming with one movin element”, *Proc. SPIE* **2539**, 105901C (2017).
- [159] M. Shenker, U.S. Patent 3,252,373 (1966).
- [160] M. Sholl, M. Ackermann, C. Bebek, et al., “BigBOSS: a stage IV dark energy redshift survey”, *Proc. SPIE* **8446**, 844667 12 pp. (2012).
- [161] B. Singaravelu and R. Cabanac, “Obstructed telescopes versus unobstructed telescopes for wide field survey – a quantitative analysis”, *PASP* **126**, 386–397 (2014).
- [162] G. Smith, *Practical Computer-Aided Lens Design*, Willmann-Bell, Richmond (1998).
- [163] R. Smith, R. Dekany, C. Bebek, et al., “The Zwicky transient facility observing system”, *Proc. SPIE* **9147**, E..79 (2014).
- [164] A. Sonnefeld, DRP (Zeiss) 697 003, 19.11.1936 (1936).

- [165] B. Starr, C. Claver, S. Wolff, et al., “LSST Instrument Concept”, *Proc. SPIE* **4836**, 228–239 (2002).
- [166] K. Strehl, “Ideales Fernrohr”, *Central Zeitung fur Optik und Mechanik*, **XXVI**, No. 7, p. 82 (1905).
- [167] H. Suiter, *Star Testing Astronomical Telescopes*, Willmann-Bell, Richmond (1994).
- [168] K. Taylor and P. Gray, “Design study for a new wide-field AAT Prime-focus – The 2dF”, *Proc. SPIE* **1236**, 290–299 (1990).
- [169] K. Taylor and P. Gray, “2dF: the AAT’s planned wide-field multifiber spectroscopic survey facility: report on commissioning the 2dF corrector/ADC”, *Proc. SPIE* **2198**, 136–142 (1994).
- [170] V. Terebizh, “Optimal baffle design in a Cassegrain telescope”, *Experimental Astronomy* **11**, 171–191 (2001a).
- [171] V. Terebizh, “All-spherical catadioptric telescopes with diffraction-limited image quality”, *Bull. of Crimean Astroph. Obs.* **97**, 101–113 (2001b).
- [172] V. Terebizh, “Concept optical design for a very wide-field corrector for the Blanco 4-m telescope”, *AURA-CTIO Report No. C10430A* (2003).
- [173] V. Terebizh, “Wide-field corrector in prime focus of a Ritchey-Chrétien telescope”, *Astronomy Letters* **30**, 200–208 (2004).
- [174] V. Terebizh, “Two-mirror Schwarzschild aplanats. Basic relations”, *Astronomy Letters* **31**, 129–139 (2005a).
- [175] V. Terebizh, *Modern Optical Telescopes* (in Russian), Moscow, Fizmatlit (2005b).
- [176] V. Terebizh, “Wide-field corrector for a Gregory telescope”, *Astronomy Reports* **51**, 597–603 (2007a).
- [177] V. Terebizh, “Wide-field optical telescopes” (in Russian), in *Astronomy 2006: Traditions, Present, and Future*, St.-Petersburg Univ. Press, 362–395 (2007b).
- [178] V. Terebizh, “Wide-field telescopes with a Mangin mirror”, *astro-ph/0710.2165v1*, 10 Oct (2007c).
- [179] V. Terebizh, “A purely reflective large wide-field telescope”, *Bull. of Crimean Astroph. Obs.* **104**, 240–248 (2008); *astro-ph/0707.1731v2*, 31 Sep (2007).
- [180] V. Terebizh, “New designs of survey telescopes”, *Astron. Nachr.* **332**, 714–742 (2011).
- [181] V. Terebizh, “Autocollimating compensator for controlling aspheric optical surfaces”, *Monthly Notices of RAS* **440**, 1824–1827 (2014).
- [182] V. Terebizh, “All-spherical telescope with extremely wide field of view”, *Astron. Nachr.* **337**, 571–575 (2016a).
- [183] V. Terebizh, “On the capabilities of survey telescopes of moderate size”, *Astron. J.* **152**, 121–130 (2016b).
- [184] V. Terebizh, “Space telescope designed for accurate measurements”, *Astron. J.* **154**, 244–246 (2017).

- [185] V. Terebizh, “Compact survey telescope with a diameter of 3.6 meters”, *Astron. J.* (2019) In press.
- [186] J. Tonry, “An early warning system for asteroid impact”, *PASP*, **123**, 58–73 (2011).
- [187] J. Tonry, L. Denneau, A. Heinze, et al., “ATLAS: a high-cadence all-sky survey system”, *arXiv:1802.00879v2* [astro-ph.IM] 28 Mar (2018).
- [188] M. Tuell, H. Martin, J. Burge, et al., “Optical testing of the LSST combined primary/tertiary mirror”, *Proc. SPIE* **7739**, 77392V–1 (2010).
- [189] H. Turnbull, *The Correspondence of Isaac Newton*, **I**, 1661–1675, Cambridge (1959).
- [190] J. Tyson and S. Wolff, “Survey and other telescope technologies and discoveries”, *Proc. SPIE* **4836**, 10- (2002).
- [191] Y. Väisälä, “Über Spiegelteleskope mit großem Geischtfeld”, *Astron. Nachr.* **259**, 197 (1936).
- [192] D. Valls-Gabaud, MESSIER Collaboration, “The MESSIER surveyor: unveiling the ultra-low surface brightness universe”, *Proc. of the IAU Symp.* **321**, 199–201 (2017).
- [193] A. Wachmann, “From the life of Bernhard Schmidt”, *Sky & Telescope* **XV**, 1–9 (1955).
- [194] A. Walker, “The Large Synoptic Survey Telescope (LSST) and its impact on variable star research”. *Mem. S.A. It.* **73**, 23–27 (2002).
- [195] S.-G. Wang, D.-Q. Su, Y.-Q. Chu, et al., “Special configuration of a very large Schmidt telescope for extensive astronomical spectroscopic observation”, *Appl. Optics* **35**, 5155–5161 (1996).
- [196] S. West, R. Nagel, D. Harvey, et al., “Progress at the Vatican Advanced Technology Telescope”, *Proc. SPIE* **2871**, 74–85 (1997).
- [197] W. Wetherell, “Evaluation of image quality”, in *Applied Optics and Optical Engineering*, **8**, R. Shannon and J. Wyant, Eds, Academic Press (1980).
- [198] W. Wetherell, “Effects of mirror surface ripple on image quality”, in *Advanced Technology Optical Telescopes*, *Proc. SPIE* **332**, 429–443 (1982).
- [199] W. Wetherell and M. Rimmer, “General analysis of aplanatic Cassegrain, Gregorian, and Schwarzschild telescopes”, *Appl. Optics* **11**, 2817–2832 (1972).
- [200] D. Whiteside, *The Mathematical Papers of Isaac Newton*, **III**, 1670–1673, Cambridge (1969).
- [201] E. Wiedemann, Deutsches Patentamt 3121044 A1 (1981).
- [202] G. Williams, E. Olszewski, M. Lesser, and J. Burge, “90prime: a prime focus imager for the Steward Observatory 90-in. telescope”, *Proc. SPIE* **5492**, 787–798 (2004).
- [203] R. Willstrop, “The Mersenne-Schmidt: a three-mirror survey telescope”, *Monthly Notices of RAS* **210**, 597–609 (1984).

- [204] R. Willstrop and D. Lynden-Bell, “Exact optics – II. Exploration of designs on- and off-axis”, *Monthly Notices of RAS* **342**, 33–49 (2003).
- [205] R. Wilson, *Reflecting Telescope Optics, I*, Springer (1996).
- [206] R. Wilson, *Reflecting Telescope Optics, II*, Springer (1999).
- [207] F. Wright, “An Aplanatic Reflector with a Flat Field Related to the Schmidt Telescope”, *PASP* **47**, 300–304 (1935).
- [208] C. Wyman and D. Korsch, “Aplanatic two-mirror telescopes: a systematic study. 1: Cassegrainian configuration”, *Appl. Optics* **13**, 2064–2066 (1974a).
- [209] C. Wyman and D. Korsch, “Aplanatic two-mirror telescopes: a systematic study. 2: The Gregorian configuration”, *Appl. Optics* **13**, 2402–2404 (1974b).
- [210] C. Wynne, “New wide-aperture catadioptric systems”, *Monthly Notices of RAS* **107**, 356–368 (1947a).
- [211] C. Wynne, “Chromatic correction of wide-aperture catadioptric systems”, *Nature* **159**, 91–92 (1947b).
- [212] C. Wynne, “Field Correctors for Parabolic Mirrors”, *Proc. Phys. Soc.* **B62**, 772 (1949).
- [213] C. Wynne, US Patent 2,509,554 (1950).
- [214] C. Wynne, “New Lens Systems”, *Progress in Physics*, **19**, 298–325 (1956).
- [215] C. Wynne, “Field correctors for large telescopes”, *Appl. Optics* **4**(9), 1185–1192 (1965).
- [216] C. Wynne, “Afocal Correctors for paraboloidal mirrors”, *Appl. Optics* **6**(7), 1227–1231 (1967).
- [217] C. Wynne, “Ritchey-Chrétien telescopes and extended field systems”, *ApJ* **152**, 675–694 (1968).
- [218] C. Wynne, “Field correctors for astronomical telescopes”, in *Progress in Optics*, **X**, 139–164 (1972).
- [219] C. Wynne, “Data for some four-lens paraboloid field correctors”, *Monthly Notices of RAS* **165**, 1P–8P (1973).
- [220] C. Wynne, “A new wide-field triple lens paraboloid field corrector”, *Monthly Notices of RAS* **167**, 189–197 (1974).
- [221] C. Wynne, “Shorter than a Schmidt”, *Monthly Notices of RAS* **180**, 485–490 (1977).
- [222] C. Wynne, “The optics of the achromatized UK Schmidt telescope”, *Quat. J. of the RAS* **XXII**, 146–153 (1981).
- [223] N. Zacharias, U. Laux, A. Rakich, and H. Epps, “URAT: astrometric requirements and design history”, *astro-ph/0606193 v1*, 8 Jun (2006).
- [224] G. Zhao, Y. Zhao, Y. Chu, et al., “LAMOST Spectral Survey”, *arXiv:1206.3569* [astro-ph.IM] (2012).
- [225] P. Zimmer, J. McGraw, and M. Ackermann, “Affordable Wide-field Optical Space Surveillance using sCMOS and GPUs”, *Proc. AMOS Conf.*, (2016).

Index

A

achromatic meniscus, 76, 88, 91, 93
achromaticity condition, 88, 90
ADC telescope, 86
Airy disk, 22, 69
Airy pattern, 22
aliasing, 24
anastigmatic, 26
anastigmats, 44
Anglo-Australian Telescope, 7
aperture stop, 12, 29, 31, 42, 64, 96
aplanat, 65
aplanat field size, 35
aplanats, 32
aplanatic, 38, 61
aplanatic Cassegrain, 2
approximate aplanats, 33, 38
asphericity gradient, 43, 57, 70, 73, 85, 121
asphericity gradients, 55, 58, 67
astigmatism, 13, 34
ATLAS, 11
atmosphere dispersion, 54
atmosphere dispersion corrector, 58
AZT-16 telescope, 90

B

back focal length, 21, 37, 60, 108
baffles system, 37
Baker three-mirror telescope, 43, 69
Baker Super-Schmidt camera, 103–104
Baker, 16

Baker–Nunn camera, 101, 107
Blanco, 57
Blanco 4-m telescope, 7, 54
Blanco telescope, 57, 73
Blanco-R, 55
Blanco-R (VT-014d), 52
Blanco-S (VT-014e), 52
Blanco-S, 52, 54–55
Blanco-T (VT-014f), 52
Bouwers camera, 76

C

Cassegrain system, 18, 29, 36, 65
Catalina Real-Time Survey, 11
charge-coupled devices (CCDs), 20, 60
chromatic aberration, 17, 50, 57–58, 89, 93, 98, 104
chromatic difference of magnification, 17
circles of least confusion, 34
classical Cassegrain telescope, 1, 31
classical Gregorian telescope, 3
classical telescope field, 32
classical two-mirror telescopes, 31
coma, 26, 34, 55, 90
complementary metal-oxide semiconductors, 21
conic constant, 18, 63
conic constants, 32, 33
conic sections, 18, 33, 38, 44
concentric meniscus, 76
corrected Cassegrain telescope, 59, 61

corrected Gregorian telescope,
 3, 59, 67
 Couder anastigmat, 39
 curved, 14
 curved detectors, 14
 curved focal surface, 10, 37, 98, 102,
 104, 107
 cutoff frequency, 22

D

Dark Energy Survey (DESI), 7, 48,
 56, 57
 Dark Matter Telescope, 70
 DARPA Space Surveillance
 Telescope (DSST), 7, 43
 DCT, 7
 DECAM, 7, 10, 21, 54, 58, 73
 delivered image quality, 5, 115
 design VT-050k, 66
 design VT-056y, 7, 24
 design VT-110f, 84
 design VT-110k, 87
 design VT-110p, 86
 design VT-119j, 109

E

effective aperture, 4
 effective aperture diameter, 63
 entrance pupil, 5, 12, 42, 71, 109
 Epps and Fabricant, 60
 equivalent focal ratio, 29
 ESO Schmidt, 7
 étendue, 4, 116
 even aspheres, 19, 43, 58, 63,
 72, 78
 exit pupil, 12, 29, 31, 39,
 41, 65

F

fiber optic, 14, 40
 fibers, 57
 field flattener, 83
 field curvature, 13, 34, 70, 83

focal gap, 77, 81
 focal ratio, 10, 22, 26
 full width at half maximum, 53
 functions of a bounded spectrum,
 22, 23

G

Gabor camera, 76
 Gattini-IR project, 100
 GEODSS, 7
 global, 50
 global minimum, 54
 gradient of asphericity, 63
 Gregorian system, 18, 29, 65, 122
 Gregory–Maksutov, 3, 65
 Gregory–Maksutov telescope, 68

H

Hamilton telescope, 17, 95, 104
 Hawkins–Linfoot camera, 91, 104,
 107
 Herschel, 5
 Hubble Space Telescope, 34, 36,
 121, 123

I

‘ideal’ telescope, 16
 IKONOS satellite, 45

J

James Webb Space Telescope, 45

K

Kepler mission, 83
 Kepler space telescope, 14, 24
 Korsch, 25
 Korsch anastigmat, 7, 44
 KPNO 84-inch reflector, 34

L

LAMOST, 7, 25, 40
 Large Binocular Telescope, 122
 Large Synoptic Survey Telescope
 (LSST), 7, 21, 43, 62, 70

lateral color, 17, 77, 87, 90, 99
lengthening systems, 31
limiting stellar magnitude, 6, 41, 96, 115
linear obscuration coefficient, 5
linear obstruction, 29
longitudinal color, 16–17, 76–77, 83, 87, 90–91, 95, 99
loss of light, 56

M

Maksutov, 28
Maksutov diagram, 29, 46
Maksutov parameters set, 117
Maksutov telescope, 18, 76, 91
Mangin, 17
Mangin mirror, 16, 95, 105
Mareschal limit, 123
Mayall, 48
Mayall telescope, 7, 57
McDonald Observatory 105-inch, 50
medial, 17
meniscus lens, 75
Mersenne system, 29, 41
modulation transfer function, 22, 123

N

near-Earth asteroids, 63
Nyquist frequency, 23, 24

O

OMI, 7

P

Palomar, 48, 87
Palomar 200-inch reflector, 32
Palomar 48-inch Schmidt, 106
Palomar Sky Survey, 10
Pan-STARRS, 7
Pan-STARRS survey, 11, 70
Pan-STARRS-1, 59
Panoptes-1AB system, 100

paraboloid field size, 26
Paul, 25
Paul three-mirror telescope, 42
Paul–Baker design, 43
Petzval condition, 13
PHOENIX telescope, 102
point spread function, 22
point symmetry, 101, 15, 77, 90, 93, 95, 108
polysag, 19
polysag surface, 43
Project MESSIER, 67

Q

quantum efficiency, 21, 97
Quasi-Ritchey–Chrétien (QRC) system, 2, 59, 61

R

reflecting Schmidt camera, 25, 40
Ritchey–Chrétien (RC) telescope, 2, 60
Richter–Slevogt, 18
Richter–Slevogt telescope, 92, 98
ripples, 53, 123, 124
Ritchey–Chrétien, 33, 57
Ritchey–Chrétien telescope, 1, 11, 40, 48, 59
Ross, 48
ROTSE-III telescope, 59

S

sampling factor, 24, 54, 92
sampling frequency, 23
sampling theorem, 23
Schmidt, 15
Schmidt camera, 18, 40, 42, 76–77, 88, 106, 108
Schmidt corrector, 77–78, 80, 82, 90
Schmidt–Cassegrain camera, 86–87
Schmidt–Houghton camera, 98, 101
Schmidt–Wynne camera, 87

- Schwarzschild aplanat, 38, 39, 118, 120
shortening systems, 31
signal-to-noise ratio, 6, 72, 97, 115
sine condition, 33, 39, 117
sky survey rate, 5, 96, 116
SkyMapper, 7
SNAP, 7
SNAP design, 45
Sonnfeld camera, 105
spatial frequency, 22
spherical aberration, 15, 34, 77, 81, 88
spherochromatism, 17, 87
SPM-Twin, 7
STA1600 CCD, 7, 92, 97
standard, 18
Steward 90", 7
Strehl, 14, 75, 93
Strehl 'ideal' telescope, 31, 42
Subaru Hyper Suprime Camera (HSC), 7, 10, 21, 57, 58
surface of medium curvature, 34
survey speed, 1, 6, 96–97
symmetry, 83
system VT-110k, 87
- T**
T250 ACTUEL telescope, 7, 63
TEC-VT300mm, 99
Terebizh, 51, 96, 105
Terebizh PF-corrector, 52
Terebizh symmetrical camera, 101, 108
thick lens, 89
three-mirror anastigmat (TMA), 3
three-mirror Paul telescope, 71
tolerances, 26, 61, 67, 72–73, 91–92, 122
- U**
United Kingdom Schmidt Telescope, 7, 87
- URAT system, 93
- V**
Vatican Advanced Technology Telescope, 55, 122
VAU camera, 104, 107
vignetting, 45, 64, 70–71, 87, 92, 96, 98, 106
VISTA, 7
VLT Survey Telescope, 7, 60
VT-014j, 54
VT-014j design, 125–126
VT-050k, 67
VT-050m design, 67
VT-060q system, 105
VT-061b design, 43
VT-078e design, 99
VT-090j design, 43
VT-098v design, 106
VT-102j, 105
VT-110k design, 77, 82, 84, 106
VT-114b design, 88–89
VT-119g, 18, 108
VT-119g design, 107
VT-119w design, 101–102
VT-133c, 68
VT-135e design, 101
VT-137d design, 64
VT-137d, 64
VT-137q, 65
- W**
wide-field, 4
WIYN ODI, 7
Wright, 83
Wynne, 48–50, 54, 58, 60, 93
Wynne RC corrector, 50
Wynne symmetrical camera, 91, 108
Wynne three-lens design, 99, 102
- Z**
Zeiss 643-mm telescope, 91



Valery Terebizh graduated from St. Petersburg University with a Doctor of Science in theoretical astrophysics. His main interests are related to the diffusion of radiation, time series analysis, extragalactic astronomy, inverse problems of mathematical physics, and astronomical optics. Terebizh has written four monographs on these topics. Many wide-field telescopes with a diameter of up to 4 m have been built around the world according to his designs. He was previously a leading researcher at the Byurakan Astrophysical Observatory and Moscow State University; currently, he is the principal investigator at the Crimean Astrophysical Observatory.